Sara Pinto dos Santos Matias

Master of Science

Dynamics of serotonergic neurons revealed by fiber photometry

Thesis submitted in partial fulfillment of the requirements for the degree of Doctor of Philosophy in

Bioengineering Systems

Adviser: Zachary Frank Mainen, Ph.D.,
Champalimaud Research Director,
Champalimaud Center for the Unknown

Co-adviser: Manuel Nunes da Ponte, Ph.D., Full Professor,
NOVA University of Lisbon

Examination Committee

Chairperson: Doctor João Paulo Serejo Goulão Crespo, Full Professor, NOVA University of Lisbon

Raporteurs: Doctor Naoshige Uchida, Full Professor, Harvard University
Doctor Tiago Vaz Maia, Assistant Professor, University of Lisbon

Members: Doctor Margarida Casal Ribeiro Castro Caldas Braga, Assistant Professor, NOVA University of Lisbon
Doctor Michael Brian Orger, Principal Investigator, Champalimaud Research
Doctor Rui Manuel Marques Fernandes da Costa, Director, Champalimaud Research

FACULDADE DE CIÊNCIAS E TECNOLOGIA
UNIVERSIDADE NOVA DE LISBOA

December 2015

Sara Pinto dos Santos Matias

Master of Science

Dynamics of serotonergic neurons revealed by fiber photometry

Thesis submitted in partial fulfillment of the requirements for the degree of Doctor of Philosophy in

Bioengineering Systems

Adviser: Zachary Frank Mainen, Ph.D.,
Champalimaud Research Director,
Champalimaud Center for the Unknown

Co-adviser: Manuel Nunes da Ponte, Ph.D., Full Professor,
NOVA University of Lisbon

Examination Committee

Chairperson: Doctor João Paulo Serejo Goulão Crespo, Full Professor, NOVA University of Lisbon

Raporteurs: Doctor Naoshige Uchida, Full Professor, Harvard University
Doctor Tiago Vaz Maia, Assistant Professor, University of Lisbon

Members: Doctor Margarida Casal Ribeiro Castro Caldas Braga, Assistant Professor, NOVA University of Lisbon
Doctor Michael Brian Orger, Principal Investigator, Champalimaud Research
Doctor Rui Manuel Marques Fernandes da Costa, Director, Champalimaud Research

FACULDADE DE CIÊNCIAS E TECNOLOGIA
UNIVERSIDADE NOVA DE LISBOA

December 2015

Dynamics of serotonergic neurons revealed by fiber photometry

This work was developed in the context of the MIT Portugal Program, area of Bioengineering Systems, in collaboration with the Champalimaud Research Programme, Champalimaud Center for the Unknown, Lisbon, Portugal. The project entitled *Dynamics of serotonergic neurons revealed by fiber photometry* was carried out at Instituto Gulbenkian de Ciência, Oeiras, Portugal and at the Champalimaud Research Programme, Champalimaud Center for the Unknown, Lisbon, Portugal, under the scientific supervision of Zachary F. Mainen, Ph.D, and under the guidance of the Thesis Committee composed by Rui M. Costa, Ph.D, and Michael B. Orger, Ph.D.. This work was supported by the fellowship SFRH / BD / 43072 / 2008 from Fundação para a Ciência e Tecnologia, Portugal, to Sara Matias and by the Advanced Investigator Grant 250334 from the European Research Council to Zachary F. Mainen.

Acknowledgments

To Zach, for the opportunity to dwell in systems neuroscience

To Guillaume, for guidance and constant support

To Eran, for guidance and a fruitful collaboration

To Patrícia, for shared laughs and frustrations

To the rest of the Mainen Lab, for eclecticism

To Fatuel and Rui, for genuine drive

To Tatiana, for kindness and teachings

To Enrica and Matthieu, for friendship and leisure

To Susana Lima, for support and the molecular biology times

To Rui and Mike, for guidance

To Rita and Guga, for DançAr

To the Ar team, for unlimited ideas and efforts

To Catarina, Susana and Marta for friendship

To OCNC 2015 organization, for the opportunity to attend such a good course

To Prof. Manuel Nunes da Ponte and Prof. José Silva Lopes for support from the MIT Portugal Program

To Filipek, Geisa, António, Paulo, Swarna, and Maria, for the early days as Ph.D. students

Ao Guga, pela Capoeira

Ao Magoo, Doutor, Manel, Catarina, Lulu, Batman, Nanete, RaparIgor, Júlia e todos os membros do Grupo de Capoeira Nova Aliança Lisboa pela amizade, pelo flow, pela mandinga

À Marisa, Vânia e Xana pela amizade de sempre e para sempre

Ao meu irmão, porque ser irmão não se explica

Aos meus pais, pelo apoio incondicional

Ao João, por acreditares em nós, mais do que em qualquer outra coisa

Abstract

Serotonin is an important neuromodulator implicated in the regulation of many physiological and cognitive processes. It is one of the most studied neuromodulators and one of the main targets of psychoactive drugs, since its dysregulation can contribute to altered perception and pathological conditions such as depression and obsessive-compulsive disorder. However, it is still one of the most mysterious and least understood neuromodulatory systems of the brain.

In order to study the activity of serotonergic neurons in behaving mice, we used genetically encoded calcium indicators and developed a fiber photometry system to monitor neural activity from genetically defined populations of neurons. This approach was developed to study serotonin neurons but it can be used in any genetically defined neuronal population.

To validate our approach, we first confirmed that increased neural activity, induced by electrical microstimulation, indeed produced increases in fluorescence detected by the system. We then used it to monitor activity in the dorsal striatum of freely behaving mice. We show that the two projection pathways of the basal ganglia are both active during spontaneous contraversive turns. Additionally, we show that this balanced activity in the two pathways is needed for such contraversive movements.

Finally, we used the fiber photometry system to study the role of serotonin in learning and behavioral control and to compare it to that of dopamine, another important neuromodulator. Dopamine and serotonin are thought to act jointly to orchestrate learning and behavioral control. While dopamine is thought to invigorate behavior and drive learning by signaling reward prediction errors, *i.e.* better-than-expected outcomes, serotonin has been implicated in behavioral inhibition and aversive processing. More specifically, serotonin has been implicated in preventing perseverative responses in changing environments. However, whether or how serotonin neurons signal such changes is not clear. To investigate these issues, we used a reversal learning task in which mice first learned to associate different odor cues with specific outcomes and then we unexpectedly reversed these associations. We show that dorsal raphe serotonin neurons, like midbrain dopamine neurons, are specifically recruited following prediction errors that occur after reversal. Yet, unlike dopamine neurons, serotonin neurons are similarly activated by surprising events that are both better and worse than expected. Dopamine and serotonin responses both track learned cue-reward associations, but serotonin neurons are slower to adapt to the changes that occur at reversal. The different dynamics of these neurons following reversal creates an imbalance that favors dopamine activity when invigoration is needed to obtain rewards and serotonin activity when behavior should be inhibited. Our data supports a model in which serotonin acts by rapidly reporting erroneous associations, expectations or priors in order to suppress behaviors driven by such errors and enhance plasticity to facilitate error correction. Contrary to prevailing views, it supports a concept of serotonin based on primary functions in prediction, control and learning rather than affect and mood.

Key words: Serotonin, dopamine, fiber photometry, reversal learning, surprise

Resumo

A serotonina é um neuromodulador envolvido em diversos processos de regulação fisiológica e cognitiva. Apesar de ser um dos neuromoduladores mais estudados por estar envolvido em acções psicoactivas de diversos fármacos e na patologia de condições como a depressão ou a doença obsessiva-compulsiva, ainda é um dos neuromoduladores mais misteriosos do cérebro. De forma a estudar a actividade dos neurónios que produzem serotonina durante o comportamento animal, usámos proteínas indicadoras de níveis de cálcio e desenvolvemos um sistema de fotometria por fibra óptica para registar a actividade de populações de neurónios. Este sistema foi desenvolvido para ser usado nos neurónios de serotonina, mas pode ser usado em qualquer população de neurónios geneticamente definida.

Para validar a técnica desenvolvida, começámos por confimar que conseguíamos detectar actividade neuronal induzida artificialmente através de estimulação eléctrica. De seguida, usámos o sistema de fotometria para adquirir informação sobre actividade neuronal no corpo estriado dorsal de ratinhos em comportamento espontâneo. Observámos que as duas vias de projecção desta estrutura se encontram activas quando os ratinhos fazem rotações para o lado contralateral ao que está a ser observado. Mostrámos também que a actividade destas duas vias de projecção tem que estar em equilíbrio para que os ratinhos consigam virar espontaneamente para o lado contralateral.

Finalmente, usámos o sistema de fotometria para estudar a actividade dos neurónios de serotonina em processos de aprendizagem e controlo comportamental. Além disso, comparámos a actividade destes neurónios com a dos neurónios que produzem dopamina, outro neuromodulador envolvido em diversas funções cognitivas. Tem sido proposto por vários investigadores que a dopamina e a serotonina funcionam em conjunto para orquestrar estes processos de aprendizagem e de controlo comportamental. Enquanto a dopamina facilita movimentos que conduzem a recompensas e a sua aprendizagem ao sinalizar eventos que são melhores do que o esperado, a serotonina tem sido implicada em inibição comportamental e no processamento de eventos aversivos. Mais especificamente, a serotonina parece ser necessária para prevenir comportamentos perseverativos quando as contingencias aprendidas pelos animais são alteradas. Contudo, não se sabe como é que os neurónios de serotonina sinalizam essas mudanças. Para investigar este assunto treinámos ratinhos para aprenderem a associar estímulos olfactivos neutros a estímulos incondicionados, como recompensas e castigos. Depois de os ratinhos terem aprendido estas contingências, revertêmo-las inesperadamente de modo a surpreendê-los e a que eles tivessem de reaprender as novas associações. Observámos que tanto os neurónios de dopamina como os de serotonina responderam a eventos melhores do que o esperado. Contudo, os neurónios de serotonina responderam da mesma forma a eventos que eram melhores do que o esperado e a eventos piores do que o esperado. Tanto os neurónios de serotonina como os de dopamina mudaram as suas respostas aos estímulos olfactivos após a reversão das contingências, no entanto os neurónios de serotonina mostraram uma dinâmica mais lenta do que os de dopamina. Esta diferença na dinâmica das adaptações de serotonina e de dopamina permite que, depois da mudança de contingências, a acção da dopamina seja favorecida no caso de a

reaprendizagem necessitar de estimular acções para recolher a recompensa enquanto que a acção da serotonina é favorecida em situações em que é necessário deixar de responder à omissão de uma recompensa.
Os nossos dados suportam um modelo de acção da serotonina em que ela está envolvida na sinalização de associações erradas e erros na predição de eventos. Esta interpretação sugere que a influência da serotonina nas emoções pode ser indirecta, sendo a sua acção directa relacionada com a aprendizagem e o controlo comportamental.

Palavras-chave: Serotonina, dopamina, fotometria por fibra óptica, mudança de contingências, surpresa

Table of Contents

List of Figures

List of Abbreviations

5-HT	5-hydroxytryptamine, serotonin
ACC	Anterior cingulate cortex
Ach	Acetylcholine
AOM	Acousto-optic modulator
CCD	Charge-coupled device
ChR2	Channelrhodopsin-2
CNS	Central nervous system
CS	Conditioned stimulus
DA	Dopamine
DNA	Deoxyribonucleic acid
DRN	Dorsal raphe nucleus
GABA	Gamma-aminobutyric acid
GECI	Genetically encoded calcium indicator
GFP	Green fluorescent protein
GPe	Globus pallidus external segment
IS	Inescapable shock
L-DOPA	Levodopa
LED	Light emitting diode
LFP	Local field potential
LHb	Lateral habenula
LSD	Lysergic acid diethylamide
MHb	Medial habenula
mPFCv	Ventral medial prefrontal cortex
NA	Numerical aperture
NAc	Nucleus accumbens
NADH	Reduced form of nicotinamide adenine dinucleotide
NE	Norepinephrine
OCD	Obsessive-compulsive disorder
PAG	Periaqueductal gray
PMT	Photomultiplier tube
rAAV	Recombinant adeno-associated virus
REM	Rapid eye movement sleep
RL	Reinforcement learning
RMTg	Rostromedial tegmental nucleus
RPE	Reward prediction error
S.D.	Standard deviation
S.E.M.	Standard error of the mean
SERT	Serotonin transporter

SNc	Substantia nigra pars compacta
SNr	Substantia nigra pars reticulata
SPN	Spiny projection neuron
TD	Temporal difference
TPH2	Tryptophan hydroxylase 2
TTL	Transistor-transistor logic
US	Unconditioned stimulus
VTA	Ventral tegmental area
YFP	Yellow fluorescent protein

1. General Introduction

In this chapter I introduce the serotonergic system. The motivation for this thesis was to record activity from neurons that produce serotonin located in the brainstem during behavior. I discuss the major theories that have been proposed for serotonin's function, which involve it in motor facilitation, aversive processing, behavioral inhibition or reward processing. The main results of this thesis represent a tentative effort to integrate a seemingly disparate set of functions for this neuromodulatory system.

Results published:
Dugué, G. P., Lörincz, M.L., Lottem, E., Audero, E., Matias, S., Correia, P.A., Léna, C., Mainen, Z.F.. Optogenetic recruitment of dorsal raphe serotonergic neurons acutely decreases mechanosensory responsivity in behaving mice. *PLoS One* **9,** e105941 (2014). DOI: 10.1371/journal.pone.0105941

Author contributions
Conceived and designed the experiments: GD CL ZM. Performed the experiments: GD ML EL EA SM PC. Analyzed the data: GD CL ZM. Contributed to the writing of the manuscript: GD CL ZM.

1.1 Introduction

Serotonin (5-HT, 5-hydroxytryptamine) is an important neuromodulator in the brain, but its primary role and function are still an enigma.

Serotonin was discovered independently in the late 1930s and 40s as an abundant compound in the gastrointestinal tract (called *enteramine*) where it increases smooth muscle tone[1,2] and as a vasoconstriction compound of blood serum[3,4] (thus its name *serotonin*). In 1945 its structure was resolved[5] and during the 1950s 5-HT was isolated from a number of organs, including the brain, and proposed as a synaptic transmitting agent[6]. The cell bodies containing this monoamine were later discovered in the brainstem[7] along with their nerve terminals which spread to a number of areas of the mammalian central nervous system (CNS)[8] . Only in the 1960s it became anatomically evident that 5-HT, like dopamine (DA) and norepinephrine (NE), was a central neurotransmitter[8], however there were hypotheses about an important role for 5-HT in mental disorders since the 50s[9]. These were based on the use of both natural and synthetic compounds related to 5-HT's structure, such as lysergic acid diethylamide (LSD). Consequently, the interest to develop and test drugs to interfere with the serotonergic system in humans was increasing[10].

Since then, scientists have implicated 5-HT in a diverse set of physiological and cognitive functions. These include cardiovascular[11] and respiratory[12,13] activity, feeding[14], fluid homeostasis[15], thermoregulation[12,16], nociception[17,18], motor control[19–21], sleep[22–25], sexual[26–29] and other social[30–32] behaviors, anxiety[33–35], depression[36–38], mood[39–43], behavioral flexibility[41,44,45], to name a few[46–48].

Despite all the interest and research that this molecule has inspired, it is still one of the most enigmatic neuromodulators of the brain: Barry Jacobs has memorably commented that the problem is that "*It is at once implicated in virtually everything, but responsible for nothing*"[49]. In fact, the mystique by which serotonin is surrounded affects not only scientists but also lay people who can relate to its effects on altered states of consciousness by hallucinogenic drugs[50,51] or by conditions related to psychiatric disorders such as schizophrenia[52–54], depression[36–39,42] or obsessive-compulsive disorder (OCD)[55,56].

In this thesis the development and use of a system to record neuronal activity from 5-HT neurons in behaving mice over the course of days will be presented. The system was also used in other neural populations, namely in midbrain DA neurons and in medium spiny neurons of the dorsal striatum, but the primary goal of its development was to record population signals from the neurons that produce this neuromodulator, serotonin. Our approach can be used to study any function of the serotonergic system, but we focused on learning, value representation, and behavioral flexibility. Consequently, in the following sections I will briefly introduce the anatomical organization of the 5-HT system and then summarize some of the theories proposed to explain its function and which are relevant to our experiments and analysis.

1.2 The serotonergic system

Brain serotonin is produced from the essential amino acid L-tryptophan inside specific neurons. L-tryptophan is obtained from dietary ingestion and these neurons have a set of proteins that carry out two chemical reactions to produce serotonin. The rate limiting factor on serotonin's production is the enzymatic activity of tryptophan hydroxylase (TPH2) whose presence in a cell is used to define it as a 5-HT neuron or not[57,58]. After production, serotonin is stored in vesicles which protect it from degradation (by another enzyme named monoamine oxidase B). When an action potential is triggered, these vesicles fuse with the plasma membrane as calcium ions enter the nerve terminals, releasing their content in the synaptic cleft. Here serotonin will interact with post- and pre-synaptic receptors (binding to the releasing neuron itself), be degraded by monoamine oxidase A, and / or reuptaken inside 5-HT neurons by the serotonin transporter (SERT) to be restored or destroyed[59]. The activity of 5-HT neurons is tightly controlled[60] and it is thought that by diffusing beyond the synaptic space serotonin can affect some neurons through volume transmission[61].

The number of neurons that produce serotonin is relatively small (approximately 26,000 in mice[62] and about half a million in humans[63]), but their axon terminals can be found in almost all areas of the brain.

The serotonergic system might be the most diffuse of all neurotransmitter systems, but this does not make it a nonspecific projection system: the patterns of efferent and afferent projections are highly organized and it includes an impressive panoply of 5-HT receptors that modulate its effects on target neurons. Briefly, there are at least 14 5-HT receptor subtypes grouped in 7 families[64]. These have variable orders of 5-HT affinity and are generally G-protein coupled receptors that trigger intracellular signaling cascades to either decrease or increase the excitability of the neurons that express them, and to modulate the release of other neurotransmitters, such as glutamate, gamma-aminobutyric acid (GABA), DA, acetylcholine (ACh) and NE. Only one 5-HT receptor, 5-HT3, is a ligand-gated ion channel[65,66]. Some of these receptors are also expressed in 5-HT neurons themselves (autoreceptors). Of particular relevance is the somatodendritic 5-HT1A autoreceptor (though it is also expressed in non 5-HT neurons) which controls 5-HT neural activity through a local negative feedback mechanism particularly important in situations of high levels of 5-HT neuronal activity[67].

In mammals, the somata of 5-HT neurons are mostly concentrated in nine nuclei in the brainstem. These nuclei are grouped in the caudal and the rostral groups, which have been shown to have distinguishable transcriptomes[68]. A code system was introduced to number these nuclei from the most caudal to the most rostral one (B1-B9)[7] . The caudal group of raphe nuclei includes the raphe obscurus, raphe magnus, raphe pallidus and parts of the lateral reticular formation (areas B1-B5) which project mainly to the spinal cord. The rostral group, on the other hand, has mostly ascending projections to the forebrain. This last group comprises the caudal linear nucleus, median raphe (B8-B9), and the dorsal raphe nucleus (areas B6-B7)[69].

5-HT neurons are known to be heterogeneous in terms of location, morphology and neurotoxin sensitivity, but there are already some tools that can be used to target groups of 5-HT neurons based on their embryonic development through rhombomere-defined genetic lineage[70]. In this respect, the 5-HT cells in the dorsal raphe nucleus (DRN) originate from a single rhombomere and develop to be located ventrally to the periaqueductal gray matter in the midbrain.
This is the 5-HT nucleus of most interest for us: it is the largest raphe nucleus, containing about 9,000 5-HT neurons in mice[62], and it is the nucleus that includes area B7 which has the strongest 5-HT projections to areas involved in learning and decision making[71–74], such as the ventral tegmental area (VTA), frontal cortices and the dorsal striatum.

Projections of DRN 5-HT neurons

5-HT neurons in the DRN have widespread and diffuse projections to the forebrain. These fibers are generally very fine, with small fusiform butons[69], and can be branched in ways that the same individual 5-HT neuron in the DRN targets several distinct but functionally related structures[75]. Some of the main projections of DRN 5-HT neurons include the substantia nigra pars compacta (SNc) and pars reticulata (SNr), the VTA, nucleus accumbens (NAc) shell, globus pallidus, ventral pallidum, the caudate putamen or dorsal striatum, the substantia innominata, central and basolateral amygdala, lateral habenula (LHb), hypothalamus, medial septum, nucleus of the diagonal band, olfactory related areas such as the olfactory bulb, the anterior olfactory nuclei and the piriform cortex, and various cortical areas, particularly orbital, medial prefrontal, infralimbic and insular[73,74].
5-HT neurons in the DRN also innervate local neurons in the DRN itself and in the other raphe nuclei, which suggests that an inhibitory feedback loop through 5-HT1A autoreceptors would be possible[65,73].

Inputs to DRN 5-HT neurons

Inputs to the DRN have been studied since the late 1970s using retrograde tracers such as horseradish peroxidase and wheat germ agglutinin, and found to be, also, very diverse[76].
Recent developments in monosynaptic retrograde tracing strategies using modified rabies viruses[77] have enabled the identification of afferent projections of specific cell types using Cre-driver mouse lines[78–80]. Using this approach, three independent studies[81–83] have shown that DRN 5-HT neurons receive their main inputs from local 5-HT neurons, from DRN GABA neurons, from glutamatergic projections from the prefrontal cortex, particularly from the insular, motor and orbital cortices, from the LHb, the lateral hypothalamus, the amygdala, D1 receptor-containing neurons in the ventral striatum, and from the VTA and SNc.

Heterogeneity of DRN neurons

As has been implied already, the DRN is an heterogeneous structure, containing not only 5-HT neurons, but also neurons expressing GABA, DA, glutamate, ACh, a variety of peptide transmitters, and nitric oxide[82,84–91]. In fact, 5-HT neurons are estimated to represent between one and two thirds of the cells in the DRN of rats[76,84,92]. This is an important point, given that it has been extremely difficult until recently[93], with the advent of optogenetics, to record from

identified 5-HT neurons in behaving mice. As a consequence, many electrophysiological studies have relied on action potential and firing properties of the recorded units to select putative 5-HT neurons. Classically, 5-HT neurons were considered to discharge in a stereotyped, clock-like manner, with an intrinsic frequency of 1-3 spikes/s and with spike duration over 2 ms with large afterhyperpolarization potential[76]. One of the first characteristics to be established for DRN 5-HT neurons *in vivo* was the relationship with the sleep-wake cycle[24,76,94]: these neurons slowly decrease their firing rate, and also their regularity, as animal transitions from wake state to drowsiness and to slow wave sleep. During rapid eye movement (REM) sleep these neurons are silent and their firing rate increases before the end of the REM epoch. Notwithstanding, other studies have shown that 5-HT neurons in the DRN actually have diverse firing properties (for example, the majority of 5-HT neurons might be slow-firing, but there are some fast-firing and even bursting ones), and that some non-5-HT neurons have properties previously associated with classical 5-HT neurons, both *in vitro*[95–97] and *in vivo*[98–102]. These realizations also include the observation of decreased firing upon administration of 5-HT1A agonists in both 5-HT and non-5-HT neurons. As a result, some researches choose not to classify their units when recording from the DRN. The limitations of these approaches are at the root of the experimental technique developed in this thesis to record activity from DRN 5-HT neurons.

1.3 Theories of Serotonin function

Here I present the most influential theories of 5-HT function. Due to the diversity of results from research focused on manipulation and monitoring of this system, these share some commonalities but also some apparent contradictions.
At the end of this thesis, based on the experimental results shown in Chapter 4, we will try to integrate these views into a novel theory of how to look at the role of the serotonergic system in learning and behavioral control.

1.3.1 The (sensori-) motor hypothesis

The motor hypothesis of 5-HT's function was developed by Barry Jacobs and colleagues based on a series of studied of electrophysiological recordings in the DRN of freely behaving cats performed in the 1980s and 90s. It states that the primary function of 5-HT is to facilitate motor output while inhibiting sensory information processing[19,49]. Specifically, the result of this tradeoff is that activation of the 5-HT system results in the coordination of the autonomic and neuroendocrine systems to generate repetitive or tonic motor output (for example, chewing, grooming), while its inactivation would result in the opposite (facilitation of sensory information processing and motor inhibition)[103,104].
These *in vivo* electrophysiological recordings were performed in cats during drug induced atonia[105], throughout the natural and manipulated sleep wake cycle[106,107], and when cats were engaged in repetitive behaviors such as central pattern generator movements[20,108] which were correlated with increases in activity of DRN neurons. This hypothesis is also supported by dense targeting of primary and secondary motor areas, substantia nigra and globus pallidus by

5-HT neurons[19], and by the fact that in invertebrates, whose nervous systems are organized in ganglions, 5-HT's functions are mostly motor-related[109,110].
This hypothesis, however, has significant caveats, such as the fact that putative serotonergic neurons were selected based on certain electrophysiological characteristics which, we know now, are not good indicators of neurochemical identity as discussed above, and the fact that it underestimates the role of the diverse 5-HT projections to non-motor related areas.

1.3.2 5-HT in behavioral inhibition

The hypothesis of 5-HT's involvement in behavioral inhibition was proposed by Philippe Soubrié in 1986[111] and is based mainly on pharmacological and lesion studies on anxiety and impulse control. It states that 5-HT's action is brought into play in situations of competition or conflict between behavioral suppression and active responding. In particular, decreased 5-HT activity would decrease passivity. An idea about the role of 5-HT in withholding responses associated with punishment had been proposed in the seventies, as a system that would possibly interact with a different reward system associated with reinforcement of behavior[112]. Soubrié reviews diverse literature in which decreased brain 5-HT signaling caused by pharmacological manipulations or lesions attenuates punishment-induced inhibition and passive avoidance behaviors, facilitates active avoidance, decreases novelty-induced inhibition, increases locomotion in the open field and Y maze, and increases resistance to extinction after a history of positive reinforcement. He claims that most of the associations between 5-HT and anxiety or aggression might be a result of a failure in behavioral inhibition (or impulsivity) instead of an effect on these emotions *per se*. He also discusses how the results of the reviewed manipulations might be context-dependent, with less or no results in conditions of "chronic", well-learned conflict, meaning that the familiarity of the environment or the animal training duration and/or experience might influence the results. This is an interesting observation, because it suggests that these effects are not purely motor, but might be influenced by a higher and more abstract brain function which depends on the expected volatility of, or control over, the environment.
Interestingly, Mark Geyer comments that one important limitation of Soubrié's proposal is the lack of distinction between the mesostriatal 5-HT pathway, which originates in the DRN and which he argues is better positioned to interact with dopamine, and the mesolimbic pathway from the MRN, better positioned to interact with norepinephrine. He therefore suggests that Soubrié's model should be tested in conditioning paradigms, specifically when focusing on the roles of the former mesotriatal pathway.
More recently, studies focusing on DRN 5-HT neurons have shown that their activity is involved in waiting for delayed rewards[113–119]. These studies used behavioral paradigms in which animals need to nose poke for a variable interval of time in order to get a delayed reward, otherwise either a small reward is delivered or no reward at all is obtained. Specific stimulation of DRN 5-HT neurons using optogenetics increased the time mice were willing to wait for a delayed future reward. Depending on the results obtained in other parameters besides waiting (such as

movement time), this result can be interpreted under this behavioral inhibition framework[119] or under the theory proposed by Kenji Doya that serotonin promotes waiting by modulating the discount factor, a parameter used in reinforcement learning models (RL) to determine how far into the future an agent should consider the prediction of rewards and select an action according to it (the more delayed a reward is, the more its value is discounted)[118,120,121].

1.3.3 Serotonin, aversive processing, and mechanisms of defense

J. F. Deakin, inspired by Wise *et al*.[122], has proposed in 1983[123] that ascending 5-HT projections are involved in mediating anticipatory responses to pain and aversive events, an idea related to Frederico G. Graeff's view, stated in 1974[124], that 5-HT could mediate the behavioral suppression induced by punishment.

Deakin agreed with Soubrié in that 5-HT seemed to show important parallels with DA, namely in terms of their efferent projections and antagonistic motor functions, but, unlike Soubrié, he was convinced that DA and 5-HT were involved in emotions of opposite valence. Consequently, 5-HT's activity should be enhanced by predictive cues of aversive reinforcers and function as a negative incentive system[123]. He argued that the involvement of DA in reward processing should be an important hint to how 5-HT would be involved in aversive processing. Therefore he specifically argued for a role of 5-HT in aversive or nonrewarded stimuli needing latent-inhibition, extinction or habituation, a theory that was more relevant for the functioning of the MRN.

So while Soubrié claimed that 5-HT effects in aversion and anxiety are a consequence of the lack of proper inhibitory control in a conflicting situation, Deakin, and also Graeff, defended that 5-HT activity is not only responsible for behavioral inhibition, but also for decreased aversion and anxiety.

However, the results of pharmacological studies were diverse and often contradictory, with 5-HT either increasing or decreasing anxiety. To overcome this confusion, Deakin and Graeff[125] proposed, in 1991, a role for 5-HT in defense mechanisms, suggesting that different 5-HT pathways would mediate distinct responses to aversive events of different kinds. According to this theory 5-HT is involved in adaptive responses to aversive events, such as behavioral suppression, withdrawal and fight/flight response[126] depending on the proximity of, and the level of control over, the threat. They looked at the 5-HT system, particularly the DRN, as an anticipatory anxiety system[127] which would be responsible for triggering negative incentive and inhibit areas involved in approach behavior when activated by DA, such as the NAc.

In fact, several more recent studies have shown increased activity of putative or identified 5-HT neurons to punishments[30,93,128–131], however responses to cues that predict them have never been reported.

This theory of 5-HT's involvement in aversive processing has seen considerable support from other scientists, with new theories of 5-HT function emerging from its influence.

1.3.4 The Dopamine – Serotonin opponency theory and beyond

Theories that oppose the actions of serotonin to those of catecholamines have been proposed since the 1950s[6], but the opponency between 5-HT and DA has been the most cherished[40,41,71,123,132–134]. These views are strongly influenced by opponent–process theories of motivation and behavioral control[135,136].

DA neurons are mostly located in the VTA and SNc, and receive strong projections from DRN 5-HT neurons[137]. DA has long been associated with reward learning, positive reinforcement, incentive salience and action invigoration[138]. A memorable point in DA's research, and neuroscience research in general, was the realization that the phasic activity of the neurons that produce it matched, almost perfectly, a computational parameter used in reinforcement learning (RL) algorithms[139,140].

Midbrain DA neurons' firing is initially triggered by unexpected rewards and, through associative learning, increased activity shifts to cues that predict these rewards. DA activity increases when an event is better than expected and decreases when it is worse than expected[139,141–144], consistent with the representation of a reward prediction error (RPE), posited by temporal difference (TD) reinforcement learning models[145–147]. In accordance with this model, DA signals impact downstream targets[148–150] to drive approach responses in appetitive reinforcement learning[151–154] as well as to directly invigorate actions[155–158]. (As expected from the complexity of neural systems, some DA neurons show responses to other type of events which have been argued to be aversive[159] or just salient[160,161] responses. Although it is likely that different DA neurons participate in different components of adaptive behaviors[162–166], such as value, salience, and motor control, the representation of a RPE signal constitutes its most general characteristic).

This realization has tempted computational neuroscientists to match the activity of other neuromodulators to the remaining parameters of reinforcement learning models[40,120,155,167].

Peter Dayan's group specifically proposed a role for 5-HT in learning that is complementary to that of DA's: the coding of an aversive prediction error by phasic activity and opposite effects on the modulation of tonic activity.

Their proposal was influenced by several factors: 1) the idea suggested by Deakin and Graeff[125] that the balance between DA and 5-HT transmission in the NAc could mediate the approach / withdrawal behavioral output, 2) additional experimental evidence showing that agonizing 5-HT opposes behaviors that are activated by DA and vice-versa[26,133,168–173], 3) the fact that DA neurons have a large dynamic range to increase their firing to better than expected outcomes but a very limited range to decrease their firing to worse than expected outcomes (baseline firing rate of 3-6 spikes/s), and 4) the fact that the classic TD algorithm is trial-based, not accounting for long-term modulations and accumulations of rewarding or aversive events. Thus, they used an average reward RL algorithm[174] that optimizes the long-term average reward and simulates the type of dynamics suggested by Solomon and Corbit's[135] for opponent systems controlling motivation to establish the following hypothesis:

- tonic 5-HT release signals the long-term reward delivery;

- phasic 5-HT release mirrors that of DA, signaling a prediction error for future punishment;
- tonic DA release signals the long-term punishment delivery.

Some years later, a review from the same lab revisited the concept of opponency between 5-HT and DA[134]. In it they discuss how the opponency between these two neuromodulators presents some important complexities. They review experimental data supporting the inhibitory effect of 5-HT on DA activity, both in the VTA/SNc and in target structures, and also contradictory evidence suggesting that the activation of certain 5-HT receptors actually enhances DA release. They discuss these issues in relation to Pavlovian and instrumental learning (both model-based and model-free) and the difficulty in isolating components of action from those of valance (whose classification might depend on expectations / context). Therefore, from the more simplistic view presented by Daw *et al*. 2002[40], they now account for a more complex definition of valance and asymmetries in Pavlovian effects (such as the biased association of reward with approach and of threat with avoidance). They also abandoned the idea that tonic DA activity could code for long-term average punishment to adopt a view more related to Niv *et al*. 2007's modeling centered on opportunity cost[155]. This variable would integrate both average future rewards and controllable punishments to modulate vigor. In this framework, tonic 5-HT activity would lead to quiescence by reporting the average punishments as an opportunity benefit for the passage of time[175].

In a related review, Cools *et al*. 2011[41] also use the model developed by Niv *et al*. 2007[40], which supports an inseparable relationship between reward processing and action invigoration in tonic DA activity, to inspire a parallel proposal for 5-HT. The consequent argument is that 5-HT could report the average punishments on the opportunity cost and thus aversive and inhibitory actions of 5-HT would be necessarily coupled (active avoidance would be under the command of a different system). This implies that rewards and punishments would be evaluated from a baseline or set point that is reported by this opportunity cost whose function is to control the balance between behavioral activation and withholding.

1.3.5 Serotonin in reward processing

Although the theories presented above mostly focus on a role for 5-HT in aversive processing and / or motor output, the experimental truth is that electrophysiological recordings from DRN neurons show heterogeneous responses and, unlike the case of DA neurons, a signal that has a computationally specific interpretation has not been found yet.
This is due, in part, to the contradiction between the theories that relate 5-HT's function to aversive processing and the fact that, quite often, DRN firing has been reported to correlate with reward parameters. Some examples are DRN sustained activity during reward anticipation and delivery[176–178], during reward omission[179], and a tonic modulation in baseline firing rate that is correlated with the expected and received reward value[43,93,131,176,177,180].

To evaluate the possibility that tonic 5-HT neural activity was indeed tracking the expected reward in a given context, two recent electrophysiological recording studies of DRN neurons[131] or of identified 5-HT neurons in the DRN[93] developed a classical conditioning task for non-human primates or mice, respectively, in which animals experienced (at least) one appetitive and one aversive block which were switched without cueing the animal. These studies have confirmed that a significant percentage of the recorded neurons show tonic modulations that are correlated with the reward context (block) and argued that such a signal would be well positioned to represent the level of motivation in a task and, consequently, be associated with the animal's cognitive state or mood.

1.4 Limitations of classical approaches to study 5-HT function

As discussed in the articles that proposed the theories outlined above, the contributions and effects of 5-HT in several behaviors have been studied over many years using mostly pharmacological and genetic manipulations. These approaches have the potential of being neurochemically very specific, targeting receptors or enzymes of the serotonergic system (although several drugs activate more than one receptor subtype). However, they generally lack spatial resolution, having systemic or whole-brain effects, and certainly lack fine temporal resolution: the effects of drugs take minutes to hours and genetic manipulations take even longer, if not the entire life of the animal, which makes them prone to compensatory effects and blind to the roles of transient modulations.

An approach with much better spatial and temporal resolution is the use of electrical stimulation to activate the neurons and use electrical single-unit recordings to look for correlates of 5-HT neuron firing with behavioral events. The limitation of these approaches is that they are neurochemically non-specific. As we have discussed already, the DRN is heterogeneous and selecting 5-HT neurons based on firing properties is not a reliable method of identification. The best current solution to this problem is to use optogenetic tagging[181] of 5-HT neurons expressing channelrhodopsin-2 (ChR2) to identify them[93]. Substantiating the heterogeneity of 5-HT neurons firing properties, a recent study using this technique has found that although in general DRN 5-HT neurons have longer spike durations, their mean firing rate and inter-spike intervals to not differ from DRN non-serotonergic neurons and clustering algorithms were unable to identify them as a separate class of neurons using these three measures[93].

Still, the DRN is a difficult area to record from and most electrophysiological studies have yielded a small number of neurons which are hard to follow over days. It is therefore hard to understand if there is a unitary signal reported by 5-HT neurons or if there is a way of reconciling the diversity of responses that have been observed in DRN neurons and even in 5-HT neurons in particular. In fact, two recent studies have shown that single DRN and single DRN 5-HT neurons can respond to both rewarding and aversive events[93,131].

In our laboratory we have been developing and applying optogenetic tools to study the 5-HT system and guarantee neurochemical specificity to our investigations[17,119]. Here we propose a complementary approach to classical electrophysiological recording methods, fiber photometry,

to measure activity of neurochemically specific cell populations in general, and 5-HT neurons in particular, over the course of days.

1.5 Objectives and organization of the thesis

The work presented in this dissertation had two main objectives:

1) to develop an alternative method to electrophysiological recordings that would be appropriate for the recording of neural activity from genetically defined cell populations and that could be easily used in different behavioral paradigms;
2) to use the developed system to record activity from 5-HT neurons over the course of days as animals are engaged in tasks with both rewarding and aversive events and which require behavioral flexibility and learning.

In **Chapter 2** I describe the development of a system to record neural activity from defined cell populations, fiber photometry with genetically encoded calcium indicators (GECI), and show its validation in anesthetized and behaving mice. In this last case, we recorded activity from freely moving mice expressing the calcium indicator in D1-expressing medium spiny neurons in the dorsal striatum to verify that movement artifacts could be a problem of our technique. We therefore improved our system to cope with this limitation.
In **Chapter 3** I show the result of an investigation done in collaboration with the laboratory of Dr. Rui Costa and which resulted from the validation of our technique in freely behaving mice: we show that both the striatonigral and the striatopallidal pathways are activated during contraversive spontaneous turns and that proper control of turning requires tightly balanced activity between the two.
In **Chapter 4** I used the fiber photometry system for what it was originally developed for: activity recordings from 5-HT neurons in a reversal learning task in which mice first learn to associate different odors with rewarding, neutral or aversive outcomes and then experience a sudden reversal of the stimulus-outcome contingencies. We have also recorded activity from DA neurons in the same task to compare the activity of the two neuromodulators in these conditions. We show that both 5-HT and DA have prediction error activity, but that 5-HT neurons report an unsigned prediction error or surprise signal.
Finally, in **Chapter 5** I discuss the implications of our approach and experimental findings.

2. Development of fiber photometry for acquisition of neural activity

In this chapter I present the development of a fiber-optic based technique to monitor activity from genetically defined neuronal populations in behaving mice. To complement the limitations of classical techniques to record activity from serotonergic neurons, we decided to use an approach based on the use of genetically encoded calcium indicators. I show validation of the working principle of this technique done in anesthetized and behaving mice. Then I discuss some of the limitations of our technique and present an improved version of the setup to deal with artifacts caused by animal movement.

Results published:

Lopes, G., Bonacchi, N., Frazão, J., Neto, J. P., Atallah., B.V., Soares S., Moreira, L., Matias, S., Itskov, P.M., Correia, P. A., Medina, R.E., Calcaterra, L., Dreosti, E., Paton, J.J., Kampff, A. R.. Bonsai: an event-based framework for processing and controlling data streams. *Front. Neuroinform.* **9**:7 (2015). DOI: 10.3389/fninf.2015.00007

Author contributions

Conceived and developed the project: G.L., N.B., J.F.; Developed software: G.L.; conceived and developed the experiments: G.L.,N.B., J.F., J.P.N., B.V.A., S.S., L.M., S.M., P.M.I., P.A.C., R.E.M., L.C., E.D., J.J.P., A.R.K.; performed and analyzed experiments: G.L., J.F., J.P.N., B.V.A., S.S., L.M., S.M., P.M.I., P.A.C., R.E.M., L.C., E.D.; wrote the manuscript: G.L., A.R.K..

2.1 Introduction

Fiber optic-based methods, together with biochemical sensors, have been used to measure physiological variables at least since the 1970s[182,183]. In general, these methods consist in acquiring the emitted fluorescence of a molecule (fluorophore) that needs to be excited using a light source. The delivery and collection of the different wavelengths in the area of interest is done using a single multimode optical fiber and therefore *fiber photometry* is a term that has been used to describe this type of methods[184].

In early studies about energy metabolism in the surface of the brain and other organs[185,186] researches took advantage of the autofluorescence of the mitochondrial nicotinamide adenine dinucleotide in its reduced form (NADH), whose intensity varies with the metabolic state of the mitochondria[186], and included this technique under the term *fluorometry*[183]. This approach was later used in a deep brain structure to monitor NADH's autofluorescence in the PAG and DRN during the sleep-wake cycle over the course of a month[187].

A similar approach was used more recently using multi-cell bolus loading[188] of a fluorescent calcium dye (Oregon green BAPTA-1[189]) and a single multimode optical fiber (Ø 200 µm) implanted in the cortex of newborn[190] or adult mice[191,192]. Calcium ions are involved in a plethora of cellular functions[193] and, because action potentials induce calcium transients in the soma and dendrites of neurons[194], neuroscientists use dynamics in calcium activity as a proxy for neuronal activity[188,195,196]. These experiments using a chemical calcium dye were either preceded or followed by two-photon imaging of the same cortex area to show that the signals acquired through the optical fiber were equivalent to those detected by a CCD (charge-coupled device) camera and that they resulted from the coordinated activity of thousands of cells[190,191]. However, synthetic calcium indicators cannot be targeted to genetically defined cell populations and limit the duration of the experiments to a few hours.

With the advent of optogenetics[197] the use of optical fibers and genetically encoded probes to study the brain spread rapidly[198]. In particular, the continuous and accelerated development of genetically encoded calcium indicators (GECI) in recent years[199–205] spured the results of functional imaging studies in general and made the use of fiber photometry more attractive. Because these are protein-based calcium indicators, their DNA sequence can be delivered to cells using recombinant adeno-associated viruses (rAAVs)[204,206] and therefore be expressed with cell-type specificity using either known promoters or transgenic lines based on site-specific recombinases, such as the Cre-lox system[78–80]. Since the cells transduced with these probes keep expressing them over time, these indicators allow for long-term recordings of neural activity. Indeed, the number of publications using fiber photometry with GECIs has increased in recent years[166,184,192,207–211] showing the usefulness of monitoring population calcium signals from genetically defined neurons.

As discussed in Chapter 1, electrical recordings in the DRN have not, until very recently[93,178], been able to determine the neurochemical identity of the recorded neurons in behaving animals[20,43,114,131,176,177,179,180,212–217]. These studies have also not yet converged on a model or hypothesis for 5-HT neurons' function during behavior[218]. For this reason we developed a fiber

photometry setup to record population signals from genetically defined 5-HT neurons. Our assumptions were that such calcium signals would reflect correlated activity of 5-HT neurons and that we would be able to follow their activity across several days. Thus, we would have an appropriate dataset to help us understand the general role of this intriguing neuromodulator.

2.2 Results

Our fiber photometry technique is based on two main principles: 1) the successful expression of the GECI, to the neurons of interest and its ability to report neural activity; and 2) the design of an optical setup capable of delivering and collecting the excitation and emission lights of the GECI, respectively. In this section we will present how the photometry technique was developed, how it was validated and how it was later improved for use in the DRN of behaving mice.

2.2.1 Targeting GCaMP expression to 5-HT neurons

During the years in which the work presented in this thesis was developed several versions of the calcium indicator GCaMP were developed and used. Initial work was done using GCaMP3[204] but all data presented in this thesis will be with GCaMP6s[205].
To guarantee that we could specifically target GCaMP to 5-HT neurons in the DRN we used Cre-dependent viruses obtained from the University of Pennsylvania Vector Core[219] (UPenn) and injected them in the DRN of SERT-Cre[220] mice which express Cre recombinase under the serotonin transporter gene (Tg(Slc6a4-cre)ET33Gsat/Mmucd)[220], obtained from GENSAT[221]. This strategy guarantees that only the neurons expressing Cre will express the calcium indicator, which was confirmed using histological methods in four mice. The injection surgeries, as well as all other surgeries targeting the DRN mentioned in this thesis, were performed with an angled approach from the back of the mouse to avoid disrupting the transverse sinus.
Three weeks after injection we sacrificed the mice to collect their brains and prepare tissue sections for immunohistochemistry. We performed anti-5-HT and anti-GFP immunostainnings and DAPI staining in the brain sections. We analysed these sections using a confocal microscope and Fiji software[222] and quantified the specificity of expression (93.2 ± 0.3 %, mean ± s.e.m) and the infection success (73.3 ± 3.5 %, mean ± s.e.m). To achieve this we counted all 5-HT-stained and GFP-stained cells in a 200 x 200 µm window in the center of infection in each of the 3 brain slices that better represented the center of infection of each mouse (**Figure 2.1**).

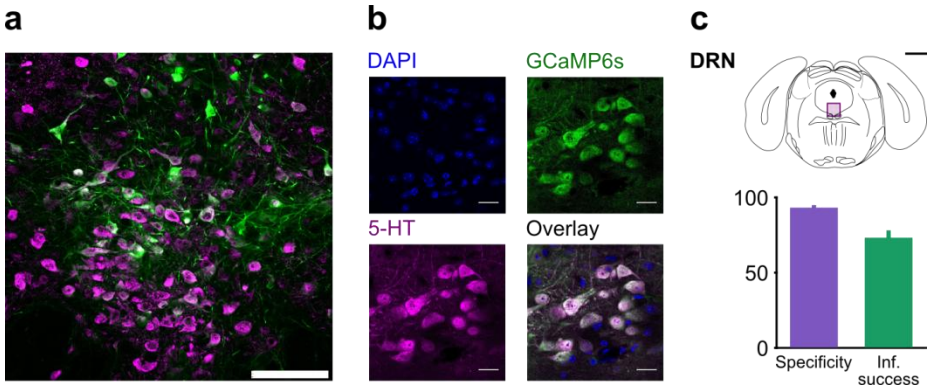

Figure 2.1. Specificity of GCaMP6s expression in DRN 5-HT neurons.

a. Confocal picture of a coronal slice showing restricted GCaMP6s expression to DRN 5-HT neurons in a SERT-Cre mouse; scale bar: 100 µm.

b. Confocal pictures showing DAPI staining, GCaMP6s expression and 5-HT immunoreactivity. Scale bar: 20 µm.

c. Top: schematics of a coronal slice view of the DRN signaling the area shown in *a.* (violet rectangle); black scale bar: 1 mm. Bottom: quantification of specific expression of GCaMP6s in 5-HT neurons (specificity: 93.2 ± 0.3 %, infection success: 73.3 ± 3.5 %, mean ± s.e.m, n = 4 mice).

2.2.2 Design and development of the photometry setup

To collect fluorescence from any activity-dependent indicator one needs to provide the excitation light for the molecule (unless it is a bioluminescence protein[223,224]) and have a means of acquiring its emission. We used the excitation and emission spectrum of GCaMP to select the optical components needed: a blue light source to excite GCaMP (a 473-nm diode-pumped solid-state laser from Crystalaser[225]), an excitation filter to prevent other wavelengths from entering the setup (bandpass filter LD01-473/10-25 from Semrock[226]), a dichroic mirror to separate the excitation and emission lights (Chroma[227] T495LP) and an emission filter to collect only GCaMP's emission (Chroma ET525/50m) (**Figure 2.2**).

A black case was designed, together with Doric Lenses[228], to accommodate all the components, protect the acquisition from ambient light and to be versatile (to change components easily when needed).

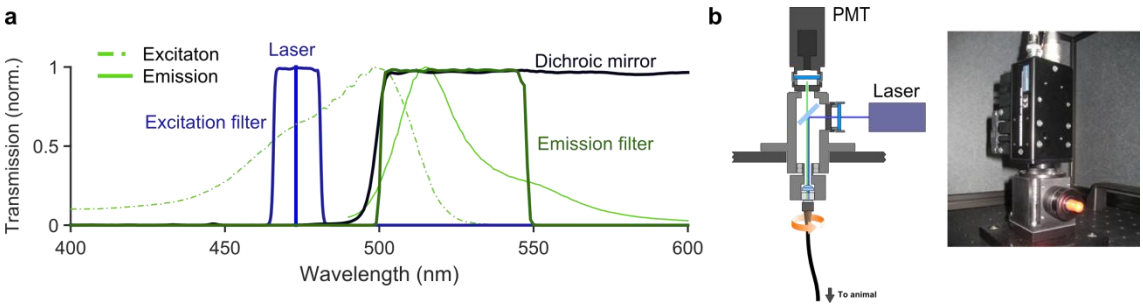

Figure 2.2. Photometry setup.

a. Excitation and emission spectra of GCaMP together with the transmission spectra of the filter and dichroic mirror used to build the setup .

b. Left: schematics of photometry setup consisting of a laser, excitation filter, dichroic mirror, collimating lens, emission filter and PMT, and collimation in the patchrod fiber that will be connected to the implant. Right: picture of the setup.
PMT – photomultiplier tube.

The black case can be adapted to use either a laser or a pigtailed LED as light source. The main advantages of using a laser are its well defined wavelength and its collimated beam, while LEDs have much broader emission spectra and are not collimated, but show much smaller emission amplitude variations than lasers (**Figure 2.1 a**). We tested both light sources and chose to use the laser, because the lack of proper collimation of the LED light made it a lot more difficult to focus it on the center of the dichroic mirror, whose optical specifications are guaranteed at 0° ± 5° and 45° ± 1.5°, and on the optical fiber core (**Figure 2.1 b-c**).

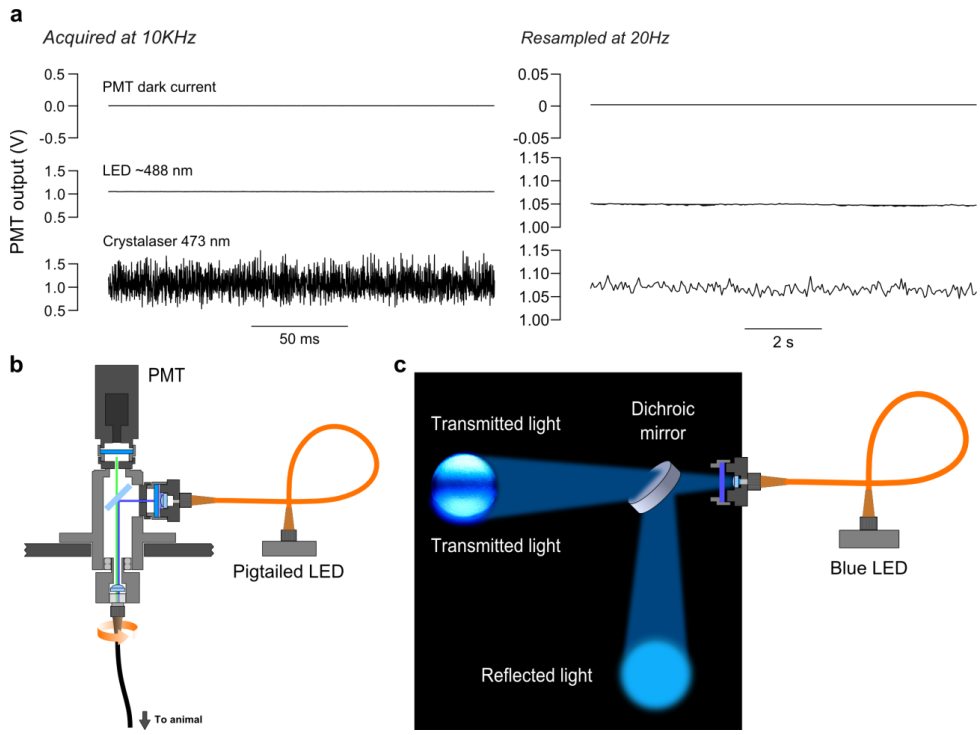

Figure 2.3. Photometry setup tested with and LED as light source.

a. Measured PMT output in the dark showing its dark current (top), using and LED as light source (middle), and using a laser as light source (bottom).
b. Schematics of photometry setup using and LED as light source
c. Schematics showing picture of transmitted light through the dichroic when the LED light is not collimated enough to be restricted to the interval defined by the dichroic specifications.

The black case also has a rotatory joint at the bottom with a FC/PC connector for the optical fiber that conducts the light to the brain. However, in all our experiments with behaving mice we fixed this joint, because its rotations altered considerably the transmission of light (**Figure 2.4**). To guarantee that the animals could move freely, we simply used a long fiber between the setup and the mouse experimental setting.

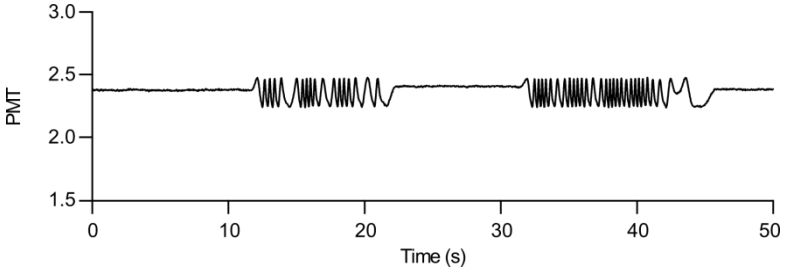

Figure 2.4. Rotatory joint creates artifacts in PMT signal. PMT signal over time showing variations when rotation of the joint was induced.

We used a collimating lens (F = 12 mm, numerical aperture (NA): NA = 0.50, Doric Lenses) to focus the laser beam on a multimode optical fiber that can transmit the two wavelengths to and from the implant on the mouse head. Our goal was to find a tradeoff between the diameter of the fiber (the larger diameter the larger the brain damage), and the amount of light collected, which should be enough for reliable detection. We did not know how much light we were going to be able to collect at the fiber tip implanted in the brain, but the expected levels of fluorescence were very low, so we wanted to use a fiber with large numerical aperture. However, these fibers are generally made with a polymer cladding, which causes a strong autofluorescence background. Thus we chose to use fibers with silica core and fused silica cladding, although the maximum NA obtained in this configuration is 0.22.

We used a single optical fiber of 300 µm (MFP_300/330/900-0.22_2.5m-FC_CM3 from Doric Lenses) and worked on the development of a good connection system that would allow us to have small fiber cannulae permanently implanted in the heads of the mice. The goal of having chronic fiber implants is to reduce the inflammation and damage that can be triggered by repeated insertion of an optical fiber through an implanted guide cannula, and which can alter the optical signal measured[187].

With such individual implants we could always use the same patchcord fiber attached to the FC/PC connector of the setup and simply connect its free end to the implants. We started out by developing magnetic connectors for the interface between the patchcord fiber and the implantable fiber cannulae (**Figure 2.5**) and collaborated with Doric Lenses to fabricate them (**Figure 2.6 a**). In the end these evolved to mini-SMA connectors (**Figure 2.6 b**) to allow better fitting of the two fibers and later to M3 connectors (**Figure 2.6 c**). The transmission of light in these connectors is above 80 % and these are the connectors that we used in all behavioral experiments described in the following chapters (MFC_300/330-0.22_5mm_RM3_FLT polymide removed).

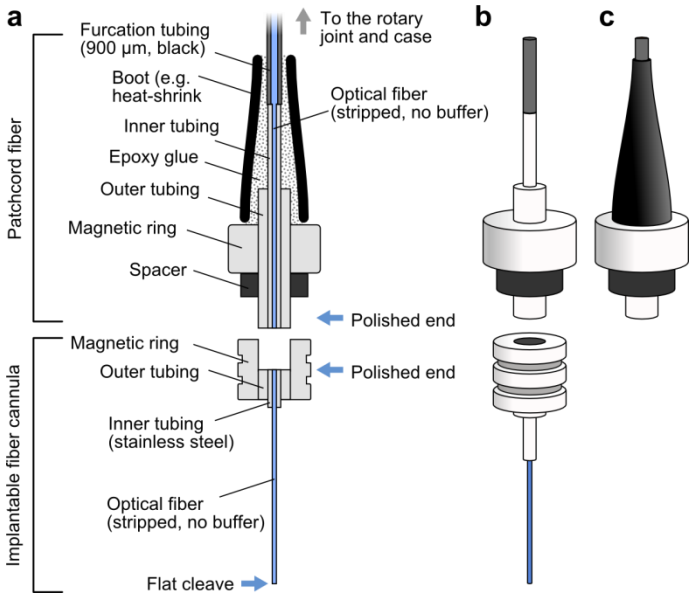

Figure 2.5. Development of magnetic connectors for optical fibers.
a. Cross-section of the magnetic connector to be used between the patchcord fiber and the fiber cannula.
b. Outside view of the connector.
c. Outside view with boot.

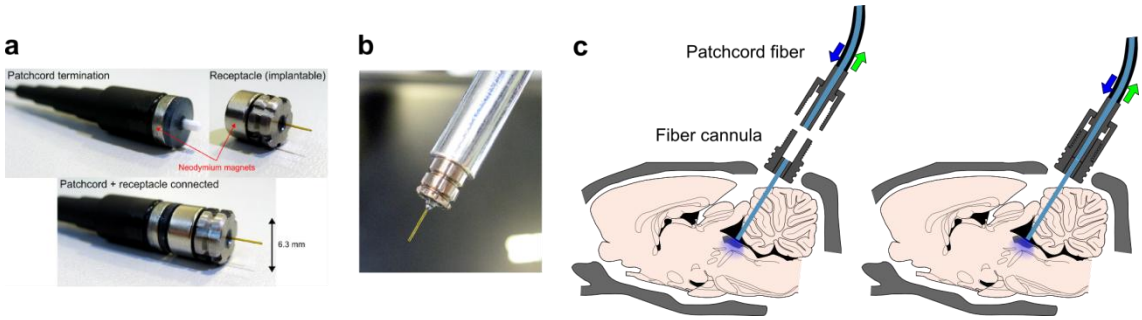

Figure 2.6. Connectors designed together with Doric Lenses.

a. Magnetic connector used in the patchcord fiber and receptacle (implant).
b. Fiber cannula with mini-SMA connector (attached to rod for stereotatix implantation).
c. Schematics of connection between the fiber cannula implanted in the DRN and the patchord fiber using a M3 connector.

Finally, the fluorescent light emitted by the calcium indicator was focused by a plano-convex spherical lens (F = 40 mm, Thorlabs[229]) and collected by a photomultiplier tube (PMT) module (H7422-02, and preamplifier C7319, Hamamatsu Photonics[230]) with high sensitivity between 500 and 550 nm, controllable gain, low dark current and linear response to increases in light power.

2.2.3 Conceptual validation

To validate our photometry technique we first tested the optical setup using non-activity dependent fluorophores and only then in mice. In this case we started by validating this approach in anesthetized mice using electrical microstimulation of the DRN to artificially activate the neurons and then we tested it in behaving mice transduced with GCaMP in the striatonigral pathway, which we predicted would generate strong signals during natural behaviors.

To prove that our optical setup could indeed report signals that varied according to the amount of fluorescence emitted by fluorophores, we measured the fluorescence emitted by solutions with increasing concentrations of fluorescein, a synthetic organic compound that emits green fluorescence (

Figure 2.7 a). We verified that, as expected, the PMT output increased with increasing fluorescein concentration (

Figure 2.7 b-c) and that the limit of detection of the PMT was, in these conditions, close to 10 nM (

Figure 2.7 d).

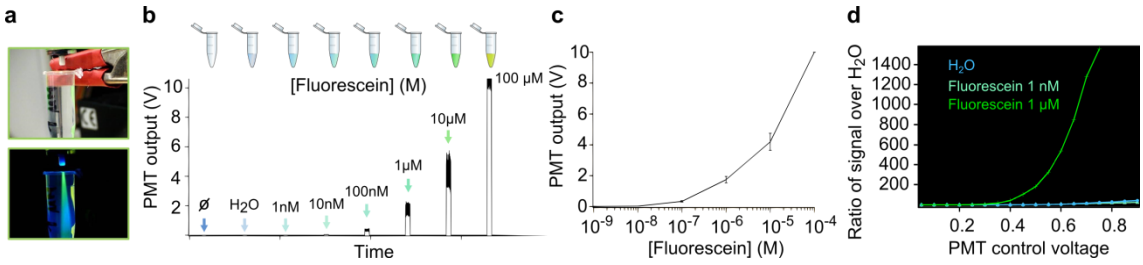

Figure 2.7. PMT output increases with increasing fluorescein concentrations.

a. Picture of eppendorf containing fluorescein (1 µM).
b. PMT output in response to different solutions put at the tip of the optical fiber.
c. PMT output to increasing fluorescein concentrations.
d. Response of PMT to two different fluorescein concentrations (1 µM and 1 nM) as a function of the control voltage used.

We then performed surgeries to inject a solution containing an rAAV virus transporting the DNA sequence of ChR2-YFP (1µl, from UPenn) into the DRN of SERT-Cre mice and implanted each with a fiber cannula targeting this structure. We measured the baseline fluorescence in the DRN of these mice across days and verified that it increased, as expected from such viral strategy: as expression levels of YFP increased over days so did the photometry signal (**Figure** 2.8).

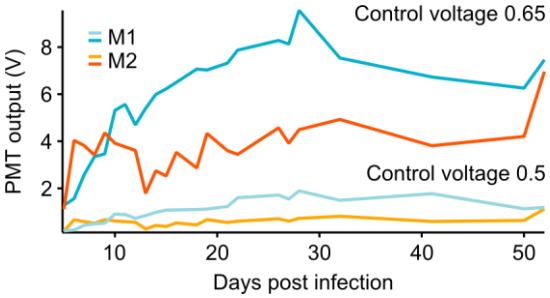

Figure 2.8. Fluorescence acquisition in vivo.
PMT signal in two mice (M1 and M2) infected with AAV2/1-ChR2-YFP in the dorsal raphe nucleus across days using two different control voltages for the PMT.

2.2.4 Validation of fiber photometry and GCaMP as appropriate tools to record activity of DRN 5-HT neurons

Given the reported heterogeneity of responses of DRN neurons *in vivo*, instead of starting by doing acquisitions in behaving animals, we decided to do electrical microstimulation in the DRN of mice under urethane anesthesia (1.5 g/kg) in a stereotaxic frame. From previous studies[231] we knew that we should be able to artificially activate 5-HT (and other) neurons in this region and with our fiber photometry we could record specifically the activity of 5-HT neurons in SERT-Cre mice.

Since there are no described recordings of calcium activity in 5-HT neurons of mice *in vivo*, these experiments were also useful to confirm that the use of photometry together with the genetically encoded calcium indicator GCaMP6s were adequate to monitor the activity of these neurons.

To accomplish this, the previously described photometry setup was adapted to be used in an anesthetized preparation. Instead of using patchcord fibers with adaptors for cannulae to be implanted in mice, we used a cleaved and polished fiber with the same optical specifications and glued it to a concentric bipolar electrode (CBAPB25, FHC[232]), so that its tip was 200 µm above the microelectrode tip (optrode) (**Figure 2.9 a**). The laser beam was passed through a 10:90 beamsplitter cube (BS025, Thorlabs) so that 10% of it was collected by a photodiode (SM1PD1A, Thorlabs) for precise laser pulse monitoring.

We performed acute experiments in mice that had been transduced with 1 µl of AAV2/1 - Syn.Flex.GCaMP6s.WPRE.SV40 (preliminary experiments were done using GCaMP3 - data not shown) for at least two weeks. The optrode was lowered in the brain using the previously

mentioned angled approach from the cerebellum using an IVM micromanipulator (Scientifica[233]). The electrophysiological signal from the optrode was amplified (x1000) and filtered (0.1–10 kHz) by an 1800 AC amplifier (AM Systems[234]), and digitized (by a Micro1401-3 interface and acquired using Spike2,Cambridge Electronic Design[235]).

During the acute experiment we run several electrical stimulation protocols which created a small damaged area in the DRN (**Figure 2.9 b**).

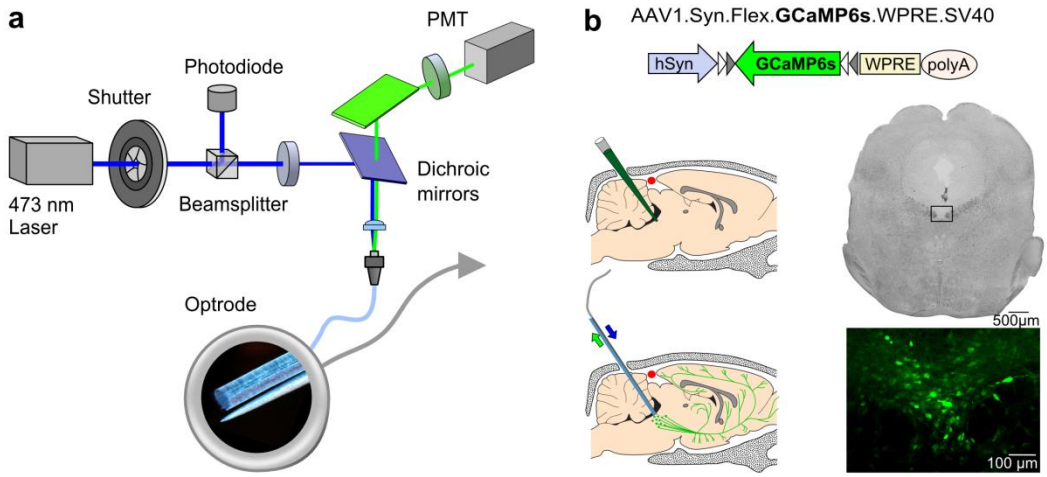

Figure 2.9. Electrical microstimulation in the DRN of anesthetized mice was used to validate the photometry approach in DRN 5-HT neurons.

a. Photometry setup adapted for acquisition in anesthetized mice preparation showing the microelectrode used for electrical stimulation glued to the optical fiber (optrode).

b. Left: schematics of angled approach for infection and for anesthetized acute recordings in the DRN of SERT-Cre mice infected with Cre-dependent GCaMP6s virus (top). Right: picture of a brain slice showing damage in the DRN caused by electrical micro-stimulation (top) and GCaMP6s expressing cells in the boxed area (bottom). Scale bars: 500µm and 100µm, respectively.

To excite GCaMP6s, we always used 100 µW measured at the tip of the optrode. The electrical stimulation protocols were run at several points in the brain, from the penetration area above the cerebellum until the optrode tip had passed through the DRN. We also measured, at each acquisition point, the baseline fluorescence. As expected, this baseline fluorescence increased at penetration depths that correspond to the location of the DRN and decreased after it, showing that expression of GCaMP6s was successful (**Figure 2.10 a**). In addition, we quantified the maximum change in fluorescence in response to one of the electrical stimulation protocols (10 pulses at 100 Hz) across these depths and found the maximum responses in the DRN location (**Figure 2.10 a,b**).

We also found that within the DRN, for the same electrical stimulation duration, protocols with higher frequencies and higher number of pulses elicited stronger increases in fluorescence (**Figure 2.10 c,d**). After the initial calcium transient elicited by electrical stimulation, we sometimes observed a delayed but sustained response that decreased slowly over time (**Figure 2.10 b,c**). We didn't investigate the reason for this delayed response, but it is probably caused by recurrent activity, given that DRN neurons are highly interconnected[73,82,83].

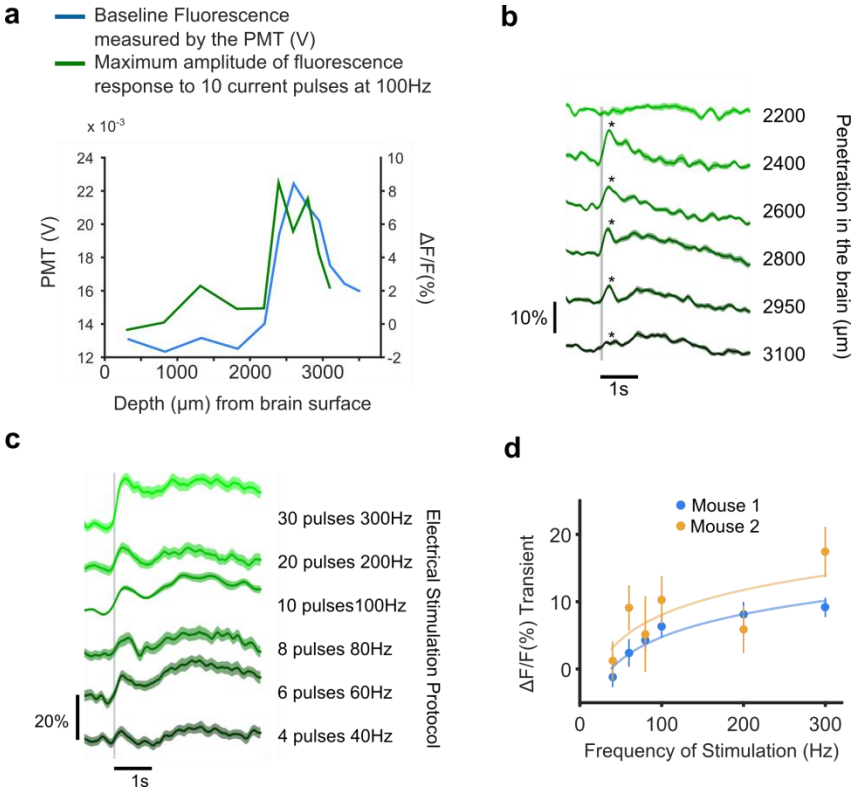

Figure 2.10. GCaMP6s reports calcium transients in the DRN of SERT-Cre mice triggered by electrical microstimulation.

a. Fluorescence measurement in the PMT (green, left axis) and maximum amplitude change in response to electrical stimulation (10 1ms and 300 μA pulses at 100Hz) (blue, right axis) profiles in one mouse plotted against the optrode position (depth from the brain surface).

b. Average fluorescence traces for mouse represented in *a* caused by electrical microstimulation at different depths. Until 2200 μm deep there is no significant change in fluorescence caused by electrical stimulation (paired *t*-test comparing mean of 1s before and after electrical stimulation onset, $p < 0.001$).

c. Average fluorescence traces for one mouse caused by different protocols of electrical stimulation in the DRN: different number of pulses at different frequencies while keeping the duration of stimulation constant (right).

d. Mean transient amplitude (mean of 2s after stimulation onset subtracted by mean of 1s before it) across the different stimulation protocols in *c* for 2 mice (represented in blue and orange) as well as logarithmic fitting for each mouse.

2.2.5 Validation in freely behaving mice: activity of the striatonigral pathway during spontaneous movement

As discussed in the introduction, there is no accepted model of 5-HT function or of events that reliably trigger 5-HT neurons' activity. Therefore, before testing our fiber photometry approach in 5-HT neurons of behaving mice, we tested it in a different neural population whose activity patterns are better known. We focused on spiny projection neurons (SPN) in the dorsal striatum which are known to be involved in voluntary actions[236,237]. D1-expressing SPNs form the direct pathway of outputs from the striatum to the SNr, one of the two major output nuclei of the basal ganglia, and their activity is thought to facilitate movement[238–240]. We knew that GCaMP fluorescence could be used to measure calcium transients elicited by bursting activity of these neurons[209] and therefore we thought it would be a good system to test our approach.

To monitor the activity of D1 (striatonigral) SPNs during spontaneous movement we injected a viral solution (1 μl) containing AAV2/1 - Syn.Flex.GCaMP6s.WPRE.SV40 (preliminary

experiments were done using GCaMP3 - data not shown) or AAV2/1 - Syn.Flex.YFP.WPRE.SV40 for control experiments into the dorsal striatum of D1-Cre mice (EY217)[209,220] and implanted a fiber cannula targeting the infection area (**Figure 2.11 a**). After some weeks, mice were individually placed in new cages for 10 minute periods and their behavior was recorded using a video camera (PS3, Playstation[241]). We used Bonsai[242], an open-source platform for managing and processing data streams, to track mice online and a custom software was programmed in MATLAB[243] (MathWorks) for control and acquisition of fluorescence signals through a data acquisition board (at 1 kHz, NI PCI-6229, National Instruments[244]).

Online visual inspection of the fluorescence signal immediately showed increased activity of D1 neurons during contraversive turns. We analysed data offline and used the whole-body tracking data to calculate instantaneous angular velocity and align it with the fluorescence signals (**Figure 2.11 b**). Changes in fluorescence were calculated for each session as $\Delta F/F_0 = (F-F_0)/F_0$, in which F_0 is the fluorescence value that corresponds to the 10th percentile of all the values acquired in each session after correcting them for baseline drift (using a third-order polynomial). Positive angular velocities correspond to rotations towards the right (represented in blue in **Figure 2.11 b**) and negative values correspond to rotations towards the left (represented in black). While higher fluorescence levels were observed when angular velocities were increased towards the contralateral side of the measured signal in GCaMP6s-transduced mice, this was not observed in YFP-transduced mice (**Figure 2.11 c-d**), even if movement artifacts were observed during the acquisition (**Figure 2.11 b**).

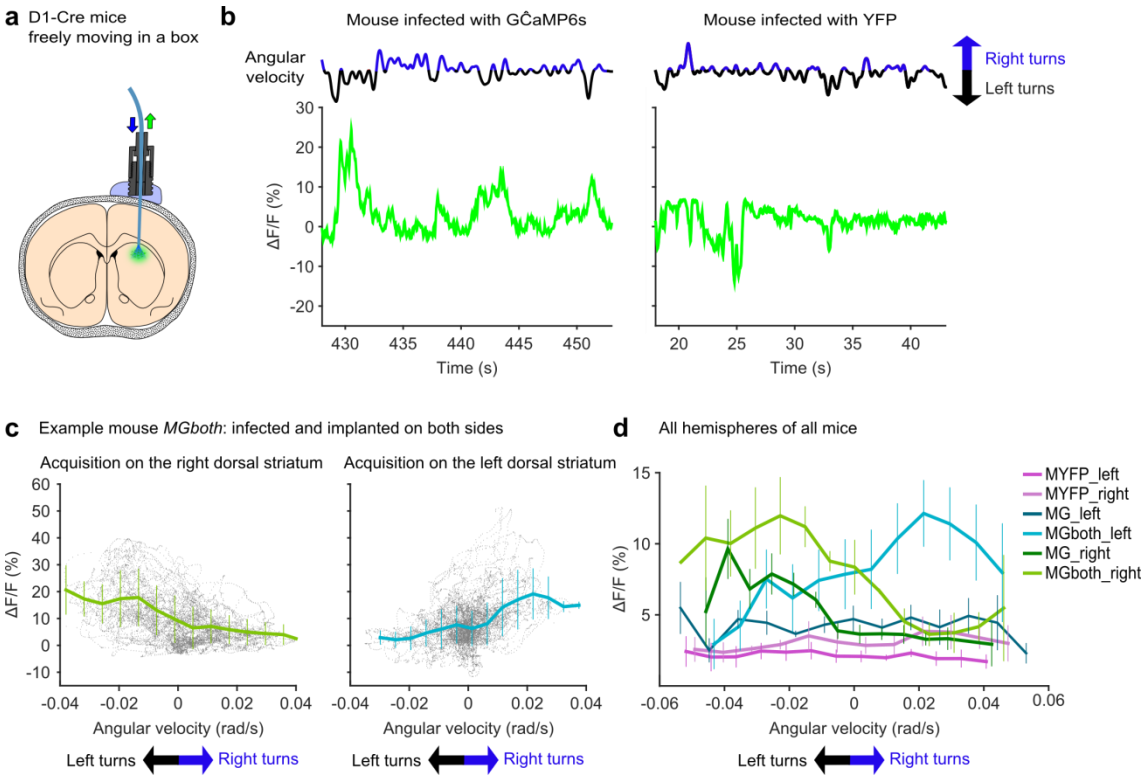

Figure 2.11. Striatonigral SPNs show increased activity during spontaneous contralateral turns.
a. Schematics of infection and fiber optic implantation in the dorsal striatum.

b. Angular velocity (top, in blue and black) and fluorescence signals (bottom, in green) from D1 SPNs expressing either GCaMP6s (left) or YFP (right) during a sample period.
c. Fluorescence values as a function of angular velocity in an example mouse implanted on both hemispheres separated by side (left: right dorsal striatum, right: left dorsal striatum), showing all fluorescence values acquired during 4 to 6 behavioral sessions for each mouse.
d. Mean fluorescence as a function of angular velocity for each mouse used in this experiment. Each line/color represents an hemisphere of a mouse (right or left as signalled in the figure legend) YFP transduced control mice are shown in pink colors.

The observed movement artifacts are a serious concern for this technique in general, because we need to distinguish artifact signals from real neural activity signals. However, in this particular application, we focused on the turns made by the animals and these were not the events that were generating the movement artifacts. To define turns in our data, we detected the points at which the derivative of the angle was null and classified them as right or left turns, depending on whether this derivative was increasing or decreasing, respectively. Only those turns occurring after 5 s in which the standard deviation of the angle was smaller than 40º and that after 5 s resulted in a change larger than 40º were included. We pooled the right and left hemispheres' data and organized it as ispsilateral or contralateral to the acquisition side; then, we aligned the fluorescence signals to these events and verified that the increases in activity were only observed in GCaMP6s-transduced mice but not in YFP mice. Similarly, the cross-correlation between the fluorescence signal and the angular velocity towards the contralateral side was highly positive in GCaMP6s mice and absent in YFP mice (**Figure 2.12**).

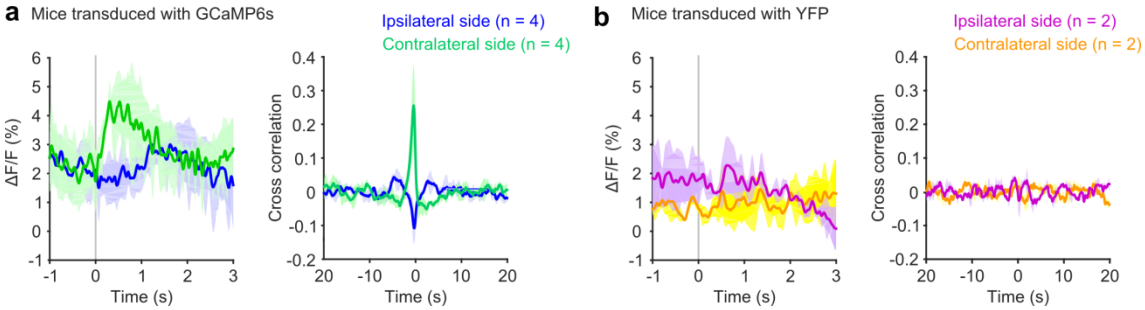

Figure 2.12. Fluorescence transients elicited by contraversive turns are observed only in GCaMP6s-transduced mice.
a. Left: mean change in fluorescence ($\Delta F/F_0$) of all trials of GCaMP6s-transduced D1-Cre mice during contra (green) and ipsilateral (blue) turns aligned to the turns. Right: cross-correlation between the fluorescence data and the angular velocity towards ipsi and contralateral sides.
b. Same as *a.* but for YFP-transduced mice (ipsi and contralateral sides in pink and yellow respectively).

We got three important outputs from this experiment in freely moving D1-Cre mice:

1) These results were extended by performing the same experiments and analysis in striatopallidal SPNs in a collaboration with Dr. Fatuel Tecuapetla and Dr. Rui Costa resulting in a scientific paper[245] published in *Nature Communications* and presented in Chapter 3 of this thesis.
2) We verified that we could also use a CCD camera instead of a PMT to acquire the fluorescence signals in this experiment. We did it by acquiring and integrating all the acquisitions (video and fluorescence) in *Bonsai*, as a possible application to use this newly developed platform published in *Frontiers in Neuroinformatics*[242].

3) We confirmed the existence of a problem we had been worried with: the susceptibility of this approach to movement artifacts. Although these were not a problem for this study in particular, because they were not correlated with spontaneous turns, they could be a problem in other studies. Therefore the need to overcome this limitation was imperious.

2.2.6 The need to correct for movement artifacts in the DRN of behaving mice

As a result of the movement artifacts' detection in YFP-transduced control mice in the striatonigral experiments we wanted to know what type of movements were causing these artifacts. We anesthetized the mice used in the previous experiments to manually move them in different ways and verified that the movement artifacts were caused by neck movements, such as lateral turns of the head in relation to the body, but especially by flexion and extension of the neck (movements in the sagittal plane). We also verified that these artifacts were much bigger in mice infected with YFP than with GCaMP6s, probably due to the higher baseline fluorescence of the first in comparison with the latter. Most movement artifacts observed in behaving mice (both in the striatum and later in the DRN) showed bigger negative changes than positive (**Figure 2.11 b**). We imagined that these neck movements cause the brain to move slightly in relation to the skull, where the fiber is firmly attached, and thus the center of infection might move away from the fiber tip causing the observed oscillations in fluorescence during cycles of flexion and extension.

If this was the case, these artifacts could represent a bigger problem for the DRN than for the striatum, because the DRN is located in the brainstem, closer to neck, and in contact with the aqueduct, which might facilitate small dislocations due to neck movement. In fact, when we compared the effects of neck movements manually caused in mice infected with YFP in the striatum or in the DRN we verified that while the first caused changes in fluorescence from -6 % to +4 % the later caused changes from -30 % to 20 %. Although, as for the striatum, these changes were expected to be smaller in GCaMP6s-infected DRN 5-HT cells than in YFP controls, we decided to develop a solution to overcome this problem. This was done by deciding to express a second, neural activity-independent, fluorophore in the same cells and use it to detect movement artifacts. This strategy would allow us to subtract detected movement artifacts from the GCaMP signal, leaving us with a corrected fluorescence that represents only neural activity.

2.2.7 Development of a photometry setup adequate for movement artifact correction

Since GCaMP6s is derived from eGFP[204,205], we decided to use a red fluorophore to be co-expressed in DRN 5-HT neurons. At first we worked on a double-floxed construct containing the sequence of GCaMP6s followed by mKate2, a far red fluorescent protein[246], with the T2A peptide sequence in between. 2A peptides are small viral elements with less than 20

aminoacids that have been reported as a “self-cleaving” and suitable for equimolar expression of two proteins[247,248]. We therefore produced rAAVs containing the sequences of GCaMP6s-T2A-mKate2 and of corresponding GFP-T2A-mKate2 for control experiments flanked by loxP and lox2272 sites. This would provide us with the closest levels of expression of GCaMP6s and mKate2 in each transduced 5-HT cell. Unfortunately, when injections were performed to evaluate the levels of expression of these constructs in 5-HT cells of SERT-Cre mice, we obtained very little success with the GCaMP6s-T2A-mKate2 expression (the best example is shown in **Figure 2.13 a** and is one out of 9 mice). In fact, when we performed electrical stimulation in the DRN of mice transduced with this construct we didn’t see any fluorescence signals in response to this stimulation, nor when we did the same experiment in the dorsal striatum of a D1-Cre mouse. Therefore, even though the GFP-T2A-mKate2 construct worked relatively well (**Figure 2.13 b**), we didn’t pursue the use of these constructs. The difference between the two could be related to the size of the final vectors: the one carrying GCaMP6s is 630 base pairs longer than the one carrying GFP and rAAVs are known to have limited loading capacity (up to 5 kb).

Still, in all mice transduced with GFP-T2A-mKate2 the expression of the red fluorophore was always lower than that of the green one. In the future, the infection success of other recombinant viruses, such as lentiviruses which have more capacity to carry foreign DNA, might be tested, as well as different types of 2A peptides to evaluate which are more appropriate to use in 5-HT neurons.

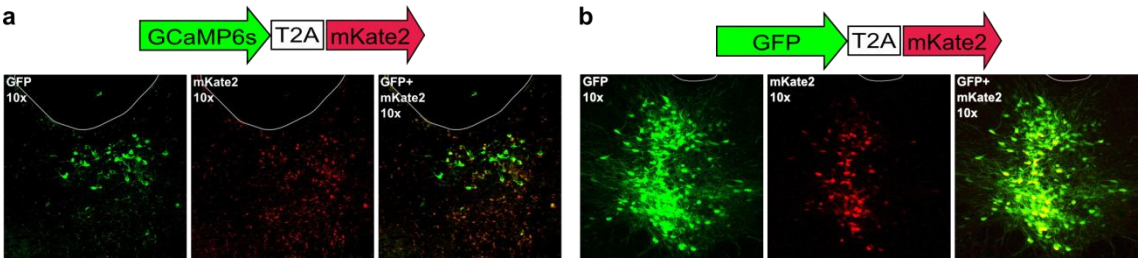

Figure 2.13. DRN 5-HT cells expressing two bicistronic constructs whose protein sequences are separated by the T2A peptide.

- **a.** GCaMP6s and mKate2 in an example mouse.
- **b.** GFP and mKate2 inand example mouse.

We then decided to use a simpler strategy to co-express a green and a red fluorophore in 5-HT neurons. We simply mixed two independent viruses (both Cre-dependent: AAV2/1 - Syn.Flex.GCaMP6s.WPRE.SV40 with AAV2/1.CAG.FLEX.tdTomato.WPRE.bGH) in equal proportions prior to injection and delivered this mixture (1.5 µl) to the DRN of SERT-Cre mice. To excite tdTomato and collect its fluorescence, we added another optical stage to our photometry setup: it includes an entrance for a yellow light source (561 nm diode-pumped solid-state laser, Chrystalaser) to excite tdTomato, the corresponding excitation filter (LL02-561-25 Semrock), two additional dichroic mirrors – one to collect the green fluorescence of GCaMP6s (FF552-Di02-25x36, Semrock) and one to separate the excitation and emission of tdTomato (Di01-R561-25x36, Semrock) -, one emission filter (LP02-568RS-25, Semrock), one convergent lens (F = 50 mm, Thorlabs) and one PMT (H7422-02, Hamamatsu Photonics) to collect the red

fluorescence of tdTomato (**Figure 2.14 a**). A new case was designed to accommodate all these components, which were chosen so that there would be the least contamination possible between channels (**Figure 2.14 c-f**, in acute experiments with electrical stimulation of the DRN no GCaMP6s fluorescence was observed in the red channel/PMT). All the components of the setup are removable and interchangeable in case a new configuration is needed in the future.

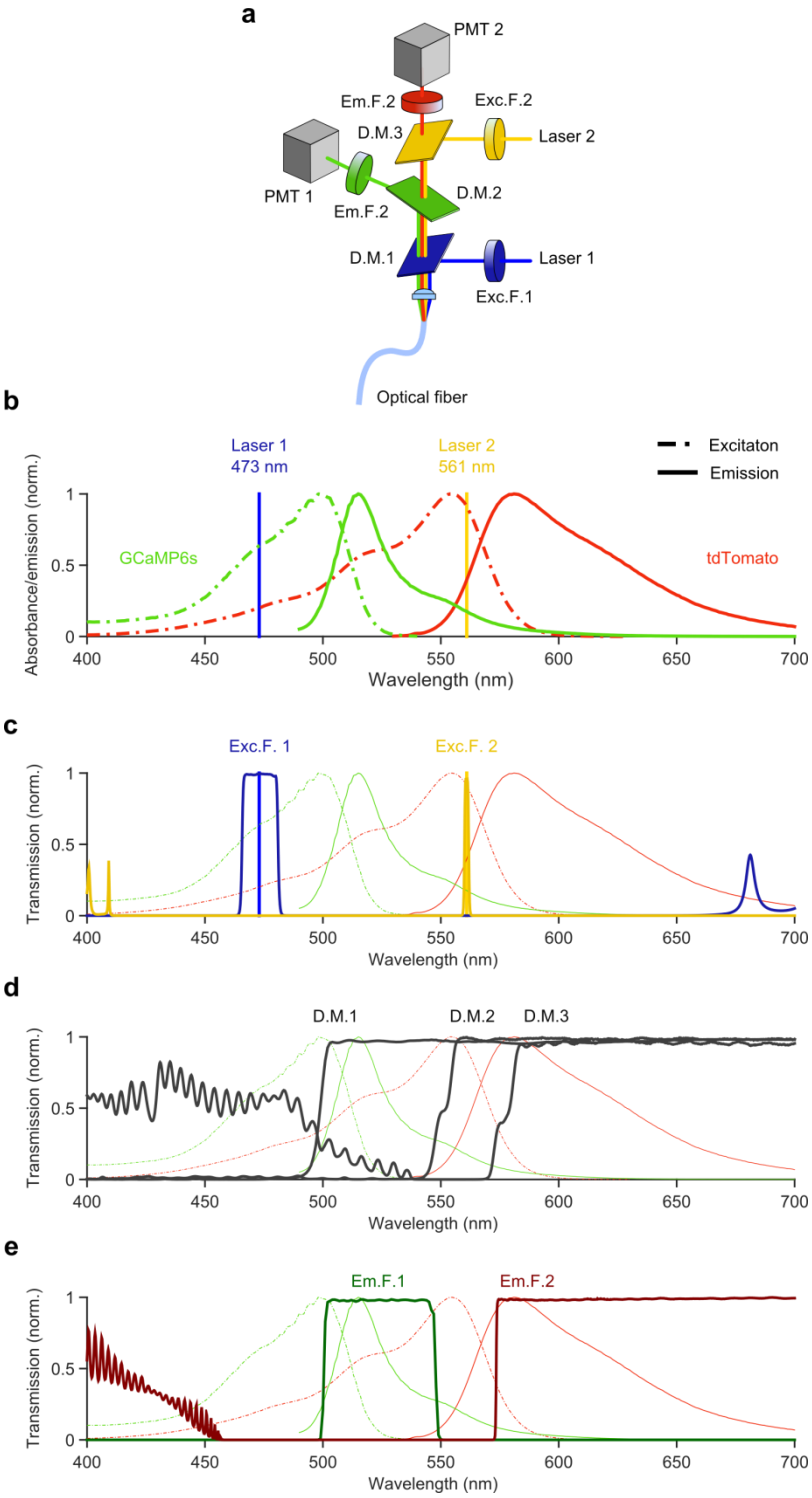

Figure 2.14. Photometry setup prepared for movement artifact correction

a. Schematics of photometry setup with two light sources and corresponding excitation filters, 3 dichroic mirrors, two photodetectors and corresponding emission filters.

b. Excitation (dash-dot line) and emission (solid line) spectra of GCaMP6s (green) and tdTomato (red) and representation of the wavelengths emitted by the lasers.
c. Normalized transmission of the excitation filters used for GCaMP6s (Exc.F.1) and tdTomato (Exc.F.2).
d. Normalized transmission of the dichroic mirrors used (D.M.1 reflects wavelengths below 495nm, D.M.2 reflects wavelengths below 552 nm and D.M.3 below 561 nm).
e. Normalized transmission of the emission filters used for GCaMP6s (Em.F.1) and tdTomato (Em.F.2).

Using this setup we performed experiments in behaving mice engaged in a classical conditioning task while recording fluorescence signals from 5-HT neurons. These results are presented in Chapter 4. The algorithm used to eliminate movement artifact signals from the green channel using information from the red channel will be explained in that Chapter, because it was developed in the context of the task in which the mice were engaged.

2.3 Discussion

Correlating neural activity with behavior is a fundamental strategy for a better understanding of brain function, just like manipulating such activity. In studying neural processing, recordings of single neurons are essential to understand how they integrate information from different inputs. However, recording of neural population activity is also indispensable in our understanding of neural information processing[249–251], especially from genetically defined neurons. We think this is particularly important in approaching neuromodulatory systems, and mainly the 5-HT system, since it has such wide and diverse projection targets and for which single cell recordings have not yet unraveled a coherent function. This system also has very distinct afferent inputs and therefore it is in a privileged position to integrate relevant information arriving from different inputs and communicate it to several brain areas.

The two main approaches that are available today to record activity of genetically defined 5-HT neurons in behaving animals are either single cell recordings of photoidentified neurons or imaging using genetically encoded indicators, such as GECIs. The DRN is located about 3 mm below bregma, rendering it impossible the use conventional microscopy to image 5-HT cells expressing GCaMP in behaving animals. Nowadays there are a few commercially available systems of miniaturized microscopes[228,252,253] or micro endoscopes[254] that can be used to image deep brain structures. However, they still have some important limitations, such as the difficulty in correcting motion artifacts especially with low frame rate acquisitions[255], the large diameter of the gradient index (GRIN) lenses inserted in the brain (~1 mm)[252,256,257], which cause extensive tissue damage, and the limited field of view in very deep structures for which GRIN lenses with high NAs are used and which are prone to optical aberrations[258]. Still, important improvements in these techniques are taking place[259] and will likely have critical impact in Neuroscience research.

As any other technique, the fiber photometry setup here developed has both advantages and limitations. As for the first, the optical fibers have much smaller diameter than conventionally used GRIN lenses, and they are light and flexible, making them appropriate to use in behaving mice. The technique is used with GECIs, which confer very good dynamic range to detect changes in fluorescence. These single-fluorophore GECIs are more susceptible to motion

artifacts than ratiometric calcium sensors such as cameleons[207], but they currently exhibit larger changes in fluorescence, faster kinetics[203], and single action potential detection[205]. As a consequence, we chose to use GCaMP6s and overcame the movement artifact problem using a second fluorophore that is not calcium sensitive (tdTomato, data will be presented in Chapter 4).

The fiber photometry technique with GECIs has two big advantages in relation to recording of electrical local field potentials (LFP): the first one is the fact that the signal is generated by a genetically defined population of neurons, a characteristic that is particularly important in areas with a diversity of neurochemical identities such as the DRN, and the second one is that LFPs might integrate neuronal activity through volume conductances of a millimeter or more[260,261].

In addition, our setup is easily adaptable for optogenetic stimulation or inhibition of cell populations, which can be done in conjunction with photometry simply by using an accustom-optic modulator controlling the laser beams.

Finally, a fiber photometry setup is a much cheaper approach than any available miniaturized microscopes for imaging deep tissue, especially if using photodiodes[166,184] instead of PMTs.

As for the limitations of this technique, the first obvious one is the lack of spatial resolution: an image is not formed and therefore single cells cannot be resolved, because the signal reflects the average activity of a group of cells. A consequence of this characteristic is that it might be difficult to detect signals in asynchronous populations showing heterogeneous responses to events in a particular environment[179]. There is both a risk of not detecting any particular signal or a potential advantage over unit recordings when these cannot help us find a general role for a population of neurons due, for instance, to small sample size.

The second main disadvantage is the propensity to be affected by movement artifacts, but this can be overcome using a second, activity independent fluorophore. Besides this function, a second calcium indicator, such as the red emitting RCaMP[262], could be used simultaneously with GCaMP to monitor the activity of two neural populations in situations where movement artifacts are not considerable.

As a concluding remark, we think the use of fiber photometry can contribute significantly for the advancement of neuroscience research: it allows the collection of average activity from populations of neurons (1), using GECIs these populations can be genetically defined (2), these acquisitions can be done in behaving animals (3) and are easily repeated across several days without brain damage by using implantable fiber cannulae (4).

This technique has helped us understand how specific cell populations, and 5-HT neurons in particular, are involved in behavior, learning, and decision making (Chapter 4) by recording the dynamics of spontaneous and evoked population activity over long time periods (weeks).

3. Balanced activity in basal ganglia projection pathways is critical for contraversive movements

In this chapter I show that both striatonigral and striatopallidal neurons are activated during spontaneous contraversive turns. Using optogenetics experiments we show that the balanced activity between these two pathways of the basal ganglia is integral for displaying behaviors that are in accordance with the spontaneous activity of the two pathways. Otherwise, behavior might be artificially biased towards a non-naturalistic pattern. Therefore, balanced activity of these two projection pathways is needed for spontaneous contraversive turns.

Results published:
Tecuapetla, F., Matias, S., Dugué, G. P., Mainen, Z. F. & Costa, R. M. Balanced activity in basal ganglia projection pathways is critical for contraversive movements. *Nat. Commun.* **5,** 4315 (2014). DOI:10.1038/ncomms5315

Author contributions
F.T. and R.M.C. designed the experiments and wrote the manuscript. F.T. performed and analysed the optogenetics experiments. S.M., G.P.D. and Z.F.M. developed the fiber photometry system. S.M. performed and analysed the GCaMP experiments.

3.1 Introduction

The control of contraversive movement by each brain hemisphere has been extensively studied in neurological patients[263,264]. Single hemisphere lesions of the dorsal striatum abolish contraversive movements and bias towards ipsiversive movements[265–267], while unilateral stimulation of the dorsal striatum induces contraversive movements[268,269]. The striatum projects to downstream nuclei through two main circuits, the so-called direct and indirect pathways, which arise from striatonigral and striatopallidal medium spiny projection neurons[238]. Several models have been proposed postulating how these different basal ganglia pathways could control movement. Some models postulate that these pathways have opposing effects on the output of the basal ganglia[236,270,271] and movement[272–274], while others say that co-activation of both pathways is necessary for movement[209,275–277]. Recent studies revealed concurrent unilateral activation of both striatonigral and striatopallidal neurons when animals perform contraversive movements in an operant task[209]. However, other studies have shown that lesion[274,277,278] or stimulation of each cell type can have opposite effects on contraversive movements[240,273]. Here we used fiber photometry and the genetically encoded calcium indicator GCaMP6s[205] to measure the activity of striatonigral and striatopallidal neurons during spontaneous contraversive and ipsiversive movements. Furthermore, we used optogenetics to selectively inhibit (or activate) either or both striatal projection pathways unilaterally, and assess their role in contraversive and ipsiversive movements. We observed that both striatonigral and striatopallidal neurons showed an increase in activity during spontaneous contraversive movements, and that inhibiting either or both striatal pathways unilaterally impaired contraversive movements and biased the animals to perform ipsilateral turns. Furthermore, we observed that simultaneous activation of both striatal projection pathways produced contraversive movements. Finally, we also show that activation or inhibition manipulations that caused a strong imbalance of activity between the striatal projection pathways can result in opposing movements being driven by each pathway.

3.2 Results

3.2.1 Striatal activity during spontaneous contraversive movements

To monitor the activity of the striatonigral and striatopallidal neurons during spontaneous contraversive movements we expressed GCaMP6s specifically in each cell type. We did this by injecting viruses that express GCaMP6s in a Cre-dependent manner (Flex, AAV2/1) into the dorsal striatum of mice expressing Cre in either striatonigral (D1-Cre mice — EY217) or striatopallidal neurons (A2A-Cre mice — KG139)[209,220]. To monitor fluorescence of GCaMP6s during activity of a specific cell population we implanted fiber cannula into the dorsal part of the striatum, and coupled these fibers with the photometry setup described in Chapter 2 (**Figure 3.1**). After 3 to 4 weeks, we placed the animals into a novel arena (a novel cage similar to the home cage) and monitored their behavior using video while acquiring fluorescence signals from

the dorsal striatum. As described in Chapter 2, we used *Bonsai*[242] to perform online tracking of the body of the animals, and offline analysis to identify spontaneous ipsi or contraversive movements (**Figure 3.1c,f**). We observed that both striatonigral and striatopallidal neurons showed an increase in activity during spontaneous contraversive movements (481 trials for contralateral turns from 4 D1-Cre hemispheres infected with GCaMP6s, $P < 0.05$; 2005 trials for contralateral turns of 4 A2Acre hemispheres infected with GCaMP6s, $P < 0.05$ from 4 A2Acre hemispheres infected with GCaMP6s, $P < 0.05$; Mann– Whitney test; **Figure 3.1d,g**). Furthermore, to better assess the temporal resolution of the increase in fluorescence, we performed a cross-correlation between the ipsi or contraversive angular velocity and the GCaMP6s signal. We observed that the significant increase in activity of both striatal pathways preceded the changes in angular velocity. Moreover, we observed a decrease in GCaMP6s fluorescence during ipsiversive movements ($P < 0.05$ for ipsi or contralateral turns; **Figure 3.1h**: n = 4 hemispheres; Mann–Whitney test). The corresponding controls expressing only eYFP did not show any significant changes in fluorescence during either contra or ipsiversive movements (inserts in **Figure 3.1d–h**: 196 trials for ipsilateral and 283 trials for contralateral turns from 2 D1-Cre hemispheres infected with eYFP; 1,514 trials for ipsilateral and 1,421 trials for contralateral turns from 2 A2A-Cre hemispheres infected with eYFP; Mann– Whitney test).

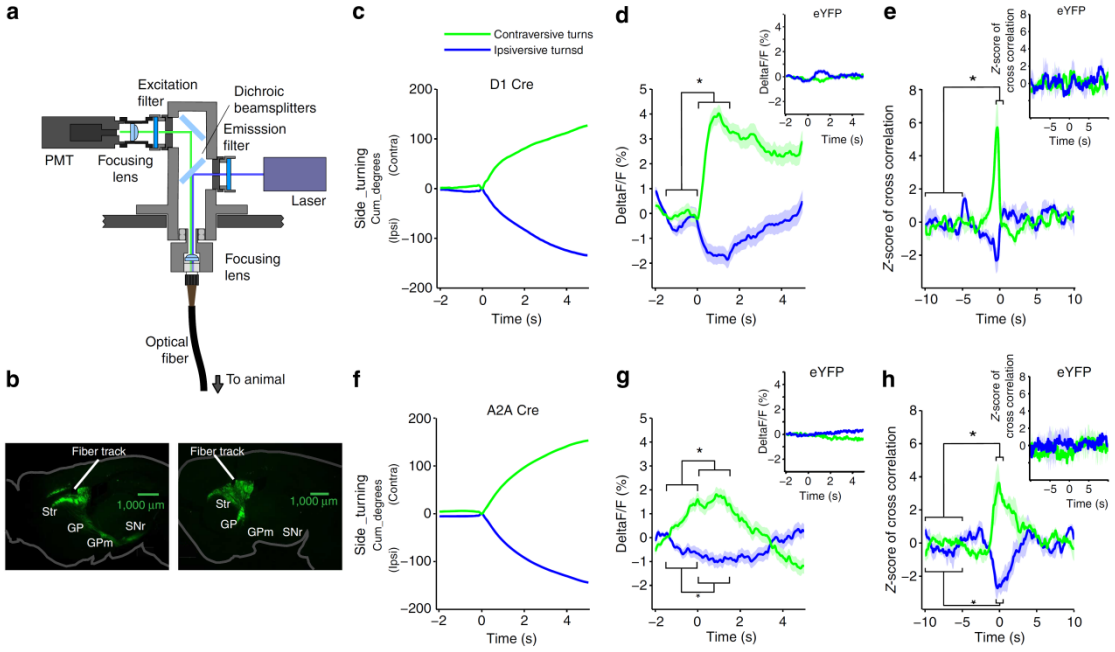

Figure 3.1. Increase activation of the basal ganglia pathways during spontaneous contraversive movements.

- **a.** Schematics of fiber optic setup for acquisition of bulk fluorescence from specific cell populations.
- **b.** GCaMP6s fluorescence in the striatonigral (left) and striatopallidal (right) pathways in brain slices of mice used in the experiments.
- **c,f.** Mean (of all trials of GCaMP6s-infected mice) temporal dynamics of the cumulative degrees of turning over 7 s in D1-Cre and A2A-Cre lines, aligned to two seconds before the turn, blue: ipsilateral side; green: contralateral side. Data is presented as mean ± s.e.
- **d,g.** Mean change in fluorescence ($\Delta F/F_0$) of all trials of GCaMP6s infected mice during contra and ipsilateral turns for the two pathways aligned to 2 s before the turn. Insets: mean $\Delta F/F_0$ for eYFP controls. * $p < 0.05$, for a Mann–Whitney test; n = 4 D1-Cre and n = 4 A2A Cre hemispheres infected with GCaMP6s.

e,h. Mean (of all hemispheres) Z-score of the cross-correlation between the fluorescence data and the angular velocity, ipsiversive and contraversive, for the D1-Cre and A2A-Cre mouse lines infected with GCaMP6s. Inset: Z-score of cross-correlation in eYFP controls. * $p < 0.05$, for a Mann–Whitney test; n = 4 D1-Cre and 4 A2A Cre hemispheres infected, same data as from d and g.
Str: striatum; GP: globus pallidus; GPm: medial globus pallidus; SNr: sustantia nigra pars reticulata.

3.2.2 Inhibiting the activity of striatal projection pathways.

To test whether the observed increase in activity of both projection pathways was necessary for contraversive movements we performed optogenetic inhibition of striatonigral and striatopallidal neurons (either simultaneously or independently) while animals performed spontaneous movements in a small open field. To optogenetically inhibit striatonigral and striatopallidal neurons we expressed Archaeorhodopsin (ArchT-GFP) in a Cre-dependent manner[279] in the dorsal striatum of mice from four different transgenic lines. To achieve simultaneous inhibition of both striatal projection pathways, we injected the ArchT-GFP virus (Flex, rAAV2/ 1) into the sensorimotor or dorsolateral striatum of RGS9L-Cre mice, and achieved strong GFP expression in both striatonigral and striatopallidal neurons[280] (**Figure 3.2**).

We verified that a similar proportion of cells from each striatal projection pathway was infected in RGS9L-Cre mice by crossing RGS9L-Cre animals with either D1-tdTomato or D2-eGFP[220,281] mice, and injecting a Cre-dependent virus expressing the other fluorophore into the dorsolateral striatum of these animals (~50% of the RGS9L-Cre cells are either D1 positive or D2 positive).

To achieve selective expression of ArchT-GFP in either the striatonigral or the striatopallidal pathways, we injected the same ArchT-GFP virus into the dorsolateral striatum of either D1-Cre mice or D2-Cre and A2A cre mice (ER43 and KG139; both lines were used to ensure that the effects observed were specific to the manipulation of striatopallidal pathway neurons, as D2 receptors may be expressed in different striatal interneurons[273]).

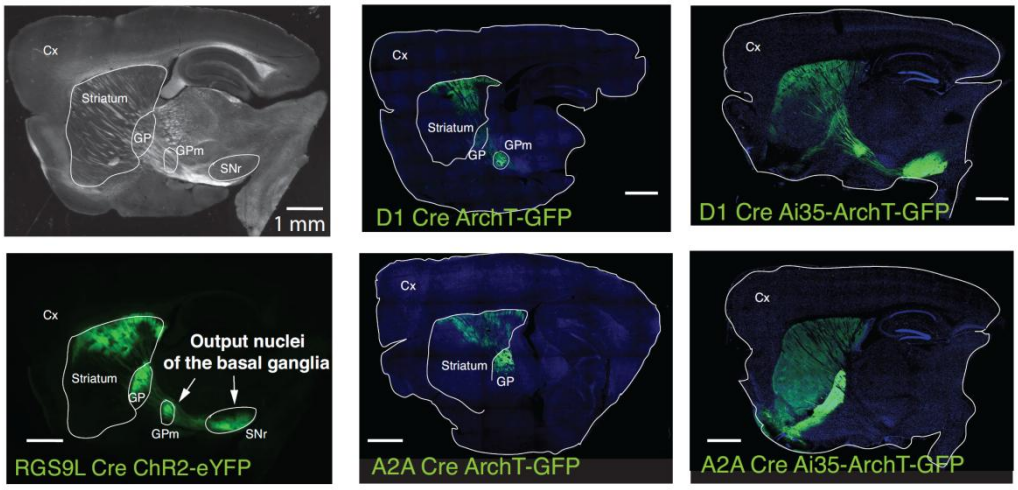

Figure 3.2. Expression of ArchT-GFP in striatonigral and striatopallidal neurons.
Photomicrographs from sagittal sections of mouse brain depicting the nuclei of the basal ganglia targeted in this study. The upper left picture shows a sagittal bright field example to illustrate the striatum and the projection target nuclei of the striatal cells (GP: globus pallidus, GPm: medial globus pallidus; SNr: subtantia nigra pars reticulata). The bottom left picture shows a sagittal brain slice of a ChR2-EYFP injection into the striatum of a RGS9L-Cre mouse. Middle column pictures show ArchT-GFP injections into the striatum of D1 Cre (ERY217) and A2A Cre (KG139) mice. Note the presence of green fluorescence in the striatum (place of injection) and in the target nuclei of the striatal cells: simultaneously in the GP, GPm and SNr in the case the RGS9 Cre line showing that it targets both the striatonigral and the striatopallidal

pathways, and selectively in GPm (and also SNr in different slices not shown) when using the D1 Cre line (striatonigral pathway) and in the GP when using the A2A cre line (striatopallidal pathway). The right column in *a* shows sagittal slices from striatonigral and striatopallidal basal ganglia pathways cross bread with the Ai35 line to express ArchT in all the cre expressing cells. Note the difference in the signals between the viral expression of ArchT (middle column in *a* and the Ai35 ArchT driven expression (right column in *a*). Scale horizontal bars in *a* correspond to 1 millimeter.

Using stereological counting, we determined that we infected on average 32.5% of striatal cells in the infected area in RGS9L-Cre mice (peak infection area ~58%), 26.5% in D1 and 31.5–32.5% in D2 and A2A Cre mice (peak infection area 45–50%, respectively). Furthermore, we verified *ex vivo* and *in vivo* that green light illumination did cause inhibition of firing in ArchT-GFP expressing neurons (556 nm, 9.2 ± 1.2mW x mm^2 was the minimum power to decrease spiking of striatal cells in the slice; *in vivo* we used 25 – 35mW measured at the fiber tip to achieve a wider modulation, 57 ms was the average latency to inhibit firing *in vivo*, **Figure 3.3**).

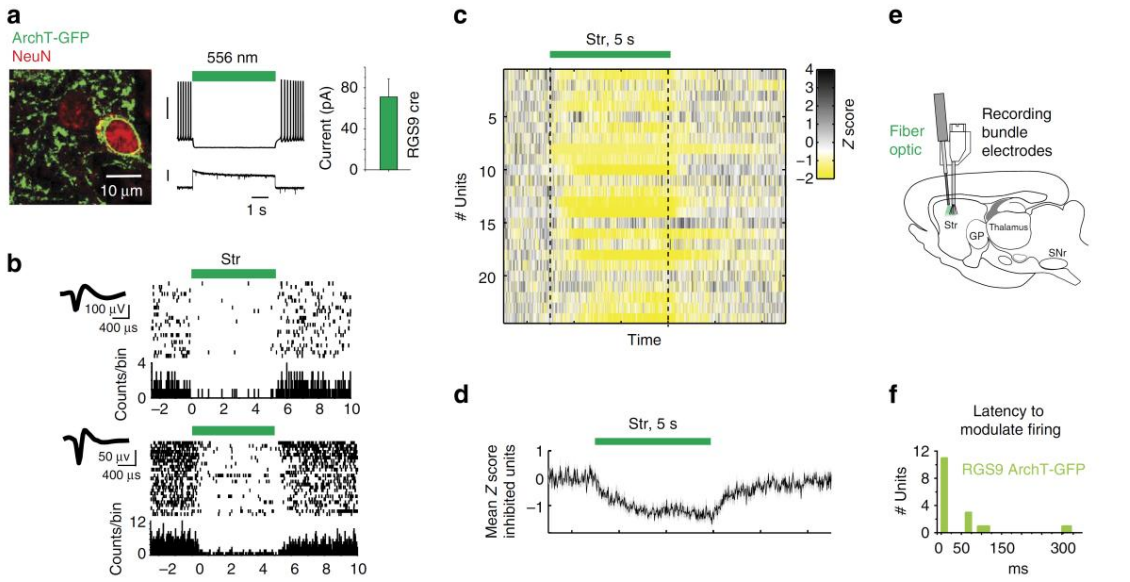

Figure 3.3. Inhibition of striatal neurons during unilateral ArchT induced inhibition and ipsiversive turns.

- **a.** Left panel, photomicrograph from a cell expressing ArchT and positive for immunolabelling the nuclei using NeuN. Right panel, voltage and current responses to green light illumination in a striatal projection neuron recorded in a brain slice, the bar on the right panel shows the mean current in response to 9.2 mW x mm^2 (minimum power to inhibit spikes in striatal neurons), upper and lower vertical bars: 30 mV and 50 pA, respectively.
- **b.** Peri-event histograms examples from individual units aligned to the onset of green light inhibition presented in *c*, bottom to top trials.
- **c.** Peri-event histograms of the Z-scored timestamps of extracellularly recorded action potentials of striatal neurons in the ipsilateral side, aligned to the onset of light in freely moving mice expressing ArchT-GFP, while turning ipsilateraly in an open field. Timestamps of each spike for the different cells, aligned to the onset of green light illumination.
- **d.** Mean Z-score for the units that were significantly modulated by the green light application.
- **e.** Representative diagram illustrating the recordings and light undiced inhibition inside the striatum of animals treated to express ArchT.
- **f.** Latency to modulate spikes in ArchT-expressing striatal cells.

3.2.3 Inhibiting either pathway favors ipsiversive movements.

We inhibited either or both striatal pathways unilaterally by delivering green light into the dorsolateral striatum through an optical fiber on either hemisphere in the same mouse (5 s of

continuous light delivery per stimulation, ~67 s time between stimulations (mean interval: 67 ± 9 s, max: 500, min: 21 s — and mean number of trials per animal: 9, max: 20, min: 3)), and evaluated contraversive versus ipsiversive locomotion in freely moving mice in an open field (using a custom-made software to analyse deviations from the rostrocaudal axis).
Assuming a cone of light emanating from the 0.48 NA fiber, and considering the minimum power intensity to modulate the spiking of striatal and the mean average of cells expressing the opsin (~30%), we estimated to be manipulating ~4,601–5,813 neurons per striatum. We observed that inhibiting either or both striatal pathways unilaterally for 5 s impaired contraversive movements and biased the animals to perform ipsilateral turns (**Figure 3.4**).
We first tested whether selective inhibition of either striatonigral or striatopallidal neurons would decrease contraversive turns and bias the animals to turn ipsilaterally. We verified that inhibiting the striatonigral neurons unilaterally resulted in ipsilateral turning (both group and interaction effects when compared with D1-eYFP controls; $F_{time} = 13.21$; $F_{group} = 4.27$; $F_{interaction\ timexgroup} = 1.64$; $p < 0.05$; repeated measures analysis of variance, **Figure 3.4 a–c**). Inhibition of striatonigral neurons in the right striatum resulted in turning towards the right side of the animal, while inhibition of striatonigral neurons in the left striatum resulted in turning towards the left (**Figure 3.4 a–c**, D1-ArchT$_{Lside\text{-}Inhibition}$: 45 ± 10 cumulative degrees to the left versus D1-ArchT$_{Rside\text{-}Inhibition}$: -39 ± 7 cumulative degrees to the right; n = 9, within-subject comparison against baseline before light stimulation, and also between left and right for each mouse; posthoc Wilcoxon test, $p < 0.05$). A similar effect was observed with unilateral inhibition of striatopallidal neurons (both group and interaction effects when compared with eYFP controls, $F_{time} = 14.54$; $F_{group} = 7.18$; $F_{interaction\ time\_group} = 5.64$; $p < 0.05$; **Figure 3.4 d–f** D2/A2A-ArchT$_{Lside\text{-}inhibition}$: 59 ± 29 versus D2/A2A-ArchT$_{Rside\text{-}inhibition}$: -86 ± 25, Wilcoxon test, $p < 0.05$, n = 10; Wilcoxon test, $p < 0.05$ against baseline and also left versus right stimulation). This was not observed if light was delivered into D1-Cre or A2A/D2-Cre animals carrying a control Cre-dependent eYFP virus (D1-Cre eYFP, n = 8, and A2A/D2-Cre eYFP, n = 6, Wilcoxon test, $p < 0.05$ against baseline and also left versus right stimulation; n = 6, D2/A2A-ArchT versus D2/A2A -eYFP, Kruskal–Wallis, $p < 0.05$; D1-ArchT versus D1-eYFP, $p < 0.05$). Furthermore, simultaneous inhibition of both striatonigral and striatopallidal neurons unilaterally resulted in ipsiversive turning (both group and interaction effects when compared with RGS9L-eYFP controls, $F_{time} = 42.48$; $F_{group} = 17.7$; $F_{interaction\ time\_group} = 16.22$; $p < 0.05$; repeated measures analysis of variance). Inhibition of both striatal projection pathways in the right striatum resulted in turning towards the right side of the animal, while inhibition of both cell types in the left striatum resulted in turning towards the left (RGS9L-ArchT$_{Lside\text{-}inhibition}$: 137 ± 35, cumulative degrees to the left, and RGS9L-ArchT$_{Rside\text{-}inhibition}$: 115 ± 27, cumulative degrees to the right; n = 9, $p < 0.05$, within-subject comparison against baseline before stimulation, and also between left and right for each mouse; Wilcoxon test, **Figure 3.4 g–i**). This was not observed if light was delivered into RGS9L-Cre animals carrying a Cre-dependent eYFP virus (n = 9, $p < 0.05$; RGS9L-ArchT-GFP versus RGS9L-eYFP, Kruskal–Wallis, $p < 0.05$). Taken together, these results indicate that activity in either the striatonigral or the striatopallidal pathways is required

for contraversive movements. Interestingly, the additive effect of inhibiting either striatonigral or striatopallidal neurons independently was equivalent to the effect of modulating simultaneously both striatal pathways (D1-ArchT: 43 ± 8 and D2/A2A-ArchT: 73 ± 19 versus RGS9L-ArchT: 138 ± 22, cumulative degrees relative to the side of stimulation), suggesting that activity in both projection pathways contributes to contraversive movements.

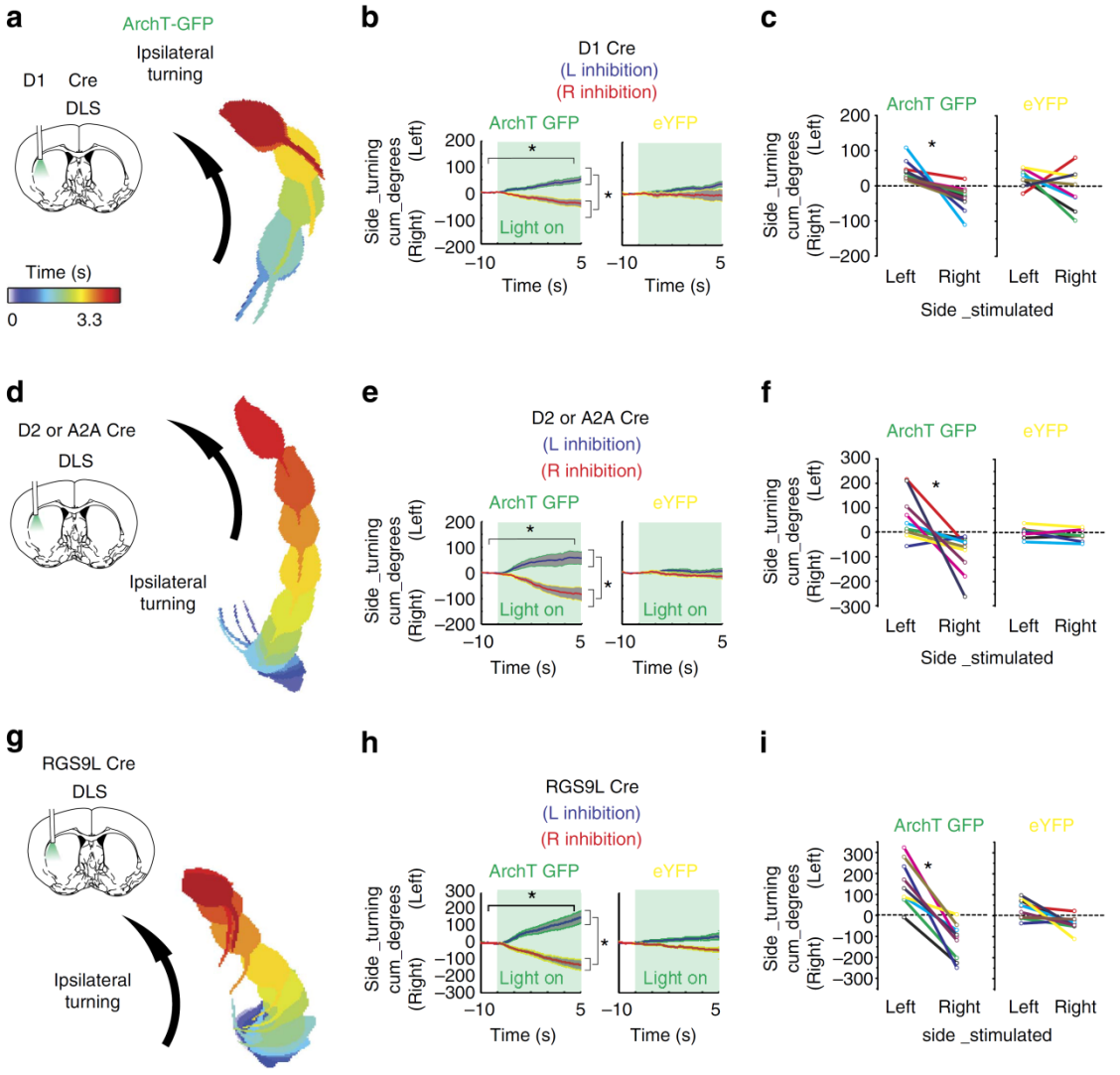

Figure 3.4. Simultaneous or independent inhibition of each striatal pathway biases towards ipsiversive movements.

a,d,g. Representative time series of video frames during the 5 s of unilateral left inhibition of the striatonigral, striatopallidal and both pathways, respectively (colours from blue to red show evolution of the behaviour during the inhibition period).

b,e,h. Temporal dynamics of the cumulative degrees of turning over the 5 s of inhibition in response to unilateral inhibition of striatal cells in the different Cre lines, aligned to one second before the illumination, blue: left side inhibition; red: right side inhibition. Data is presented as mean ± s.e.m..

c,f,i. Average cumulative degrees of turning towards left or right side, for each animal, during the last second of unilateral inhibition in the striatonigral pathway alone, in the striatopallidal pathway alone and in both striatal pathways simultaneously. *$p < 0.05$, for a within animal Wilcoxon test; n = 9 and n = 10 for D1 and D2/A2A-Cre ArchT-GFP; n = 8 and n = 6 for D1 and D2/A2A-Cre eYFP.

3.2.4 Inhibiting either pathway impairs contraversive movements.

The data presented above show that inhibition of either or both striatal projection pathways biases animals towards ipsilateral turns, but does not distinguish if inhibition of the striatal pathways impedes contralateral turns or further favours ipsilateral turns.

Therefore, we performed analyses wherein we examined separately trials where animals were turning ipsilaterally or contralaterally just before the onset of inhibition (analysing ~200ms before inhibition). These analyses allowed us to examine separately optogenetic trials in which both striatonigral and striatopallidal neurons show increased activity (contralateral turning) versus trials where they are not activated and even display a decrease in activity (ipsilateral turns) (**Figure 3.5**). We observed that the specific inhibition of striatonigral neurons impaired contralateral turns (when compared with trials with light off - no inhibition, D1-Cre$_{\text{ArchT-contra off light}}$: - 5 ± 4 cumulative degrees to the contralateral side, n = 69 trials versus D1-Cre$_{\text{ArchT-contra on light}}$: 11 ± 4 cumulative degrees to the ipsilateral side, n = 84 trials, Kruskal–Wallis, $p < 0.05$; **Figure 3.5 a,b**), but did not affect ipsilateral turns (again compared with trials with light off - no inhibition, D1-Cre$_{\text{ArchT-ipsi off light}}$: 7 ± 4 cumulative degrees to the ipsilateral side, n = 69 trials, versus D1-Cre$_{\text{ArchT-ipsi on light}}$: 12 ± 5 cumulative degrees to the ipsilateral side, n = 84 trials, Kruskal–Wallis, $p < 0.05$; **Figure 3.5 a,b**). Similarly, inhibition of striatopallidal neurons decreased contralateral turns (D2-Cre$_{\text{ArchT-contra off light}}$: - 5 ± 5 cumulative degrees to the contralateral side, n = 81 trials, versus D2- Cre$_{\text{ArchT-contra on light}}$: 18 ± 5 cumulative degrees to the ipsilateral side, n = 89 trials, Kruskal–Wallis, $p < 0.05$, **Figure 3.5 c,d**), but had no effect on ipsilateral turns (D2-Cre$_{\text{ArchT-ipsi off light}}$: 10 ± 5 cumulative degrees to the ipsilateral side, n = 81 trials, versus D2-Cre$_{\text{ArchT-ipsi on light}}$: 17 ± 6 cumulative degrees to the ipsilateral side, n = 89 trials, Kruskal–Wallis, $p < 0.05$, **Figure 3.5 c,d**). These data show that inhibition of either striatonigral and striatopallidal neurons impedes contralateral turns (when neurons from both pathways are activated) but did not further bias ipsilateral turns (when neurons from both pathways are not activated and even decrease activity), indicating that activity of each projection pathway is necessary for contralateral turning, but inhibition of an individual pathway is not sufficient to bias further ipsilateral turns.

We next examined the effect of inhibiting both striatonigral and striatopallidal neurons simultaneously. Inhibition of both projection pathways impeded contralateral rotations and further biased ipsilateral rotations (RGS9L-Cre$_{\text{ArchT-ipsi off light}}$: - 4 ± 5 cumulative degrees to the ipsilateral side, n = 86 trials, versus RGS9L-Cre$_{\text{ArchT-ipsi on light}}$: 43 ± 5 cumulative degrees to the ipsilateral side, n = 100 trials, Kruskal–Wallis, $p < 0.05$, RGS9L-Cre$_{\text{ArchT-contra off light}}$: 4 ± 4 cumulative degrees to the ipsilateral side, n = 105 trials, versus RGS9L-Cre$_{\text{ArchT-contra on light}}$: 39 ± 5 cumulative degrees to the ipsilateral side, n = 92 trials, Kruskal-Wallis, $p < 0.05$, **Figure 3.5 e,f**). These data show that activity in either striatonigral or striatopallidal neurons is necessary for contralateral turns, but inhibition of an individual cell type is not sufficient to further bias ipsilateral turns; only when both striatonigral and striatopallidal neurons are simultaneously inhibited unilaterally can ipsilateral turns be further biased (consistent with **Figure 3.1** and with Cui *et al.*, 2014[209]).

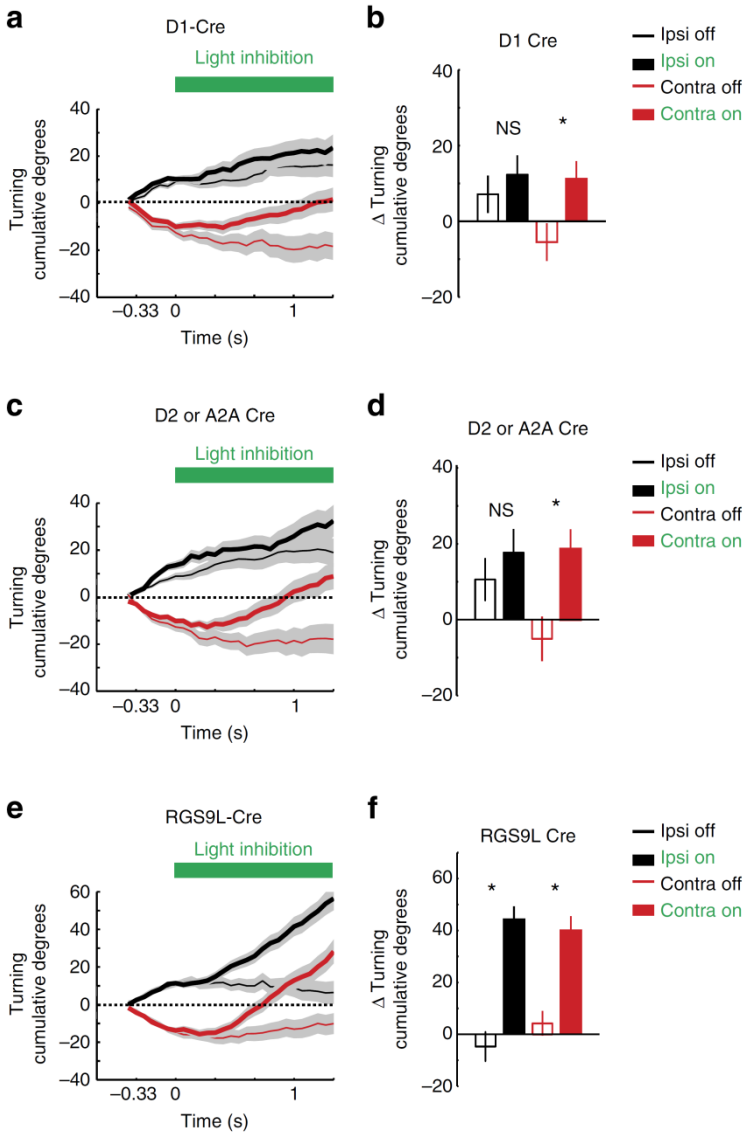

Figure 3.5. Effect of ArchT inhibition on contraversive versus ipsiversive movements.
a,c,e. Mean ± s.e.m. of the individual trials from all animals categorized as ipsilateral turning (black colour) and contralateral turning (red colour) 200 ms before the onset of light, grey shadows represent s.e.m.. The thick lines correspond to trials receiving light illumination as depicted by the green bar on top of each panel, while the thin lines corresponds to similar segments of time with no light illumination (obtained from periods of 6 s before light onset).
b,d,f. Difference between cumulative degrees at the onset of light (0 s) and 1.33 s after light onset (20 frames later).

3.2.5 Striatal activity biases head movements.

The results presented so far suggest that although we only manipulate a few thousand neurons in sensorimotor striatum, this affects whole body movements. However, as our optogenetic manipulations were targeting areas in the striatum receiving input from head areas of motor cortex[282] we decided to investigate whether our manipulations affected contraversive movements of the head in relation to the body axis. To assess contraversive and ipsiversive movements of the head in relation to the longitudinal body axis during inhibition we analysed angle of the head and of the body independently (and subtracted whole body turning, **Figure 3.6a**). These analyses revealed that inhibition of both striatonigral and striatopallidal neurons produced ipsiversive head movements (comparing 1 s before light onset versus a 1 s sliding window after inhibition; Kruskal–Wallis, $p < 0.05$, **Figure 3.6b**). To distinguish whether inhibition of the striatal projection pathways impedes contralateral turns or further favours ipsiversive movements of the head, we analysed the effect of manipulating the striatal activity in trials in

which the head was turning contraversively versus trials in which the head was turning ispiversively before the onset of inhibition (200 ms). We observed that inhibition of both striatonigral and striatopallidal neurons impeded contraversive head movements, but did not further bias ongoing ipsiversive head movements (Kruskal–Wallis, $p < 0.05$, **Figure 3.6c**, brackets to the right; after verifying overall effect, post-hoc analyses frame by frame revealed the specific period of time showing significant decrease in contraversive movements, horizontal bracket in **Figure 3.6c** corresponding to the bars presented in **Figure 3.6d**).

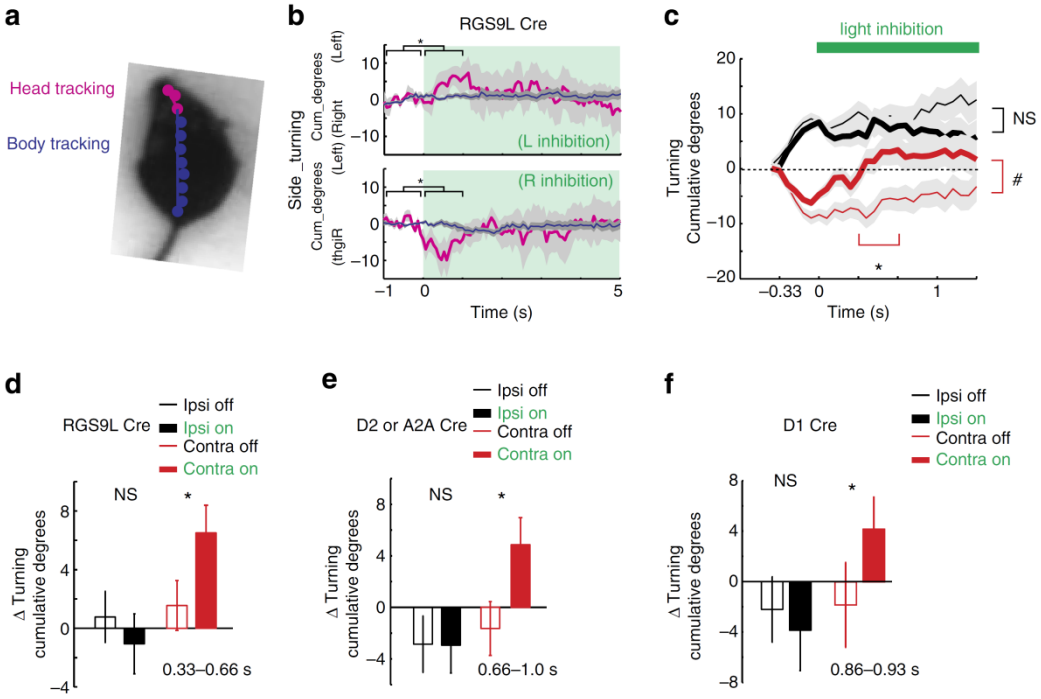

Figure 3.6. Contraversive and ipsiversive movements of the head in relation to the body.

a. Representative example of the animal segmentation separating the head tracking (magenta) from body tracking (dark blue).

b. Temporal dynamics of the cumulative degrees of head turning towards each side during the 5 s of unilateral illumination to inhibit both striatal pathways (shadowed green and blue square), magenta: head tracking, dark blue: body tracking.

c. Mean ± s.e.m. of the individual trials from all animals categorized as ipsilateral head turning (black colour) and contralateral head turning (red colour) 200 ms before the onset of light, grey shadows represent the s.e.m.. The thick lines correspond to trials receiving light illumination as depicted by the green bar on top of each panel, while the thin lines corresponds to turns in the same animals with no light illumination (obtained from periods of 6 s before light onset).

d. Difference between cumulative degrees at the onset of light (0 s) and the time depicted by the horizontal brackets in *c*.

e. Same analyses as for *c* and *d*, in this case for inhibition the striatopallidal pathways.

f. Same analyses as for *c* and *d*, in this case for inhibition of the striatonigral pathways. #Po0.05, Kruskall–Wallis, for the total period of illuminations. *$p < 0.05$ for the post hocs in the period of time depicted by the horizontal bracket. The inserted periods of time correspond to the periods in which the posthoc analysis showed significance.

3.2.6 Imbalanced activity between the pathways causes opposing effects.

In the results presented above we have described ipsilateral biases when inhibiting either of the basal ganglia pathways. This is consistent with the idea that the increased activity in both of

them during contralateral turning is critical for the foretold movements. However, there is evidence suggesting that independent activation of striatonigral and striatopallidal neurons[240,273] or lesions/decreases in the activity of these neurons[277,278] leads to opposite effects on behavior. One discrepancy between these studies and our study could be that either independent activation of each projection pathway or large lesions of one of the cell types would lead to an imbalance in the activity of both pathways, and this could result in opposing behavioral phenotypes. We therefore examined the effect of independently increasing the activity of striatonigral and striatopallidal neurons. We expressed ChR2-eYFP in striatonigral and striatopallidal neurons[240,273], using the same strategy used for expressing ArchT, and stimulated each striatum of each mouse for 5 s (we used 10 ms pulses delivered at 14 Hz, ~44 s inter-trial interval when using more than a single trial: 44 ± 4 s (max: 175, min: 14 s); number of trials when using more than a single stimulation: mean 3 (min: 2, max: 12 trials)). As previously shown[240,273], selective stimulation of striatonigral neurons favoured contralateral movements, while selective stimulation of striatopallidal neurons resulted in ipsilateral turns (**Figure 3.7 b,e**).

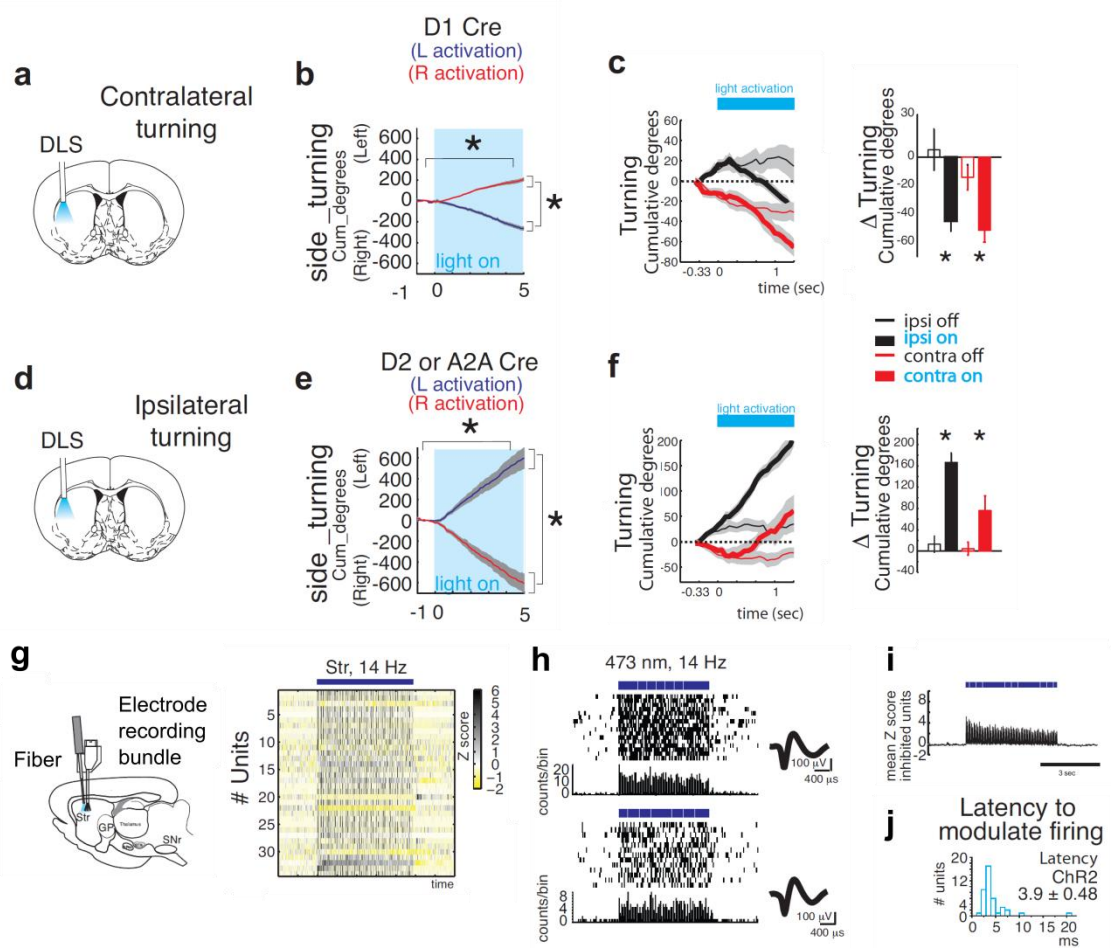

Figure 3.7. Unbalanced activation of the basal ganglia pathways show opposite effects on movements.

a, d. Representation of coronal brain mice slices depicting the unilateral stimulation in the different Cre lines.

b, e. Temporal dynamics of the cumulative degrees of turning towards each side in response to 5 seconds of unilateral illumination to activate the the striatal cells in the Ai35 mouse line, aligned to one second before the stimulation, dark blue: left side activation; red: right side activation. Data is presented as mean ± standard error. * $p < 0.05$, for a within-animal Wilcoxon test.

c, f. Left panels: mean ± standard error of the individual trials from all animals categorized as ipsilateral turning (black color) and contralateral turning (red color) 200 ms before the onset of light. The thick lines correspond to trials receiving light illumination as depicted by the blue or green bar on top of each panel, while the thin lines corresponds to similar segments of time with no light illumination (obtained from periods of 6 seconds before light onset). Right panels: difference between cumulative degrees at the onset of light (0 seconds) and 1.33 seconds after light onset (20 frames later). * $p <$ 0.05 for a Mann Whitney U test. Data: D1-Cre$_{ChR2\ ipsi\text{-}off}$: 11 trials from 8 animals (5 ± 14), D1-Cre$_{ChR2\ ipsi\text{-}on}$: 16 trials from 8 animals (-44 ± 7), D1-Cre$_{ChR2\ contra\text{-}off}$: 25 trials from 8 animals (14 ± 8), D1-Cre$_{ChR2\ contra\text{-}on}$: 20 trials on from 8 animals (-51 ± 8). D2/A2A-Cre$_{ChR2\ ipsi\text{-}off}$: 11 trials from 6 animals (12 ± 15), D2/A2A-Cre$_{ChR2\ ipsi\text{-}on}$: 13 trials from 6 animals (166 ± 17), D2/A2A-Cre$_{ChR2\ contra\text{-}off}$: 13 trials from 8 animals (4 ± 12), D2/A2A-Cre$_{ChR2\ contra\text{-}on}$: 11 trials on from 8 animals (75 ± 27).

g. Perievent histograms of the Z-scored timestamps of extracellularly recorded action potentials of striatal neurons, relative to onset of light in freely moving mice expressing ChR2-eYFP while turning contralateraly or ipsilateral in an open field.

h. Perievent histograms examples from individual units

i. Mean Z-score for the units that were significantly modulated by the blue light illumination in *g*.

j. Latency to modulate spikes in ChR2-eYFP expressing striatal cells.

However, if both pathways are simultaneously activated, as observed when monitoring their activity during contralateral turns (**Figure 3.1**), animals perform contralateral movements (RGS9L-Cre$_{ChR2\text{-}Lside\text{-}activation}$: - 187 ± 28 cumulative degrees to the left and RGS9L$_{ChR2\text{-}Rside\text{-}activation}$: 192 ± 45 cumulative degrees to the right; Wilcoxon test, $p < 0.05$, against baseline and left versus right; n = 6, **Figure 3.8**; no effect in eYFP controls).

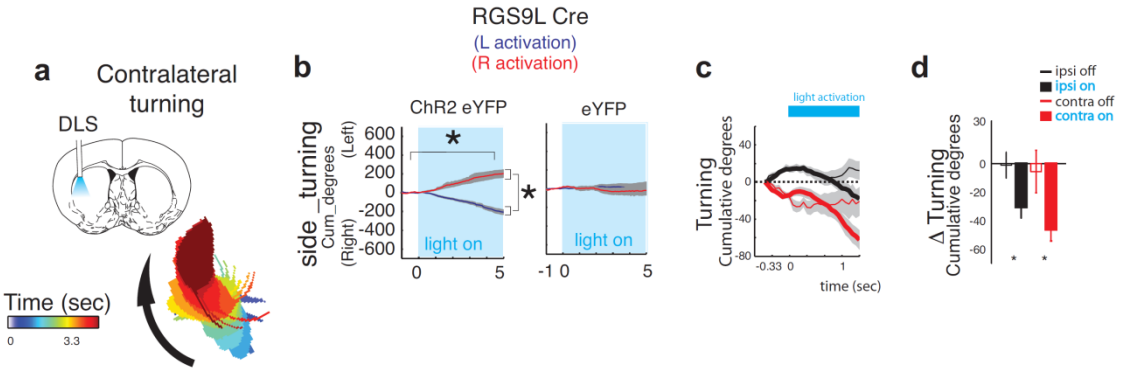

Figure 3.8. Concurrent over-activation of both striatal pathways favors contraversive movements.

a. Representation of a coronal brain mice slice depicting the unilateral stimulation in *b-d*.

b. Temporal dynamics of the cumulative degrees of turning towards each side in response to 5 seconds of unilateral illumination to activate the striatal cells, aligned to one second before the stimulation, dark blue: left side activation; red: right side activation. Data is presented as mean ± standard error. Data: RGS9L-Cre$_{ChR2Lside\text{-}activation}$: -187 ± 28 cumulative degrees to the left and RGS9L-Cre$_{ChR2Rside\text{-}activation}$: 192 ± 45 cumulative degrees to the right; Wilcoxon test, $p < 0.05$, against baseline and left vs. right; n = 6; no effect in EYFP controls.

c. mean ± standard error of the individual trials from all animals categorized as ipsilateral turning (black color) and contralateral turning (red color) 200 ms before the onset of light. The thick lines correspond to trials receiving light illumination as depicted by the blue bar on top of each panel, while the thin lines corresponds to similar segments of time with no light illumination (obtained from periods of 6 seconds before light onset).

d. Difference between cumulative degrees at the onset of light (0 seconds) and 1.33 seconds after light onset (20 frames later). * $p < 0.05$, Mann Whitney U test.

These data suggest that although simultaneous activity of both pathways is normally involved in contralateral turns, imbalanced activity between the two projection pathways can lead to opposite effects in movement, which could be relevant for some disorders. To further investigate this we also performed more extensive inhibition of each striatal projection pathway

by crossing D1 Cre or A2A-Cre animals with the Ai35 mouse line (expressing ArchT in all Cre-positive cells[283]). We observed that unilateral striatal inhibition on the dorsolateral part of the striatum in the D1-Cre Ai35 animals induced ipsiversive movements (**Figure 3.9 b**), whereas inhibition of the dorsolateral part of the striatum in A2A-Cre Ai35 animals induced contraversive movements (**Figure 3.9 e**), consistent with references [277,278].

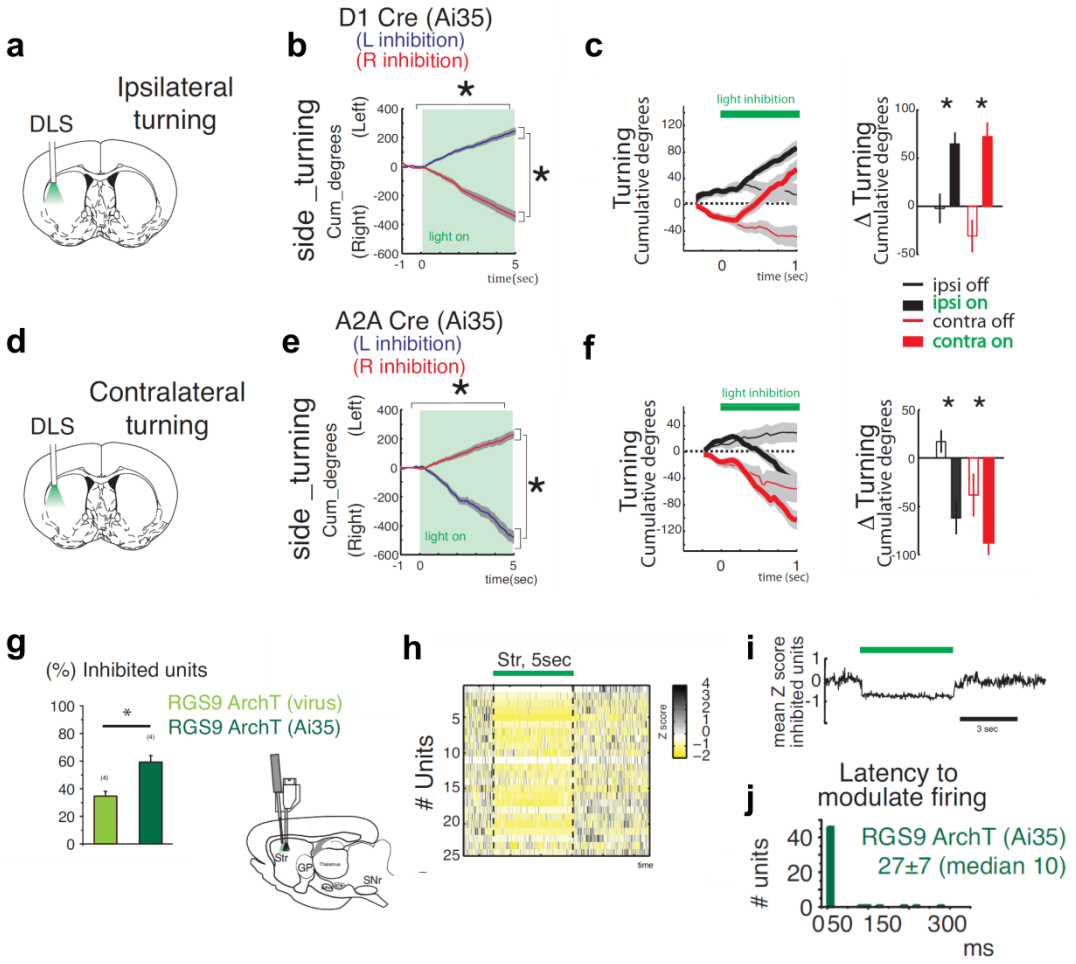

Figure 3.9. Unbalanced inhibition of the basal ganglia pathways shows opposite effects on movements.

a, d. Representation of coronal brain mice slices depicting the unilateral inhibition in the different Cre lines. **b, e,** Temporal dynamics of the cumulative degrees of turning towards each side in response to 5 seconds of unilateral illumination to inhibit striatal cells using the Ai35 mice line, aligned to one second before the stimulation, dark blue: left side activation; red: right side activation. Data is presented as mean ± standard error. * $p < 0.05$ for a within-animal Wilcoxon test.

c, f. Left panels: mean ± standard error of the individual trials from all animals categorized as ipsilateral turning (black color) and contralateral turning (red color) 200 ms before the onset of light. The thick lines correspond to trials receiving light illumination as depicted by the blue or green bar on top of each panel, while the thin lines corresponds to similar segments of time with no light illumination (obtained from periods of 6 seconds before light onset). Right panels: difference between cumulative degrees at the onset of light (0 seconds) and 1.33 seconds after light onset (20 frames later). * $p <$ 0.05 for Mann Whitney U test. Data: D1-Cre$_{\text{ArchT(Ai35) ipsi-off}}$: 11 trials from 2 animals (-5 ± 14), D1-Cre$_{\text{ArchT(Ai35) ipsion}}$: 22 trials from 2 animals (64 ± 11), D1-Cre$_{\text{ArchT(Ai35) contra-off}}$: 23 trials from 2 animals (-30 ± 15), D1-Cre$_{\text{ArchT(Ai35) contra-on}}$ 16 trials on from 2 animals (72 ±14). D2/A2A-Cre$_{\text{ArchT(Ai35) ipsi-off}}$: 14 trials from 2 animals (17 ± 11), D2/A2A-Cre$_{\text{ArchT(Ai35) ipsi-on}}$: 13 trials from 2 animals (-62 ± 16), D2/A2A-Cre$_{\text{ArchT(Ai35) contra-off}}$: 9 trials from 2 animals (-38 ± 21), D2/A2A-Cre$_{\text{ArchT(Ai35) contra-on}}$: 10 trials on from 2 animals (-87 ± 12).

g. Comparison of proportion of cells been inhibited in animals using the viral ArchT expression vs animals cross bread to expressing ArchT using the Ai35 mice line [Mean % of inhibited units Ai35-

ArchT-GFP = 59 ± 4 % versus the mean % of inhibited units viral ArchT-GFP = 34 ± 7; $p < 0.05$; Mann Whitney test].

h. Perievent histograms of the Z scored timestamps of extracellularly recorded action potentials of striatal neurons, relative to onset of light in freely moving mice expressing ArchT-GFP while turning contralateraly or ipsilateral in an open field.

i. Mean Z-score for the units that were significantly modulated by green light

j. Latency to modulate spikes in ArchT-GFP expressing striatal cells.

The results presented above suggest a more complex functional organization of basal ganglia circuits than initially thought. Therefore, we performed electrophysiological recordings of neural activity in striatum and downstream target regions (globus pallidus (GPe), SNr) and primary motor cortex) to investigate whether the effects in downstream neurons were those predicted (**Figure 3.10**). Although ArchT stimulation caused strong inhibition of striatonigral and striatopallidal projection neurons (**Figure 3.10 a,d**), the classically predicted opposing effects in basal ganglia output (SNr) were not observed (**Figure 3.10 e-g**). Inhibition of striatonigral neurons did not lead to an increase in activity in SNr (few neurons changed activity and a similar proportion of neurons increased versus decreased activity), whereas inhibition of striatopallidal neurons did result in an increase in activity in GPe, but not in a decrease of activity in SNr (**Figure 3.10 g**). Together with the effects observed in the primary motor cortex, these results suggest the existence of functional connectivity details in basal ganglia circuitry that are beyond the known feedforward connections classically reported[284–286].

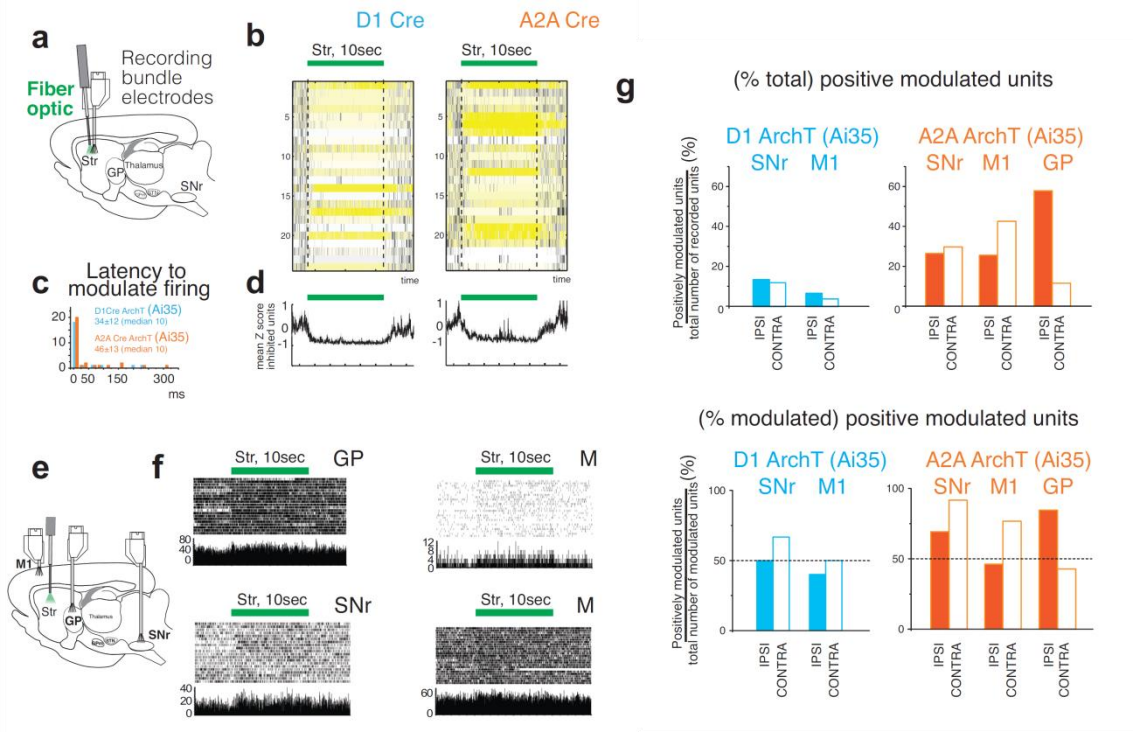

Figure 3.10. Recordings on the target nuclei of the basal ganglia pathway while unilaterally inhibiting the basal ganglia pathways.

a. Representation of a sagittal brain mice slice depicting the unilateral stimulation and recordings inside the striatum for the data presented in *b-d.*

b. Perievent histograms of the Z-scored timestamps of extracellular recorded action potentials of striatal neurons, relative to onset of green light in freely moving mice expressing ArchT-GFP using the Ai35 mice line, while turning in an open field.

c. Latency to modulate spikes from the data presented in *b*.

d. Mean Z-score for the units that were significantly modulated by the green light illumination.

e. Representation of a sagittal brain mice slice depicting the unilateral striatal stimulation and recordings on GP (globus pallidus) or SNr (sustantia nigra pars reticulata) or M1 (motor cortex) for the data presented in *f-g*.
f. Perievent histograms examples from individual units recorded in the target nuclei of the basal ganglia while inhibiting the striatum for the analysis presented in *g*.
g. Upper panels, percentage of positive modulated units from the total number of units recorded in the target nuclei of unilateral striatonigral inhibition (blue) or striatopallidal inhibition (orange). Lower panels correspond to the percentage of positively modulated units in relation to the total number of modulated cells (positive and negative). Data: D1-Ai35-ArchT IPSI Striatal inhibition SNr recordings 15 units, 2 sessions, 1 animal; D1-Ai35-ArchT CONTRA Striatal inhibition SNr recordings 17 units, 2 sessions,1 animal; D1-Ai35-ArchT IPSI Striatal inhibition M1 recordings 60 units, 3 sessions,1 animal; D1-Ai35-ArchT CONTRA Striatal inhibition M1 recordings 52 units, 3 sessions,1 animal. A2A-Ai35-ArchT IPSI Striatal inhibition SNr recordings 34 units, 4 sessions, 2 animal; A2A-Ai35-ArchT CONTRA Striatal inhibition SNr recordings 37 units, 4 sessions, 2 animal; A2A-Ai35-ArchT IPSI Striatal inhibition M1 recordings 47 units, 3 sessions, 2 animal; A2AAi35-ArchT CONTRA Striatal inhibition M1 recordings 54 units, 3 sessions, 1 animal; A2AAi35-ArchT IPSI Striatal inhibition GP recordings 18 units, 2 sessions, 1 animal; A2A-Ai35- ArchT CONTRA Striatal inhibition GP recordings 26 units, 2 sessions, 1 animal. Note that we used movable arrays that were advanced 200 microns from one session to the next.

3.3 Discussion

The findings presented here suggest that co-activation of striatonigral and striatopallidal neurons is critical for natural contraversive movements. Using a new method of fiber photometry to measure GCaMP6s activation, we observed that striatonigral and striatopallidal neurons are concurrently active during spontaneous contraversive movements, and slightly decrease activity during ipsilateral turns (**Figure 3.1**; consistent with ref. [209]). These measurements reflect the bulk activity of thousands of neurons[209], and so they probably represent the population average of the activity of striatonigral and striatopallidal neurons (which are similar in number) during contraversive movements. However, the spatial resolution of bulk activity and the temporal resolution of GCaMP6s activation are not amenable to differentiate the activity of subpopulations of neurons, or to examine small differences in the time course of activation of both populations[287]. Consistent with the findings that both projection pathways are active during contraversive movements, we showed that optogenetic unilateral inhibition of either striatal projection pathway impaired contralateral movements without affecting ipsilateral movements. Inhibition of both pathways cancelled contralateral turns and further biased ipsilateral turns. These findings support a view in which activity in both projection pathways is required to achieve a particular movement[209,275,276], where, for example, direct pathway neurons could select the desired motor programme while indirect pathway neurons inhibit competing motor programmes[209,276,287,288]. This view is further supported by the fact that concurrent activation of direct and indirect pathways caused contralateral turns. Analyses of contraversive and ipsiversive movements of the head in relation to the body axis further confirmed these findings. Still, we also show that imbalance in activity of striatonigral versus striatopallidal neurons can cause opposing motor phenotypes[236,240,270,271,273]. This could be at play in disorders in which one of the pathways is strongly activated relative to the other, as suggested, for example, for Parkinson's and Huntington's disease[236,289]. Furthermore, we verified that inhibiting striatonigral versus striatopallidal neurons does not produce the predicted effects in basal ganglia output. Taken together, these results suggest that the functional connectivity in basal ganglia is more complex than previously thought. For example, the observation that striatopallidal activation in

the absence of simultaneous striatonigral activation leads to ipsiversive movements, but in the presence of simultaneous striatonigral activation leads to contraversive movements is intriguing. One potential explanation for the apparent discrepancy is that striatopallidal neuron activation could cause inhibition of striatonigral neurons via the collaterals between them[290] (which are stronger than the converse case[291]). However, other possibilities that do not rely only on intrastriatal interactions between the pathways are likely to be at play. For example, it is possible that striatonigral versus striatopallidal neurons project to overlapping but not completely redundant downstream target areas of basal ganglia output, so that overactivation or overinhibition of each projection pathway by itself would lead to a different pattern of activation or inhibition of downstream targets than concurrent activation of both pathways. It is also likely to be, given that the main discrepancies were observed after striatopallidal manipulations, that striatopallidal neurons connect to more targets than those postulated by the 'indirect pathway', and that pallidal neurons projecting to regions other than the subthalamic neurons and SNr are mediating some of the effects observed here.

In conclusion, these data suggest that striatal projection pathways interact to produce desired movements, and that balanced activity in both types of projection neurons is required to produce contraversive movements. Imbalanced activity between the two pathways can lead to opposite motor output.

Interestingly, serotonin is thought to play an important role in this balance between the activity of the striatopallidal and striatonigral pathways through modulation of DA's activity: it is thought to facilitate DA's release in the striatum[292] (although this is most likely a very simplistic view[293,294]) and to inhibit DA cells in the SNc[295,296]. Its effects are mostly revealed in Parkinson's disease patients under levodopa (L-DOPA) treatment[297,298], but proposals for its modulation in homeostatic situations have been proposed[299].

3.4 Experimental Procedures

Animals

All procedures were reviewed and performed in accordance with the Instituto Gulbenkian de Ciência and the Champalimaud Centre for the Unknown Ethics Committee guidelines, and approved by the Portuguese Veterinary General Board (Direcção Geral de Veterinária, approval ID 018831). Male mice between 2 and 4 months of age, resulting from the backcrossing of BAC transgenic mice into Black C57BL for at least six generations (which express the Cre recombinase under the control of the dopamine D1a (EY217 line), D2 (ER43 line) or A2A (K139 line), or td-tomato or enhanced green fluorescent protein, under the promoters of D1 or D2 receptors obtained from GENSAT) into C57BL/6J (The Jackson Laboratory[300]) were used in this study.

Stereotaxic virus injections and fibre implantation

Surgeries were performed under deep anaesthesia using a mix of oxygen (1 $l.min^{-1}$) and 1 % isuoflorane (1–3 % for interventional procedures). For GCaMP6s experiments, animals were

infected and implanted either in only one hemisphere or in both. In each hemisphere, 1 ml of viral stock solution was injected using quartz pipettes and a picospritzer (Parker Hannifin[301]) in the dorsal striatum at coordinates anteroposterior 0.5 mm from the bregma, 1.7 mm mediolateral, 2.2 mm deep for D1-Cre mice, and anteroposterior 0.5 mm from the bregma, 2.0 mm mediolateral, 2.45 mm deep for D2-Cre mice. For optogenetic manipulation experiments, each animal was bilaterally injected, using glass pipettes (< 50 µm tip), with 1 ml viral stock solution (from a 4 to 5 ml viral aliquot kept at -80ºC) by pressure (4.6 nl every 5 s; 23 nl s^{-1} rate) using a nanoject II (Drummond Scientific[302]) into the dorsolateral striatum at the following coordinates: 0.5 mm anteroposterior from the bregma, 2.3 mm mediolateral and 2.3 mm below the surface of the brain. After the injection was performed, the pipette was left in place for 10 min before retraction. Subsequently, a 200 µm diameter (NA 0.22 for ChR2) or 300 µm diameter (NA 0.48 for ArchT) or 300 µm diameter (NA 0.22 for GCaMP6s) fiber optics were implanted (Doric Lenses[228]) 200 µm above the viral injection. These experiments were carried out using AAV1.Syn.Flex.GCaMP6s (titer $2.98x10^{13}$, University of Pennsylvania[219]), AAV1.EF1a.DIO.ChR2-eYFP (titer $1.4x10^{13}$; University of North Carolina), AVV1.EF1a.DIO.eYFP (titer $1.4x10^{13}$, University of North Carolina[303]), AVV1.EF1a.Flex.ArchT-GFP (titer $1.4x10^{12}$, University of Pennsylvania[219]) or AVV1.EF1aDIO.td- tomato (titer $1.4x10^{12}$, University of Pennsylvania[219]).

Monitoring activity with GCaMP6s

The fiber photometry setup used was the one described in section 2.2.2. The control and acquisition of the transistor–transistor logic (TTL) signal used for synchronization with the video through an light-emitting diode (LED) and the acquisition of the fluorescence signal were performed with an NI-PCI data acquisition board (PCI-6229) at 1 kHz and custom software programmed in Matlab (MathWorks, MA). Two to four weeks after surgery the animals were placed into a novel arena (a novel cage similar to the home cage) and video recorded as detailed in section 2.2.5. Tracking data (angle or angular velocity) and fluorescence data were lowpass filtered at 5Hz and used for further analysis. Turns were detected by finding the points at which the derivative of the angle was zero and were classified as right or left, depending on whether this derivative was increasing or decreasing, respectively. Only those turns occurring after 5 s in which the s.d. of the angle was smaller than 40º and that after 5 s resulted in a change bigger than 40º were included. Relative changes in fluorescence, $\Delta F/F_0 = (F-F_0)/F_0$ was calculated by, for each session, correcting baseline drift with a third-order polynomial. We defined F_0 as the 10th percentile of the drift-corrected fluorescence. All angle and all $\Delta F/F_0$ (resampled to match the angle data) values during the detected turns were collected in all the sessions of all the mice, separated in contra and ipsilateral sides, and averaged. For easier comparison of contra and ipsilateral $\Delta F/F_0$ traces, each was subtracted by its mean between -2 and -1 s before the turn. For cross correlation analysis angular velocity was derived from the body angle data, lowpass filtered at 5 Hz and separated into contra- and ipsilateral angular velocity by separating the positive and the negative components of the signal and rectifying them. Filtered and subsampled $\Delta F/F_0$ data and rectified angular velocity data of all sessions of

each mouse were concatenated and the cross-correlation of the z-score of the two signals was determined for each mouse.

Light manipulations *ex vivo*

Striatal brain slices were obtained as described in ref. [287]. In the case of the ChR2-eYFP versus eYFP comparison *in vitro*, optical stimuli were delivered from 200 mm multimode optical fibers coupled to a 50 mW, 473 nm, diode-pumped, solid-state laser (Laserglow Technologies[304]) or using a fiber-coupled LED (473 nm, Doric Lenses). In the case of the ArchT-GFP versus eYFP experiments, a 200 mm fiber core, 0.48 NA, coupled to a diode-pumped, solid-state laser (CNI Lasers[305], China) was used and the control of delivering the light was done using a shutter (Thorlabs). In all the recordings, the tip of the fibre was positioned 200–400 mm away from the recorded cells. No significant changes on the intrinsic properties of the cells were found when comparing Cre ChR2-eYFP versus Cre eYFP-expressing cells or Cre ArchT GFP versus Cre eYFP-expressing cells, in periods of expression < 3 weeks. The minimum power to trigger reliable spikes using ChR2 in vitro was calculated as 1.6mW.mm^{-2}. In the case of ArchT we estimated an average current of 71 ±17 pA in firing of striatal cell.

Light manipulations *in vivo*

For the ChR2 and the corresponding controls, optical stimuli were delivered from 200 mm implantable fibers (NA 0.22; Doric Lenses) coupled to a 200 mW, 473-nm, diode-pumped, solid-state laser (Laserglow Technologies) using a one-input two-outputs rotatory joint (Doric Lenses) clamped in the position that during the day of the experiment was found to deliver the same amount of light on the two outputs. To set up the parameters of ChR2 stimulation we tried different protocols with 5 Hz, 14 Hz or 5 s of continuous light delivery. Although both 5 and 14 Hz provided reliable stimulation, continuous light resulted in an initial activation that was not sustained and rapidly decreased. For ArchT and the corresponding controls, optical stimuli were delivered using 200 or 300, implantable fibers (NA 0.48; Doric Lenses) free launched to a 500 mW, 556 nm, diode-pumped, solid-state laser (CNI Lasers) using a fiber optic to get light into a one-input two-outputs rotatory joint as for the blue laser. For the blue laser, the delivery of the light was controlled via TTL pulses connected to the diode-pumped solid-state lasers (DPSSL) driver of the laser. All the experiments using ArchT were done using an acoustic optic modulator (AA Opto Electronic[306]) to control the path of the light. Measures of the power in the tip of the fiber (similar to the one implanted) were verified every day of the experiment using a powermeter (PD1000-S130C, Thorlabs) and the power adjusted at the tip of the fibre to be 1–3mW for ChR2 or 25–35 mW for ArchT, unless otherwise stated.

Neuronal recording and light stimulation *in vivo*

To verify and decide the parameters of stimulation we recorded the activity of striatal neurons while delivering light stimulation in freely moving animals in the open field (39 x 39 cm). These animals were previously infected to express either ChR2-eYFP or ArchT-GFP, and implanted with electrode arrays coupled to an implantable fiber. We used two kinds of array-fiber configurations. One of these array configurations consisted of a 2 x 8 array of platinum-coated

tungsten microwire electrodes of 35 mm diameter with 150 mm spacing between microwires, and 250 mm spacing between rows coupled to an optic fiber. The second system was a movable bundle of 16 platinum-coated tungsten microwires, which allowed us to record from different distances related to the tip of the fiber (Innovative-Neurophysiology[307]). In both cases these array-fiber configurations contained guide cannulas to introduce a fiber optic and position it 200–300 mm away from the tip of the electrodes before implantation. The neural activity and the timestamps from the light stimulation were recorded using the Cerebrus recording system (Blackrock Microsystems[308]). The spike activity was initially sorted using an online sorting algorithm (Central Software, Blackrock Microsystems), and only cells with a clearly identified waveform and relatively high signal-to-noise ratio (43:1) were used for further analyses. At the end of recording, cells were resorted using an offline sorting algorithm (Offline Sorter, Plexon Inc.[309]) to isolate single units and together with the timestamps of the light stimulation provided by a pulse generator (Master 8, AMPI[310]) were exported to MATLAB to perform analyses. To determine the volume of ArchT-positive neurons that can be effectively photostimulated to induce inhibition of spikes in neurons, we estimated the brain volume in which the light intensity achieved is greater than ~9.2 mW x mm^{-2} (threshold determined as the minimum intensity to modulate the spiking of striatal cells recorded in the slice). From experimental data measuring the light through striatal tissue we estimated that after passing through 100 µm of striatal tissue, total transmitted light power was reduced by 50%, and by 90% at 1mm. The data was fit by a Kubelka–Munk model for diffuse scattering media[311], with best-fit values for the scattering coefficient of 12.0 and 9.0 mm^{-1} for 473 nm and 561 light in the striatal mouse tissue. In addition to loss of light from scattering and absorption, light intensity also decreases as a result of the conical spreading of light after it exits the optical fibre. The light exiting the multimode fiber is not collimated and spreads with a conical angle of 41º determined by the numerical aperture of 0.48 used in the case of ArchT and 18º as determined by the numerical aperture of 0.22 used for ChR2. This effect will reduce the light intensity, which is expected to be the relevant quantitative parameter determining efficacy of ArchT or ChR2 stimulation. We therefore calculated the effective intensity, taking into account the combined effects of scattering, absorption and conical spread. These calculations allowed us to estimate the expected volume of tissue to modulate the ArchT- or the ChR2-expressing cells by the light illumination *in vivo*. If effective inhibition of spikes is achieved at 9.2 mW x mm^{-2}, in principle we were able to inhibit the spikes in 30% of the neurons (average rate of infection) at least up to 0.5 mm from the fiber tip. This distance value, together with the measured conical cross-section of 1.0 and 1.1mm diameter at 0.5 mm from the fiber tip, results in a total volume experiencing 9.2 mW x mm^{-2} light intensity of ~0.172–0.217 mm^3 (using 200 and 300 µm fiber core). Considering this volume and taking into account that ~30% of the neurons expressed ArchT we estimate that we were inhibiting between 4,601–5,813 and 7,668–9,689 ArchT-expressing cells. On the other hand, if effective activation of spikes is achieved at 1.6 mW x mm^{-2} (threshold determined as the minimum intensity to induce spikes of striatal cells recorded *in vitro*), in principle we were able to induce spikes in 30% of the neurons at least up to 0.4 mm (for 1 mW) and 0.8 mm (for 3 mW) from the fiber tip. This

distance value, together with the measured conical cross-section of 0.45 and 0.71 mm diameter at 0.4 and 0.8 mm from the fiber tip, results in a total volume experiencing 1.6 mW x mm^{-2} light intensity of ~0.0348 and ~0.179 mm^3. Considering this volume and taking into account that 30% of the neurons expressed ChR2 lead us to estimate that we were activating between 930 and 4,798 ChR2-expressing cells depending on the power used. To estimate the response latency to light illumination we estimated the onset of significant firing rate decrease in the case of ArchT and increase for ChR2 after light onset, based on the neuron's baseline firing rate peri-histogram aligned to the onset of light illumination using bins of 5 ms sliding 1 ms for ChR2 and 10 ms bins sliding 1ms. These data analyses were conducted in Matlab with custom-written programmes (MathWorks). To estimate positive- or negative-modulated units in the postsynaptic target nuclei of either D1-ArchT or A2A-ArchT striatal manipulations, we were based on 1 s baseline firing rate peri-histogram aligned to the onset of light illumination using bins of 10ms sliding 1 bin, and only if 30 bins in the first 2 s after the onset of light were different to the baseline ($p < 0.05$) a unit was considered as positively or negatively modulated.

Anatomical verification

Three to four weeks post infection, animals were killed after completion of the behavioural tests. First, animals were anaesthetized with isofluorane, followed by intraperitoneal injection of ketamine/xylaxine (~5 $mg.kg^{-1}$ xylazine; 100 $mg.kg^{-1}$ ketamine). Animals were then perfused with saline and 4% paraformaldehyde, and brains extracted for histological analysis. Brains were kept in the same solution overnight and then transferred to saline solution. Brains were sectioned sagittally or coronally in 50 µm slices (using a Leica vibratome (VT1000S) and kept in PBS 1% solution before mounting or immune staining treatment). After mounting and sealing of sections, one every five slices were selected to image the dorsal striatum using a confocal microscope equipped with Diodo 405 nm, Argon multi line 458-488-514 nm and a DPSS 561 nm lasers (LSM710, Zeiss[312]). Magnification (x 40) Z stacks (50 x 50 x 50 µm; 2 µm interslice) were acquired from the upper right quadrant using a randomly positioned grid (square grid 200 µm) covering the dorsal striatum (ZEN lite software, Zeiss). These Z-stacks were imported into the stereo investigator software (MBF Bioscience[313]) and quantification of the NeuN-positive, eYFP-positive or GFP-positive cells was done. Following this method, a total of 806/2,661 were positive for NeuN-eYFP or NeuN/GFP in ChR2 and ArchT animals (n = 4 hemispheres; 1 RGS9L-ChR2—1 RGS9L-ArchT: 97/310, 1 D1-ChR2: 236/897, 1 D2-ChR2: 473/1454 and 1 A2A-ChR2: 50/157). To evaluate whether the RGS9L-Cre line targets the two striatal pathways we injected virus expressing protein reporters into the striatum of RGS9L-Cre animals that were generated from cross breading RGS9L-Cre animals with either D1 td-tomato or D2-eGFP. This allowed us to identify from the RGS9L-Cre-infected cell (by a DIO AAV1 virus, see above) how many of them correspond to D1-td-tomato or D2-eGFP. From three sections from three different slices in one RGS9L Cre D1 td-tomato mice we estimated that out of 347 infected cells 181 were D1 td-tomato positive (52%). On the other hand, when infecting the striatum to express td-tomato in an RGS9L-Cre D2-eGFP animal (counting the infected cells from four sections from

four different slices), we estimated that 174 out of 354 infected RGS9L-Cre cells were D2-eGFP positive (49%).

Software to evaluate rotations

For *in vivo* cell manipulation experiments, videos from the animals in an open field were acquired using a charge-coupled device camera (DFK 31BF03) using the ICcapture software (Imaging Source[314]) or a custom-developed software in Labview (National Instruments[244]) at a rate of 15 frames per second signaling in the videos of the light stimulation periods. To calculate the rostrocaudal axis, the coordinates of the head centre and the tail were determined using a custom-made software developed in Python[315]. We used MATLAB for post-hoc analyses of these coordinates to estimate rotations aligned to a one second before the light onset and to detect the direction of the animal three frames before the light onset (the minimum number of frames to define a change in trajectory is two frames (sampling at 15 fps)—therefore, we used a minimum of three frames moving in a given trajectory to define where the body or the head was turning), to ensure that this was indeed a turning trajectory. Ipsilateral turning was plotted as positive and contralateral turning as negative. In these same figures for the 'light-off' condition we took trials using the same criteria 6 s before light onset. To further track the head rotations related to the body we vertically aligned the mouse in each frame by calculating the vertical axis of the whole animal and subtracting it for each frame (this is what we refer in the main text as subtracting the whole body axis). Once the image was vertically aligned we segmented the image, using the upper three segments to categorize the head angle and the remaining seven to determine the body angle (as depicted in **Figure 3.6**).

Statistics

Results were represented as mean ± s.e.m. and statistical significance was accepted for $p < 0.05$. The repetition of experiments was determined above the minimum *n* depending on the statistical test. A non-parametric Mann–Whitney test was used for comparisons of GCaMP6s activation during baseline and turning behavior. Paired non-parametric Wilcoxon test were performed to compare within-subject effects of the light stimulation, unless otherwise specifically stated in text. Non-parametric Kruskal–Wallis tests were used for between-subject comparisons. For statistical analyses, Matlab and Systat11[316] were used.

4. Dynamics of dopamine and serotonin neurons during reversal learning

In this chapter I present a study performed to understand how serotonin neurons in the dorsal raphe nucleus are involved in behavioral flexibility and compare their activity to dopamine neurons. We show that with our fiber photometry approach we can observe reward prediction error activity in dopamine neurons during reversal learning. We also show that, surprisingly, serotonin neurons show prediction error activity too. However, this activity is better explained by an unsigned prediction error or surprise signal, *i.e.* these signals are observed both when events are better than expected and when events are worse than expected. In addition, we show that dopamine and serotonin neurons have different dynamics of adaptation to reversal and we suggest that this might be a key element in understanding the long proposed opponency between these two systems in learning and behavioral control.

Results submitted for publication:
Matias, S., Lottem, E., Dugué, G. P., Mainen, Z. F.. Serotonin neurons signal surprise during reversal learning. Submitted.

Author contributions
S.M., E.L. and Z.F.M. designed the behavioral experiments and wrote the manuscript. S.M., and G.D. designed and developed the fiber photometry setup for movement artifact correction, E.L. developed movement artifact correction algorithm. S.M. performed experiments. S.M. and E.L. performed data analysis.

4.1 Introduction

As discussed in Chapter 1, midbrain neuromodulatory neurons such as DA and 5-HT are theorized to encode important scalar signals in their transient activation, which can be broadcasted to modulate critical processes throughout the brain[134].

While the phasic activity of DA neurons can be understood as representing a RPE signal, as posited by temporal difference reinforcement learning models[140,147], there is no accepted model for 5-HT neural activity. Because 5-HT and DA systems appear to be closely related, they have been theorized to act as opponent or complementary process[40,41,134]. More specifically, it has been suggested that phasic activity of 5-HT neurons could signal an aversive prediction error, or negative reward prediction error, which would be used for behavioral inhibition. However, reward related activity has also been observed in non-identified DRN[43,179,180] and identified 5-HT neurons[93].

Hence, it is not clear how 5-HT participates in affective signaling or how 5-HT signals might complement or oppose those of DA.

To investigate the responses of genetically defined DRN 5-HT neurons to predicted and unpredicted events of positive and negative valences, we trained mice to associate neutral odor cues with motivationally-significant outcomes while recording the population activity of these neurons using the fiber photometry setup described in Chapter 2. Additionally, we also recorded VTA/SNc dopaminergic activity in these same conditions so that we could compare the neural patterns of these two neuromodulatory systems and investigate how they oppose or complement each other.

The proposal that phasic activity of 5-HT neurons could represent a negative reward prediction error is compatible with a series of results from reversal learning paradigms performed in primates that show that 5-HT depletion causes perseverative errors, *i.e.* difficulties in stopping the response to previously rewarded stimuli which are no longer reinforced. In fact, both DA and 5-HT activity are thought to contribute to behavioral flexibility during reversal learning. Striatal and lateral prefrontal DA signaling is known to influence this type of errors[317–319], as well as 5-HT signaling[320,321], especially in the OFC where decreased 5-HT levels do not affect new learning or retention of learned associations but increase the number of perseverative errors during reversal[44,45]. It has been proposed that this might reflect insensitivity to reward loss, which should be signaled by a negative reward prediction error signal. Interestingly, SERT knockout rats and mice show differences in extinction[322] and increased performance in reversal learning[323] compared to controls, but DRN lesions also decrease the extinction rate of freezing responses after fear conditioning[324], suggesting that the role of 5-HT might not be restricted to extinguishing responding to worse-than-expected outcomes.

Knowing how DA and 5-HT neurons are activated during such paradigms could therefore provide insight into their function, yet very little such data is available[325].

Therefore, instead of using a simple classical conditioning task, once the odor-outcome associations in the classical conditioning task mentioned above had been well-learned, we rapidly reversed them. This allowed us to study the responses of 5-HT and DA neurons to the

robust violations of expectation that occurred upon reversal and to track their trial-by-trial dynamics as this process unfolded.

4.2 Results

4.2.1 Behavior of mice in a classical conditioning task

Water- restricted mice were trained in a head-fixed classical conditioning paradigm (**Figure 4.1 a**) in which one of four odor cues (conditioned stimuli, or CS's) was randomly presented in each trial. After a fixed trace period of 2 s each odor was followed predictably by a tone and one of four uniquely associated outcomes (unconditioned stimulus, US): large water reward, small water reward, nothing (tone-only), or a mild air puff to the eye. The four types of outcomes define the trial types. Within 1-3 days of training with the four odors (after a period of slow adaptation to the head-fixed setup and gradual introduction of the odors), mice learned the CS-reward associations, as indicated by differences in lick rate during CS and trace periods (large reward > small reward > neutral ≈ air puff) (**Figure 4.1 b**). In contrast, examination of eye blink responses indicated that mice did not learn an eyelid conditioned response (**Figure 4.1 c**), presumably due to the long trace period[326,327]. We therefore focused on the CS-reward association and reversal.

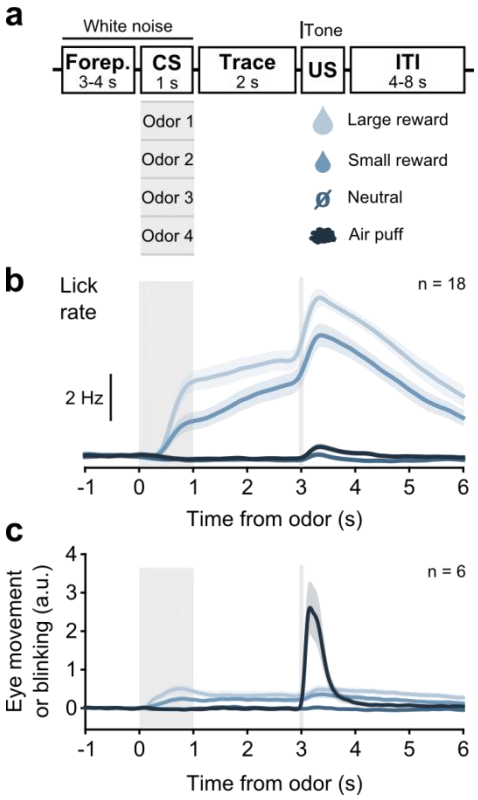

Figure 4.1. Behavior of mice trained in a classical reversal learning task.

a. Schematics of the trial structure in the classical conditioning task. In each trial one of four odors (conditioned stimulus or CS) was randomly selected and presented during 1 s after a variable foreperiod. The associated outcome (unconditioned stimulus or US) was delivered after a 2 s trace period together with a tone (same tone for all trial types). Mice were presented with 140 to 346 interleaved trials (mean ± SD: 223 ± 30) per session/day. Forep – foreperiod.

b. Mean licking rate of all mice (n = 18) along the duration of each trial type. For each mouse, three sessions were averaged. Colors code trial type according to *a*, shaded areas represent s.e.m. (3-way ANOVA with factors day, mouse and trial type; main effect of trial type $F_{3,8723}$ = 4935.17, p < 0.001; multiple comparisons with Scheffé's method with p = 0.3433 for neutral vs air puff and p < 0.001 for all other comparisons).

c. Mean eye movement of all mice (n = 6) along the duration of each trial type. For each mouse, three sessions of the classical conditioning task where initial associations had already been learned were averaged. Colors code trial type according to 1a, shaded areas represent s.e.m. (3-way ANOVA with factors day, mouse and trial type; main effect of trial type $F_{3,3290}$ = 583.74, p < 0.001; multiple comparisons with Scheffé's method with p < 0.001 for all comparisons).

4.2.2 Movement artifact correction in the context of the task

To monitor neuronal population activity reported by 5-HT neurons over the course of several days and to guarantee specificity of the recordings to the neural populations of interest we used fiber photometry to measure fluorescence signals from this genetically-defined population. As described before (Chapter 2), we targeted 5-HT neurons by stereotaxic injection of a mixture of adeno-associated (rAAV) viruses: one containing Cre-dependent vector driving GCaMP6s[205] and one containing Cre-dependent vector driving tdTomato expression into the DRN of SERT-Cre[220] (5-HT-specific) transgenic mice. To acquire the fluorescence signals *in vivo* we implanted a single multimode optical fiber that transmitted both excitation and emission lights (Chapter 2). We verified that while animals were engaged in this task we could see movement artifacts in the fluorescence signals of both GCaMP6s and tdTomato and that these movement artifacts were mostly caused by licking behavior (**Figure 4.2**). Taking advantage of the expression of tdTomato, whose changes in fluorescence only report artifacts caused by movement / licking, we developed a correction algorithm to subtract these from the GCaMP6s signal.

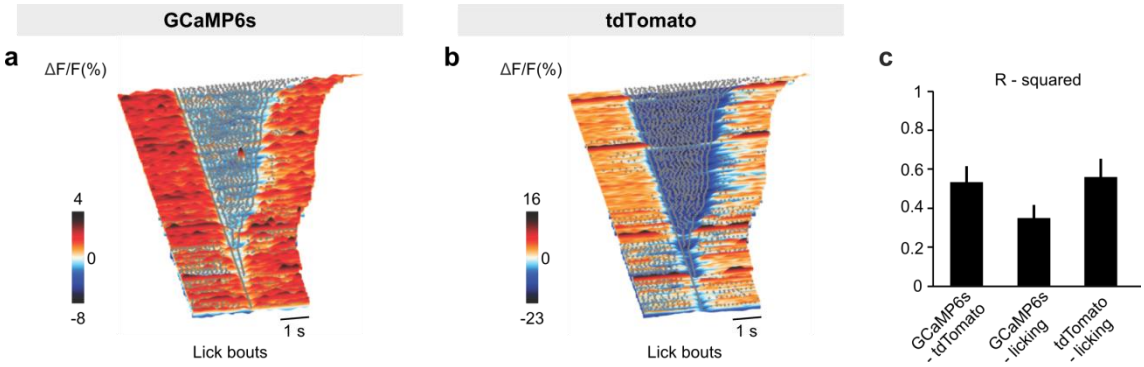

Figure 4.2. Lick bouts cause considerable changes in fluorescence of both the GCaMP6s and the tdTomato signals.

a, b. Surface plots showing raw GCaMP6s (a) and tdTomato (b) fluorescence signals aligned on the onsets of lick bouts during an example session of a SERT-Cre mouse. Gray dots represent single licks. Bouts were defined as sequences of licks separated by no more than 315 ms.

c. Bar plot showing R-squared values comparing GCaMP6s, tdTomato and licking signals calculated during 3 imaging sessions and averaged across all SERT-Cre mice (n = 10).

To validate our correction, we used another set of SERT-Cre animals infected with eYFP (instead of GCaMP6s) and tdTomato which were also trained in this classical conditioning task. These control mice are important to show that our movement correction algorithm is able to eliminate all artifacts, which should result in a flat corrected fluorescence signal in eYFP infected mice, but should not affect the calcium transients observed only in the green channel of GCaMP6s-transduced mice. In fact, the control mice showed the same type of movement artifacts in both eYFP and tdTomato fluorescence signals and we verified that, histologically, these controls were comparable to the GCaMP6s and tdTomato mice: there was a similar overlap between cells expressing the two fluorophores and the center of infection and implantation target were similar (**Figure 4.3**).

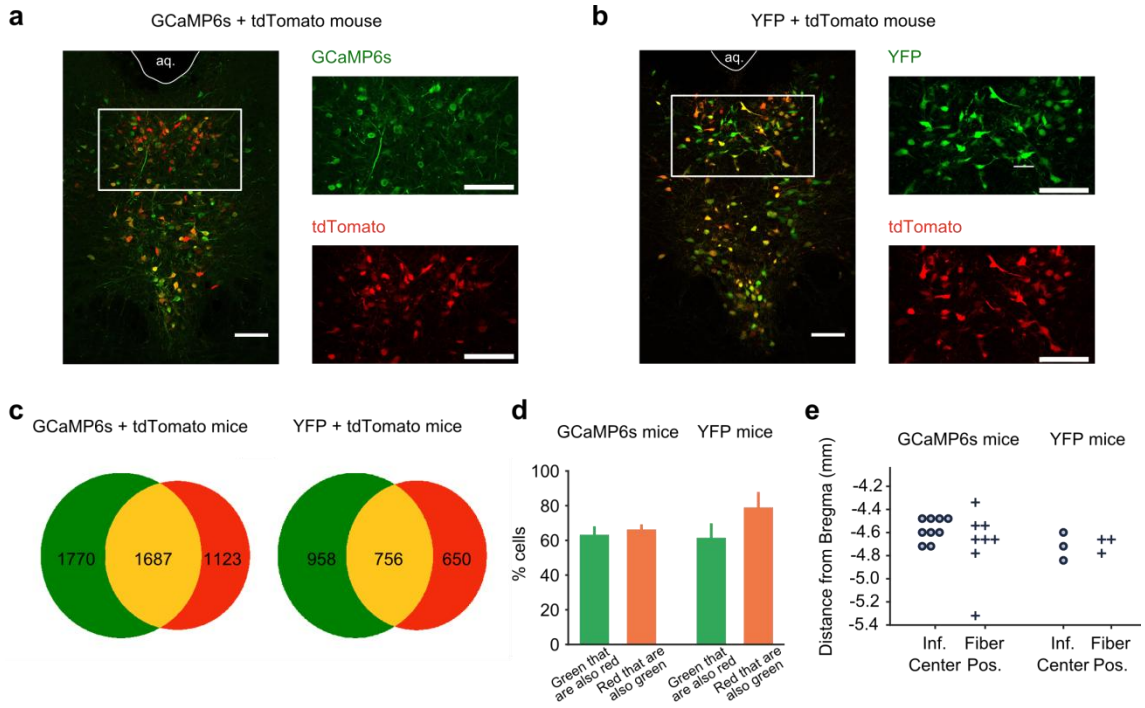

Figure 4.3. Expression of GCaMP6s and tdTomato has similar pattern to expression of YFP and tdTomato.

a, b. Confocal picture showing expression of GCaMP6s and tdTomato (a) and of YFP and tdTomato (b) in DRN 5-HT neurons. Scale bars: 100 µm. Aq. – aqueduct.

c. Total number of cells expressing green fluorophore (GCaMP6s or YFP), tdTomato, or both in SERT-Cre experimental and control mice (counted from 3 sections at the center of infection for each mouse, n = 6 GCaMP6s mice, n = 3 YFP mice)

d. Percent green and red cells that express both fluorophores in GCaMP6s and YFP infected mice (n = 6 GCaMP6s mice, n = 3 YFP mice). No statistical difference was obtained between the percentage of green cells that co-express tdTomato in GCaMP vs YFP mice, nor between the percentage of red cells that co-express a green fluorophore in GCaMP vs YFP mice (Mann-Whitney U test, n.s. for $p < 0.05$).

e. Antero-posterior location of the center of infection (circles) and of the fiber tip location (crosses) in the SERT-Cre mice used in behavioral experiments with good histology (n = 9 for GCaMP6s infection center, n = 8 for GCaMP6s fiber placement, n = 3 for YFP control mice).

To eliminate movement-related artifacts we used linear regression to decompose the green and red fluorescence signals into a shared component, which reflects movement-related changes, and a GCaMP6s-specific component, reflecting activity-dependent changes. To perform this correction, in each trial of the task, the relative change in fluorescence, $\Delta F/F_0 = (F-F_0)/F_0$, was calculated by considering F_0 the mean fluorescence during 1 s before the odor presentation for both the red and for the green channels ($[\Delta F/F_0]_{GREEN}$ and $[\Delta F/F_0]_{RED}$). Then, for each session of each mouse, the distribution of green to red values of $\Delta F/F_0$ was fitted by the sum of two Gaussians along the red channel and the crossing point between these 2 Gaussians was used as a boundary (excluding the first and last 100 ms of each trial because of filtering artifacts). All values of $[\Delta F/F_0]_{RED}$ below this boundary were used (to avoid noise fitting), together with the corresponding $[\Delta F/F_0]_{GREEN}$, to fit a linear regression line. Then, for each trial we corrected the green $\Delta F/F_0$ values using the parameters obtained with the regression model of that mouse in that session (*a* - slope; *b* - offset): $[\Delta F/F_0]_{GREEN\_corr} = [\Delta F/F_0]_{GREEN} - a*[\Delta F/F_0]_{RED} - b$ (**Figure 4.4**).

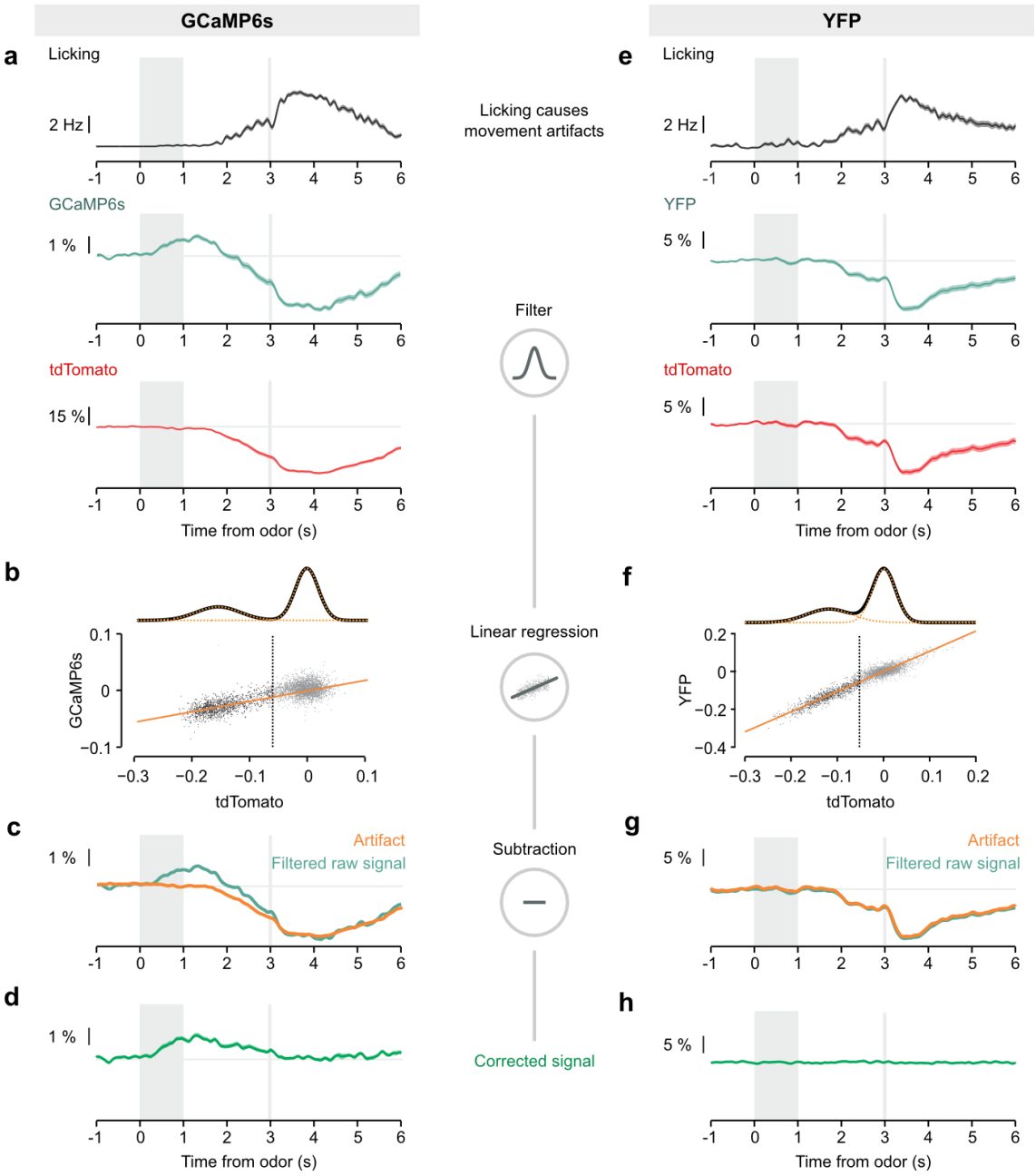

Figure 4.4. Linear regression approach to eliminate movement artifacts from neuronal imaging data.

a, e. Mean licking (top), mean filtered green fluorescence of GCaMP6s (a) or YFP (e), and mean filtered tdTomato fluorescence in large water reward trials in an example session of a SERT-Cre mouse transduced with GCaMP6s and tdTomato and of a SERT-Cre example mouse transduced with YFP and tdTomato. Data in *a* belongs to the same session represented in Figure 4.3.

b, f. Scatter plot and linear regression between tdTomato and GCaMP6s (b) or YFP (f) signals for the same sessions as before. tdTomato signals were often bimodal and well fit as a sum of 2 Gaussians (top; orange dotted curves, individual Gaussians; black curve, their sum). In order to avoid noise fitting, only data from the Gaussian not centered at 0 were included in the linear regression calculation (dark grey dots to the left of the vertical line). Orange solid lines indicate regression curves.

c, g. Mean filtered raw GCaMP6s (c) or YFP (g) signals and corresponding artifact predictions (calculated using linear regression as shown in *b* and *f*).

d, h. Corrected fluorescence signal obtained after the subtraction of the filtered raw signal by the artifact signal presented in *c* and *g*. While a calcium signal is still visible in the mouse infected with GCaMP6s (d), no signal is observed in the YFP control (h).

4.2.3 DA and 5-HT responses after initial learning

As mentioned before, we wanted not only to record 5-HT neurons' activity in the context of this reversal learning task but also to compare it to DA neuron's activity and look for evidences of any opponent interaction between the two.

Hence, we also targeted DA neurons in the VTA and SNc using the same viral vectors in TH-Cre (DA-specific) transgenic mice. We verified the specificity of GCaMP6s expression to DA neurons using histological methods (89 ± 2.5 %, mean ± SEM; n = 4 mice; **Figure 4.5**).

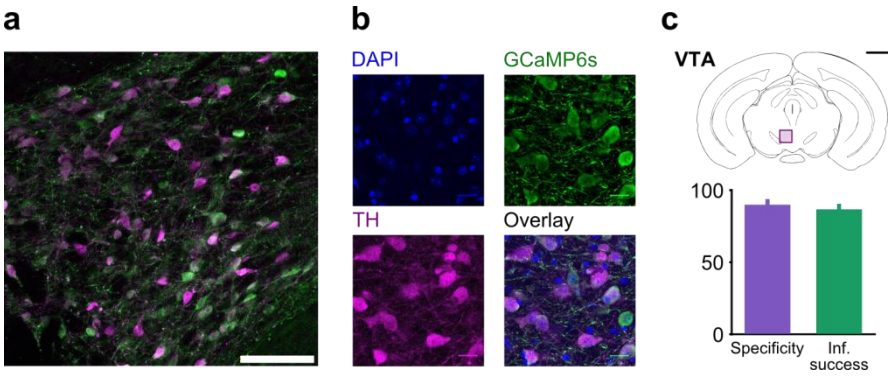

Figure 4.5. Specificity of GCaMP6s expression in VTA/SNc DA neurons.

d. Confocal picture of a coronal slice showing restricted GCaMP6s expression to VTA DA neurons in a TH-Cre mouse; scale bar: 100 µm.

e. Confocal pictures showing DAPI staining, GCaMP6s expression and TH immunoreactivity. Scale bar: 20 µm.

f. Top: schematics of a coronal slice view of the VTA signaling the area shown in figure in *a.* (violet rectangle); black scale bar: 1 mm. Bottom: quantification of specific expression of GCaMP6s in DA neurons (specificity: 89.9 ± 2.5 %, infection success: 86.7 ± 2.5 %, mean ± s.e.m, n = 4 mice).

As for SERT-Cre mice, in TH-Cre mice we also expressed tdTomato and used it for movement artifact correction of the fiber photometry system (**Figure 4.6**).

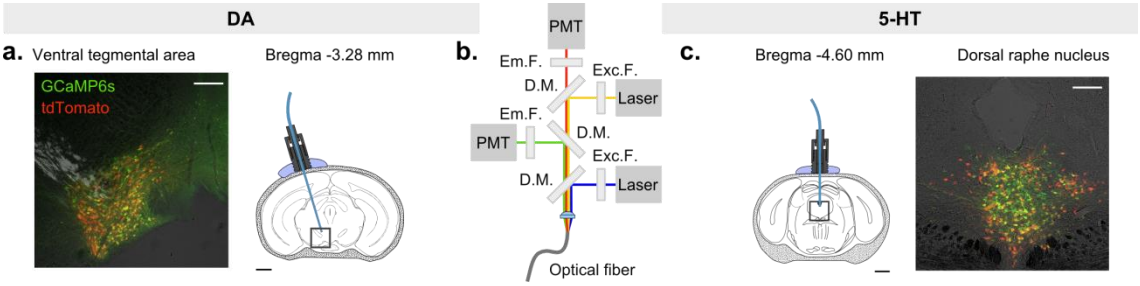

Figure 4.6. Photometry approach with movement artifact correction to dopamine and serotonin neuron population activity.

a. Coronal section showing expression of GCaMP6s and tdTomato in the VTA of a TH-Cre mouse (left) and schematics of infection and implant positioning in the VTA (right).

b. Fiber photometry setup used for excitation and acquisition of fluorescence of 2 different fluorophores: GCaMP6s (green, calcium activity dependent) and tdTomato (red, non-activity dependent).

c. Schematics of infection and implant positioning in the DRN (left) and coronal section showing expression of GCaMP6s and tdTomato in the DRN of a SERT-Cre mouse (right).
White scale bars: 200 µm; black scale bars: 1 mm. PMT – photomultiplier tube; Exc.F – excitation filter; Em.F – emission filter; D.M. – dichroic mirror.

After initial CS-US learning, different contingencies reliably elicited distinct 5-HT and DA neural responses triggered by odors and outcomes. These transient responses generally peaked within 1 s and declined to baseline again by around 2-3 s (example mice in **Figure 4.7 b, g**). As expected for a reward prediction error signal, DA neurons showed CS responses that paralleled their relative values indicated by licking rates (large reward > small reward > neutral ≈ air puff; example mouse **Figure 4.7b i.,** population data in **Figure 4.7c-e i.**). The magnitude of 5-HT CS responses also positively correlated with the relative value of the CS's (example in **Figure 4.7g i.,**, population data in **Figure 4.7h-j i.**), consistent with recent electrophysiological recordings of identified 5-HT[93] and non-identified DRN neurons[131].

Consistent with the idea that phasic activity of DA neurons reflects a balance between excitation and inhibition[143,144,164,328–330], in all TH-Cre mice we also observed a small phasic suppression to CS's that did not predict rewards. Phasic suppression of DA activity to the air puff cue is predicted by the classic TD learning algorithm, as the value of this US is negative (aversive). However, the fact that such suppression is also seen to the neutral CS suggests that, in the context of this task, the value of these neutral trials is actually below the average value of any unknown trial. This is expected given that the mice are thirsty and therefore a trial that is considered neutral in valance actually represents the omission of water which likely excites lateral habenula neurons[329]. Interestingly, in both mice infected and implanted in the VTA the suppression to neutral CS was stronger than the suppression to the air puff predicting CS, which migh reflect the contribution to the signal of a few DA neurons that are activated by aversive events[159,163] (**Figure 4.7b i.**).

As for 5-HT activity, such suppression to non-rewarded CSs was sometimes observed but not in all mice. When it was present it showed a slower and more sustained supression than the one observed in DA neurons (**Figure 4.7b i.**). This slow modulation is probably related to the changes in tonic activity that have been reported for indentified 5-HT[93] and non-identified DRN[131,177] neurons in classical conditioning tasks organized in blocks of rewarded and non rewarded trials. These studies report a considerable proportion of neurons with increased tonic activity in rewarded blocks versus in non-rewarded blocks and have attributed this characteristic to a representation of emotional state or mood.

In contrast to the CS responses, the magnitude of both DA and 5-HT neural signals to US's was small (**Figure 4.7b-e ii., g-j ii.**). For DA, the lack of response to a predictable US is explained by the theory of reward prediction error coding[140–142]. For 5-HT, this observation is also suggestive of a signal that is modulated by expectations. However, as previously reported[93], 5-HT neurons also showed a positive response to the air puff US (**Figure 4.7g-j ii.**). The close parallel between these observations and previously reported properties of DA[143] and 5-HT[93] neural responses, together with an absence of transients to either CS or US's recorded in SERT-Cre YFP-transduced control mice trained and tested in the same manner (**Figure 4.7h-i insets**), indicate that the fiber photometry fluorescence signals report a signal that is similar to that obtained in electrophysiological recordings in their respective populations.

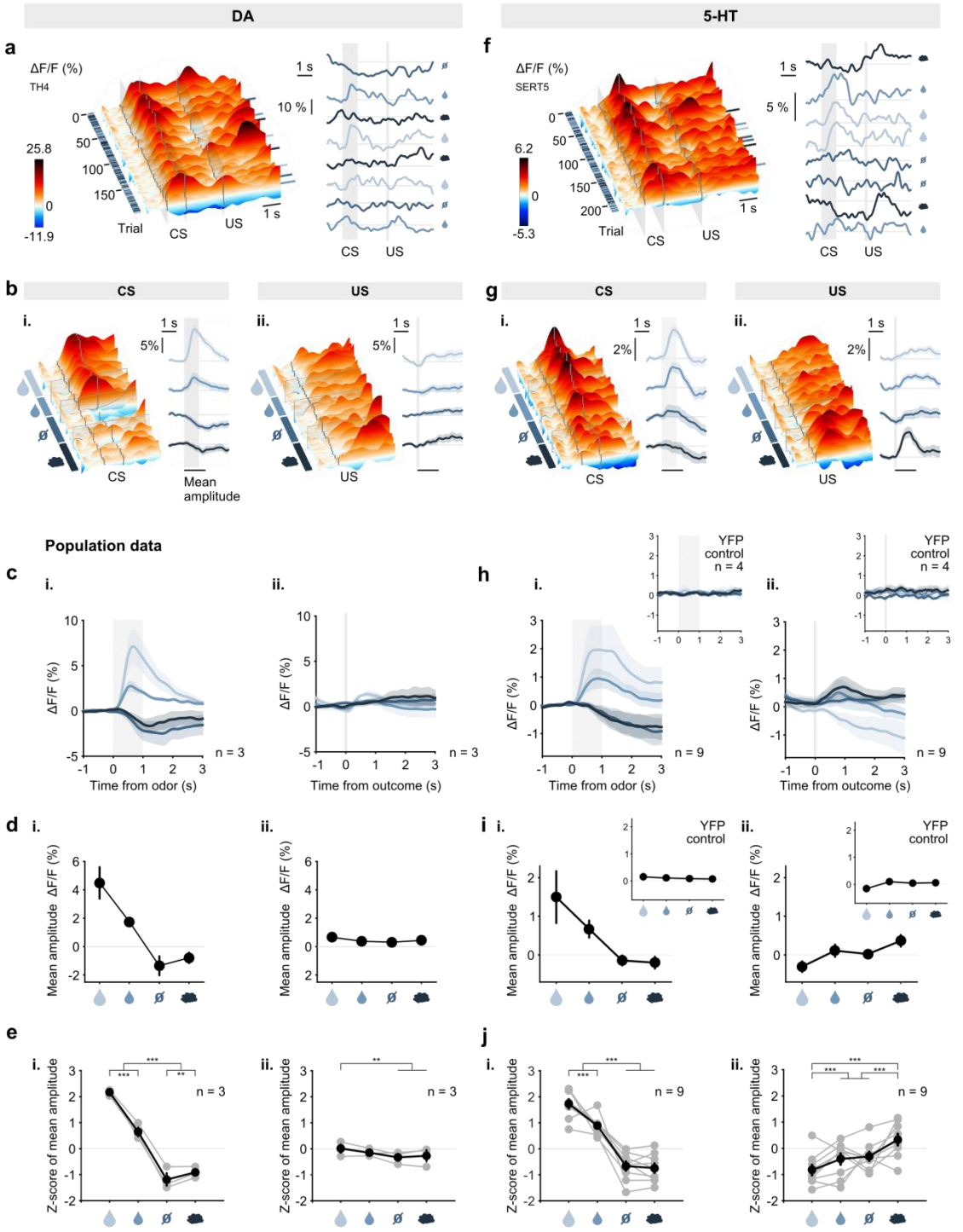

Figure 4.7. Dopamine and Serotonin neurons respond to reward predicting cues but only serotonin neurons respond to air puff.

a, f. Fluorescence data of a TH-Cre mouse example session (a) and of a SERT-Cre mouse example session (f) showing interleaved trials (left) and randomly selected example trials (2 of each type) from each session (right) signaled by small lines on the right of the surface plots.

b, g. Surface plots show the same sessions as in *a* and *f* respectively, with trials ordered by trial type. CS (i.) and US (ii.) responses are separated. Mean responses of all trials of the corresponding session (for each trial type) are shown on the right to the surface plots. Shaded areas represent 95% confidence intervals.

c, h. Mean (± s.e.m) CS (i.) and US (ii.) responses of all TH-Cre mice (c, n = 3), of all SERT-Cre mice (h, n = 9) and of all YFP infected SERT-Cre mice (insert in *h*, n = 4) after having learned the CS-US associations. Shaded areas represent s.e.m..

d, i. Mean fluorescence amplitude (mean of 1.5 s after event onset ± s.e.m) in response to CS's (i.) and US's (ii.) across all TH-Cre mice (d, n = 3), all SERT-Cre mice (i, n = 9) and all YFP infected SERT-Cre mice (insert in *i.*, n = 4) after having learned the CS-US associations. Shaded areas represent s.e.m..

e, j. Z-scores of mean fluorescence (mean fluorescence in a 1.5 s period after CS or US onset) for CS (i.) and US (ii.) across trial types for all TH-Cre mice (d, grey dots represent individual mice n = 3 mice) and for all SERT-Cre mice (g, n = 9 mice). (3-way ANOVA with factors day, mouse and trial type followed by pos hoc multiple comparisons for trial type: only statistically significant comparisons are shown: * $p < 0.05$, ** $p < 0.01$, *** $p < 0.001$).

4.2.4 DA and 5-HT responses to positive reversals

Approximately two weeks after the onset of training (12.7 ± 1.6, mean ± SD sessions) we reversed the CS-US contingencies in pairs, so that the CS's associated with large and small rewards now predicted the air puff and neutral outcomes respectively, and vice versa (**Figure 4.8a**). After reversal, mice gradually learned the new CS-US associations, as indicated by changes in their anticipatory licking during CS and trace periods (**Figure 4.8b**) for each US (trial type).

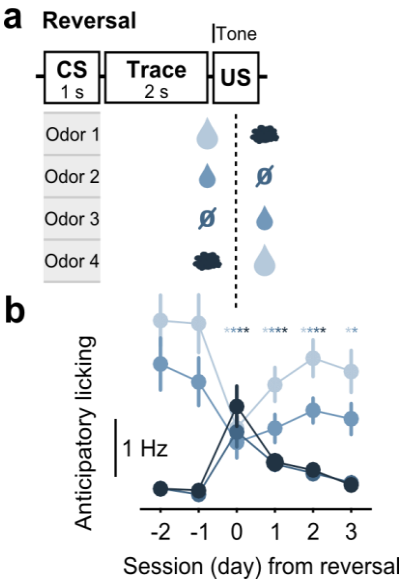

Figure 4.8. Mice adapt their licking behavior to reversed CS-US contingencies

a. Schematics of the reversal procedure. In the reversal session, after some trials with the learned CS-US associations (mean ± SD: 73 ± 12), the contingencies were reversed, so that odors 1 and 2 became to predict air puff and neutral respectively, while odors 3 and 4 became to predict small and large reward respectively.

b. Anticipatory licking (mean of odor and trace period) across mice for sessions around reversal showing that for each trial type licking is adjusted after reversal. Colors follow US identity (not odor), so that, for a given US, the reversal day shows a licking pattern that is influenced by the licking pattern of a different US that used to be associated with the odor now presented. Over time, as mice re-learn the new CS-US associations licking pattern looses the influence of the US previously associated with a particular odor (2-way ANOVA for large reward $F_{4,3449} = 192.96$, $p < 0.001$, for small reward $F_{4,3447} = 114.62$, $p < 0.001$, for neutral $F_{4,3382} = 93.17$, $p < 0.001$, for air puff $F_{4,3449} = 160.97$, $p < 0.001$; multiple comparisons with the 2 days before reversal (-1 and -2) using Scheffé's method are signaled in the figure with colored asterisks according to trial type: * $p < 0.001$).

We next examined how DA and 5-HT neural responses change when CS-US contingencies are reversed. The reversal task allowed us to examine several implications of the prediction error theory of DA. First, we examined positive surprises, which occur when, after reversal, the large reward US was delivered following the CS that previously predicted the air puff (**Figure 4.8**). This condition should generate a large positive RPE, and a large transient increase in DA signal was in fact observed (**Figure 4.9a-c**). Smaller positive RPEs would also be generated for the reversal from neutral to small reward, and this too was observed (**Figure 4.10a-c**).

More surprisingly, reversal of associations also triggered robust US responses in 5-HT neurons. As for DA neurons, 5-HT neurons responded positively to a better than expected outcome when a large reward was delivered following a CS previously paired with an air puff (**Figure 4.9d-f**).

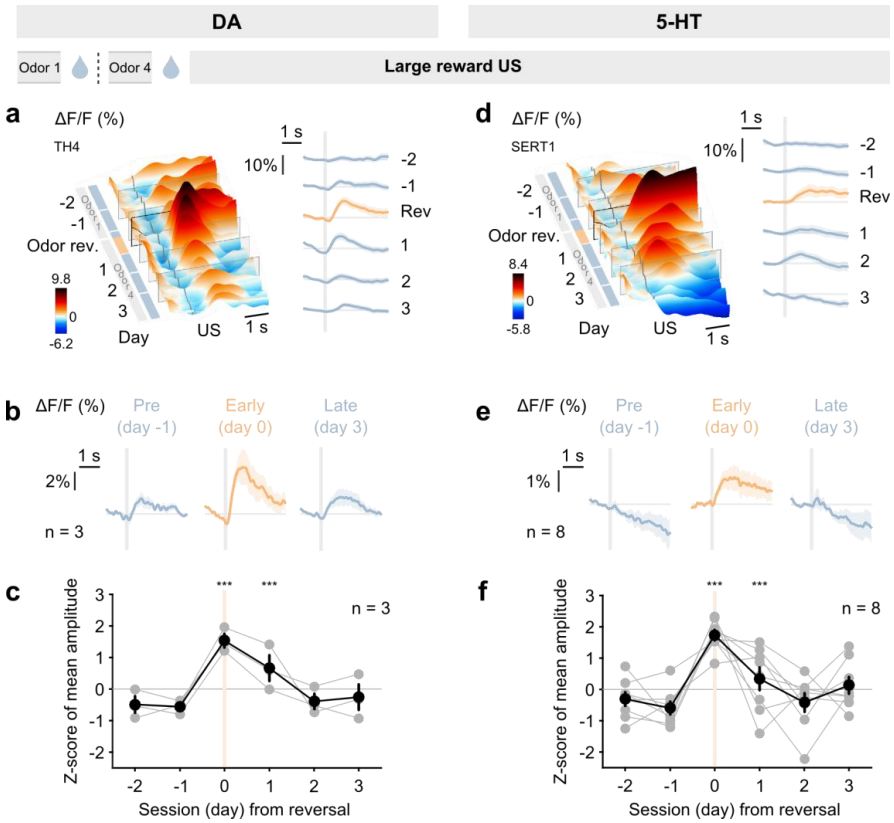

Figure 4.9. Both Dopamine and Serotonin neurons show reward prediction error activity.

Dopamine and serotonin neurons' responses to large reward unconditioned stimulus are temporarily increased after reversal of the CS-US associations.

a, d Responses to large reward delivery across sessions (from 2 sessions before reversal to 3 sessions after it) of a TH-Cre mouse (a) and of a SERT-Cre mouse (d). Surface plots on the left represent all trials of each session while plots on the right show mean of all large reward trials in each session. Reversed trials in the reversal session are shown in orange. Shaded areas represent 95% confidence intervals.

b, e Mean responses to large reward delivery in the day before reversal (Pre), in the reversal day (Early) and 3 days after reversal (Late) for all TH-Cre mice (b, n = 3) and for all SERT-Cre mice (h, n = 8). Shaded areas represent s.e.m.

c, f Z-score of the mean fluorescence transient (mean fluorescence in a 1.5 s after US onset) in response to large reward delivery across days around reversal for all TH-Cre mice (c, grey dots n = 3 mice) and for all SERT-Cre mice (f, grey dots n = 8 mice). Black dots represent mean ± s.e.m. across mice for each session (2-way ANOVA, $F_{4,853} = 30.24$, $p < 0.001$ for DA and $F_{4,2592} = 38.65$, $p < 0.001$ for 5-HT; *pos hoc* multiple comparisons with 2 days before reversal using Scheffé's method are signaled in the figure).
* $p < 0.05$, ** $p < 0.01$, *** $p < 0.001$

Similarly, 5-HT neurons also responded to unpredicted small rewards after reversal, also showing a smaller prediction error when compared to an unexpected large reward (**Figure 4.10d-f**). Together, these observations show that both DA and 5-HT neurons respond similarly to rewarding US's both during steady-state and immediately after reversals, suggesting that both systems are sensitive to violations of the expectations generated by previous associative learning.

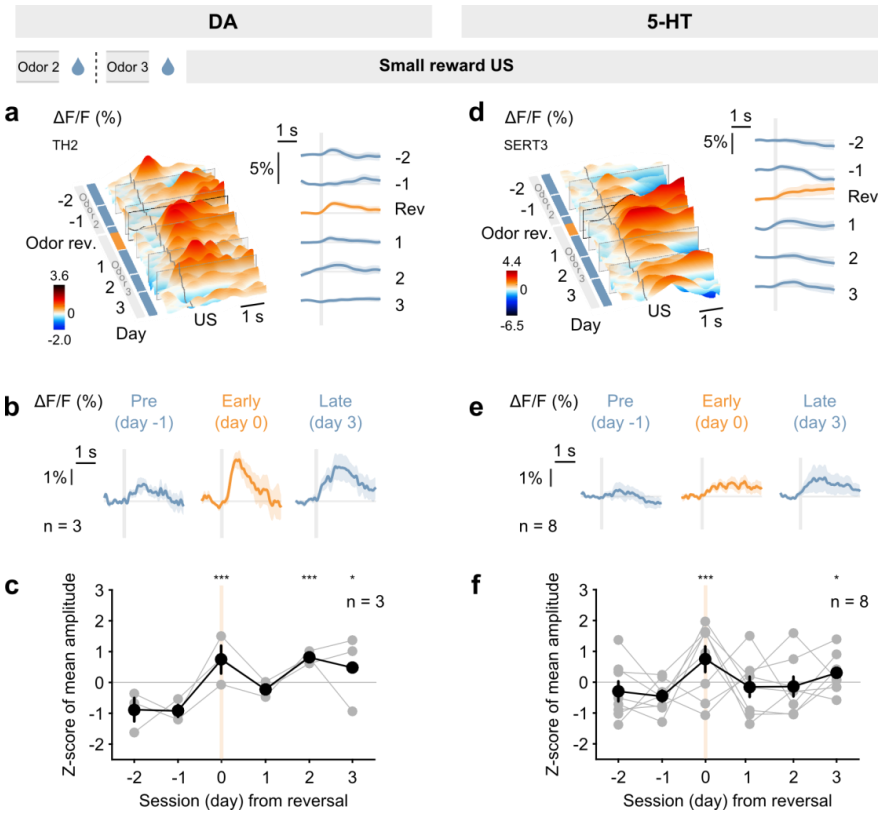

Figure 4.10. Responses of DA and 5-HT neurons to small reward during reversal.

a, d Responses to small reward delivery across sessions (from 2 sessions before reversal to 3 sessions after it) of a TH-Cre mouse (a) and of a SERT-Cre mouse (d). Surface plots on the left represent all trials of each session while plots on the right show mean of small reward trials in each session. Reversed trials in the reversal session are shown in orange. Shaded areas represent 95% confidence intervals.

b, e Mean responses to small reward delivery in the day before reversal (Pre), in the reversal day (Early) and 3 days after reversal (Late) for all TH-Cre mice (e, n = 3) and for all SERT-Cre mice (k, n = 8). Shaded areas represent s.e.m.

c, f Z-score of the mean fluorescence transient (mean fluorescence in a 1.5s after US onset) in response to small reward delivery across days around reversal for all TH-Cre mice (f, grey dots n = 3 mice) and for all SERT-Cre mice (l, grey dots n = 8 mice). Black dots represent mean ± s.e.m. across mice for each session (2-way ANOVA, $F_{4,911} = 9.22$, $p < 0.001$ for DA and $F_{4,2532} = 7.96$, $p < 0.001$ for 5-HT; multiple comparisons with 2 days before reversal using Scheffé's method are signaled in the figure). * $p < 0.05$, ** $p < 0.01$, *** $p < 0.001$

4.2.5 DA and 5-HT responses to negative reversals

To test further how 5-HT neurons encode prediction errors, we analyzed DA and 5-HT responses to "negative surprises" that occurred, immediately after reversal, for trials in which the CS that had predicted the delivery of small water reward up until that moment was now followed by a neutral outcome (tone only) (**Figure 4.8**). For these trials DA neurons showed a small but significant supression, consistent again with the RPE theory, since the difference between expected and actual outcome value was negative (**Figure 4.11a-c**). This suppression of DA firing was clearly visible for the first 1-5 trials after reward omission, but hardly visible after them.

In strong contrast, 5-HT neurons showed a robust and transient increase in activity following the same unexpected reward omissions (**Figure 4.11d-f**).

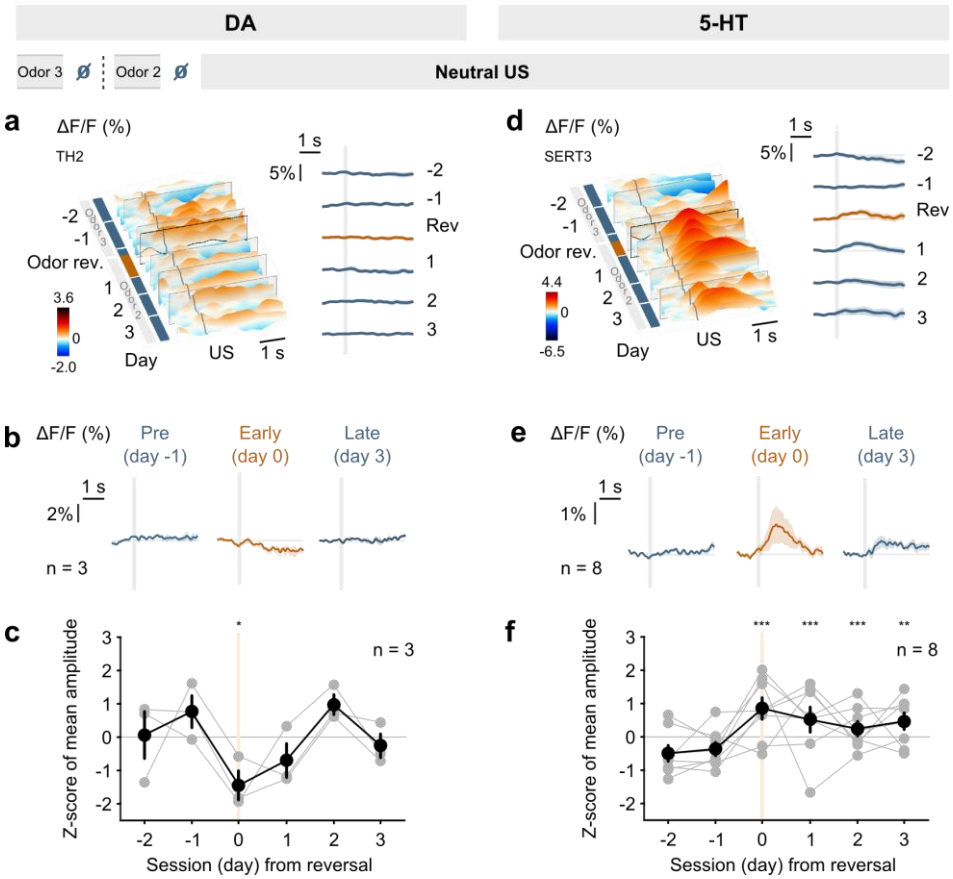

Figure 4.11. Serotonin neurons, but not dopamine neurons, are excited by reward omission.

a, d Responses to neutral (tone only) delivery across sessions (from 2 sessions before reversal to 3 sessions after it) of a TH-Cre mouse (a) and of a SERT-Cre mouse (d). Surface plots on the left represent all trials of each session while plots on the right show mean of all neutral trials in each session. Reversed trials in the reversal session are shown in orange. Shaded areas represent 95% confidence intervals.

b, e Mean responses to neutral outcome in the day before reversal (Pre), in the reversal day (Early) and 3 days after reversal (Late) for all TH-Cre mice (b, n = 3) and for all SERT-Cre mice (e, n = 8). Shaded areas represent s.e.m.

c, f Z-score of the mean fluorescence transient (mean fluorescence in a 1.5s after US onset) in response to neutral (tone only) outcome across days around reversal for all TH-Cre mice (b, grey dots n = 3 mice) (c) and for all SERT-Cre mice (f, grey dots n = 8 mice). Black dots represent mean ± s.e.m. across mice for each session (2-way ANOVA, $F_{4,843} = 4.56$, $p = 0.0012$ for DA and $F_{4,2535} = 13.39$, $p < 0.001$ for 5-HT; multiple comparisons with 2 days before reversal using Scheffé's method are signaled in the figure).
* $p < 0.05$, ** $p < 0.01$, *** $p < 0.001$

We also examined the negative prediction error that occurred when the air puff was delivered after a CS that had predicted the delivery of a large reward. For DA neurons, we observed a significant transient decrease (**Figure 4.12a-c**), again consistent with RPE theory. For 5-HT neurons, because a response to air puff was generally present even before reversal, we observed no significant change in this response after reversal (**Figure 4.12d-f**). Still, in 2 out of 8 mice, this activation was even larger after reversal.

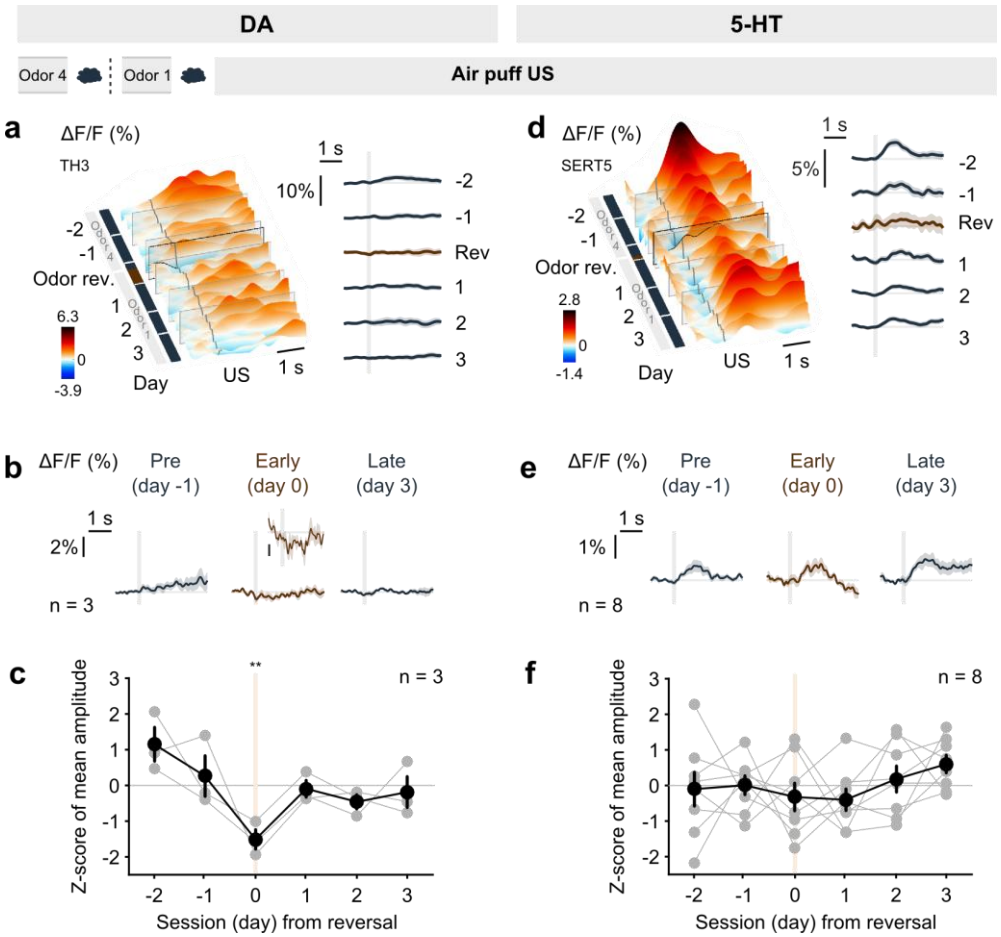

Figure 4.12. Responses of DA and 5-HT neurons to air puffs during reversal

a, d Responses to air puff delivery across sessions (from 2 sessions before reversal to 3 sessions after it) of a TH-Cre mouse (a) and of a SERT-Cre mouse (d). Surface plots on the left represent all trials of each session while plots on the right show mean of air puff trials in each session. Reversed trials in the reversal session are shown in orange. Shaded areas represent 95% confidence intervals.

b, e Mean responses to air puff delivery in the day before reversal (Pre), in the reversal day (Early) and 3 days after reversal (Late) for all TH-Cre mice (b, n = 3) and for all SERT-Cre mice (e, n = 8). Shaded areas represent s.e.m. Inset in middle plot shows the mean of the first 2 trials of reward omission / unexpected air puff delivery and bar represents again 2% change in fluorescence.

c, f Z-score of the mean fluorescence transient (mean fluorescence in a 1.5s after US onset) in response to air puff delivery across days around reversal for all TH-Cre mice (c, grey dots n = 3 mice) and for all SERT-Cre mice (f, grey dots n = 8 mice). Black dots represent mean ± s.e.m. across mice for each session (2-way ANOVA, for air puff $F_{4,881} = 5.21$, $p = 0.0004$ for DA and $F_{4,2564} = 2.72$, $p = 0.0284$ for 5-HT; multiple comparisons with 2 days before reversal using Scheffé's method are signaled in the figure).

* $p < 0.05$, ** $p < 0.01$, *** $p < 0.001$

4.2.6 DA and 5-HT responses to surprising events

To further test how DA and 5-HT neurons respond to surprising events, 5 days after reversal, we introduced 20% surprise trials in each session (**Figure 4.13**). In these trials, one of the US's was randomly selected and delivered at the time that the CS would normally be presented.

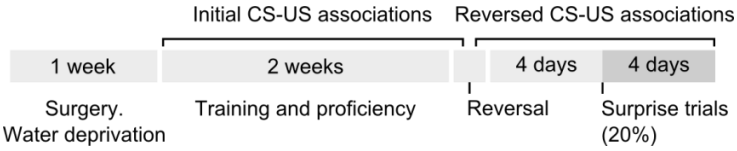

Figure 4.13. Complete experimental timeline showing introduction of surprise trials.

Consistent with the previous observations concerning positive surprises after reversal, for both DA and 5-HT neurons, surprise rewards produced larger responses than the equivalent rewards did when they were preceded by a well-learned cue (**Figure 4.14**). For DA neurons, surprise neutral trials (tone only) and surprise air puffs produced a small initial rise followed by supression, similar to previous observations in electrophysiological recordings[160]. In contrast, for 5-HT neurons, surprise neutral trials produced a small but significant increase in activity, and both surprise and predicted air puffs produced large responses (**Figure 4.14**).

The observation that all surprise trials, even neutral tones, elicited a positive transient response in 5-HT neurons supports the idea that 5-HT neurons, unlike DA neurons, are activated by mismatches between predicted and real outcomes whether they are positive, negative or neutral with respect to value.

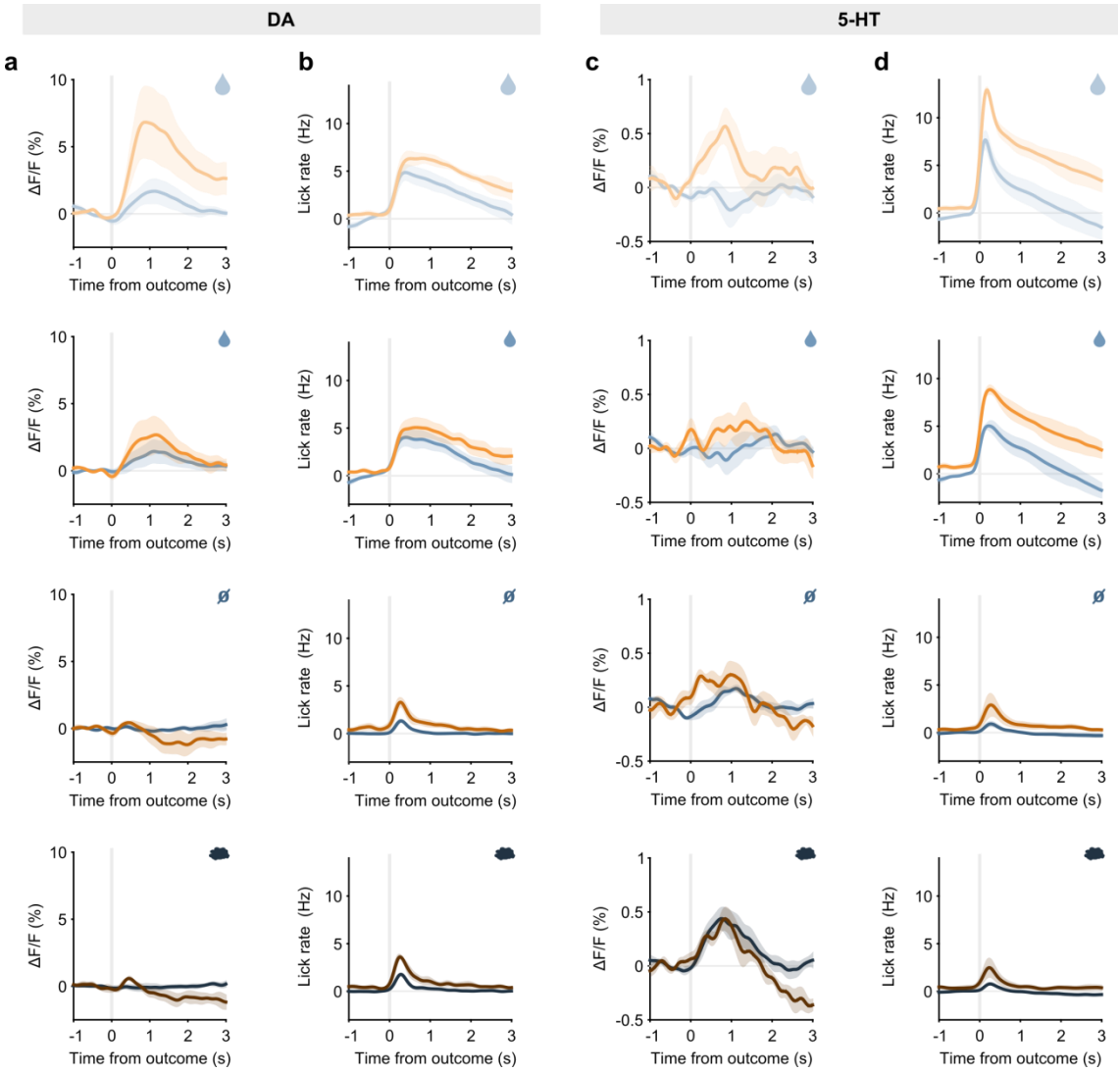

Figure 4.14. Responses of DA and 5-HT neurons to surprising outcomes.

Mean neural activity (a,c) and licking (b,d) in response to predicted and surprise US's for all TH-Cre mice (a,b, n = 3), and of all SERT-Cre mice (c,d, n = 4) to predicted (blue hue) and unpredicted (orange hue) outcomes. Lightness of colors represents trial types, shaded areas represent s.e.m.

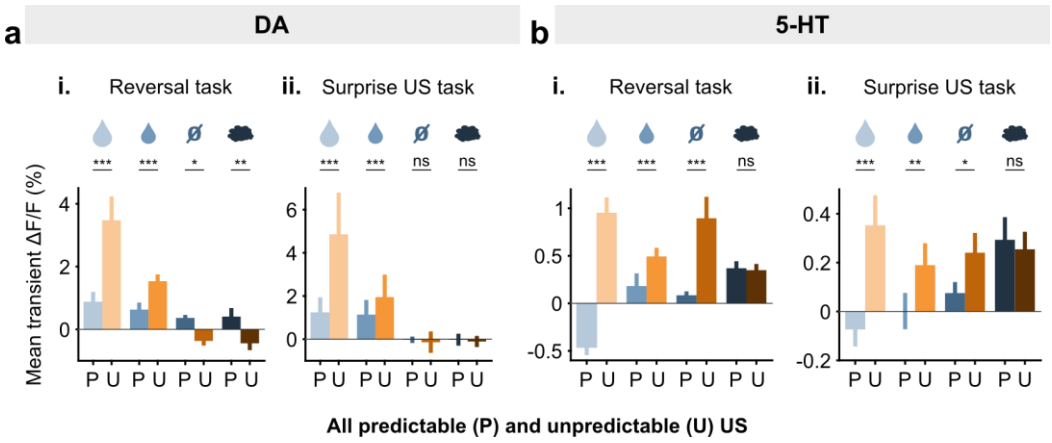

Figure 4.15. While DA neurons are activated by better-than-expected outcomes, 5-HT neurons are activated both by better-than-expected and worse-than-expected outcomes.

a, b i. Comparison of mean fluorescence transient day before reversal (P) and reversal day (U) to summarize responses to predicted (blue hues) and unpredicted (orange hues) outcomes during reversal learning for all trial types in DA (a) and 5-HT neurons (b).

a, b ii. Four sessions after reversal, surprise trials were introduced. These consisted of unpredicted US (of any of the four types) delivered instead of the odor after the foreperiod. While dopamine neurons showed stronger responses to unpredicted compared to predicted rewards only (*a*, grey dots, n = 3 mice, large reward $F_{1,642} = 175.05$, $p < 0.001$, small reward $F_{1,589} = 17.53$, $p < 0.001$, neutral $F_{1,673} = 0.52$, $p = 0.4707$, air puff $F_{1,601} = 0.28$, $p = 0.5598$), serotonin neurons also had significantly stronger responses to unpredicted than to predicted neutral US (*b*, grey dots, n = 4 mice, large reward $F_{1,923} = 43.06$, $p < 0.001$, small reward $F_{1,944} = 8.75$, $p = 0.0032$, neutral $F_{1,924} = 6.14$, $p = 0.0134$, air puff $F_{1,924} = 0.47$, $p = 0.4914$). Bars represent s.e.m. across mice for each condition (4 sessions with 20% surprise trials were pooled together).
* $p < 0.05$, ** $p < 0.01$, *** $p < 0.001$

Thus, whereas DA neurons showed opposite responses to better than and worse than expected outcomes (**Figure 4.15a i.**), 5-HT neurons showed increases for both kinds of prediction violations (**Figure 4.15b i.**). Similarly, when unpredicted US's were delivered at the time an odor would be expected, 5-HT neurons showed transient responses to the four types of US. This pattern of activations is consistent with a surprise or unsigned prediction error signal. Responses of unidentified DRN neurons to omitted rewards have previously been reported[131,179], but responses to unpredicted events may have been underappreciated in previous studies which did not focus on conditions of environmental change[93,176].

4.2.7 Distinct trial-by-trial dynamics of DA and 5-HT responses

The reversal paradigm afforded the possibility to examine not only immediate responses to changes in environmental contingencies, but also the time course of the adaptation of neuromodulatory systems to these changes. Following either positive or negative reversals, anticipatory licking rates gradually returned to pre-reversal conditions over several sessions (**Figure 4.8**). Likewise, DA and 5-HT neural responses to odor cues also returned to their pre-reversal levels (**Figure 4.16 a-f**). Interestingly, however, the two systems showed markedly different dynamics: 5-HT neurons' CS responses returned to baseline with a significantly slower time course than those of DA neurons (**Figure 4.16 g-i**). This was true both for adaptation to negative reversals (CS no longer predicting a reward, $\tau = 21 \pm 8.7$ trials for DA and 96 ± 20.4 trials for 5-HT, mean ± S.E.M. in **Figure 4.16i**) and positive reversals (CS starts predicting a

reward, τ = 33 ± 6.8 trials for DA and 127 ± 25.1 trials for 5-HT, mean ± S.E.M.). In particular, the time course of 5-HT neurons' responses is also slower than the corresponding licking time course (**Figure 4.16i** left).

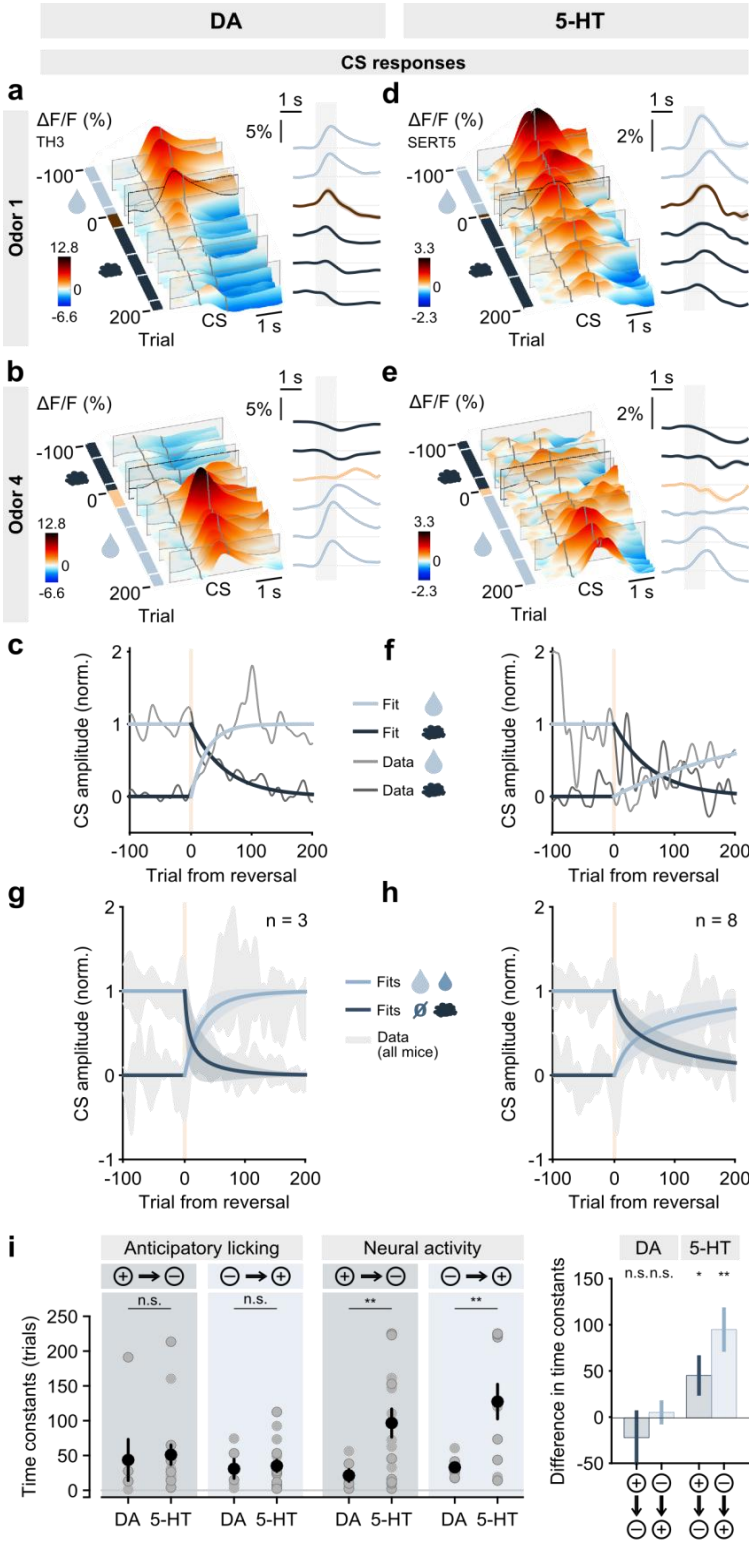

Figure 4.16. Post-reversal changes in CS activity are slower in 5-HT neurons than in DA neurons.

a, d. CS responses to odor 1 presentation which predicts large reward before reversal and air puff after it in a TH-Cre example mouse (a) and in a SERT-Cre example mouse (d). 300 trials (taken from 7 sessions) were concatenated. Surface plots on the left represent 100 trials before and 300 trials after reversal. Plots on the right show mean of the trials taken from those sessions. Shaded areas represent 95% confidence intervals.

b, e. CS responses to odor 4 presentation which predicts air puff before reversal and large reward after it for same mice as in *a* and *d*. 300 trials (taken from 7 sessions) were concatenated.

c, f. Normalized exponential fits to the mean amplitude (in 1.5 s) of the CS responses across trials around reversal for the example mice (c corresponds to mouse in *a,b*; f corresponds to mouse in *d,e*) in odors 1 and 4.

g, h. Normalized exponential fits to the mean amplitude (in 1.5 s) of the CS responses across trials around reversal for all TH-Cre (left, n = 3) and all SERT-Cre (right, n = 8) mice. Fits were performed for each odor and each mouse, odors 1 and 2 (dark blue after reversal) were averaged together as well as odors 3 and 4 (light blue after reversal), across mice; shaded areas represent s.e.m. Grey shades present average and s.e.m. of corresponding normalized average data.

i. Left: Time constants of the exponential fits obtained for dopamine and serotonin mice during reversal for both anticipatory licking and CS neural response. Time constants of change in anticipatory licking were not significantly different between TH-Cre and SERT-Cre mice for either a negative change (i.e. to decrease licking – odors 1 and 2 – unpaired t-test p = 0.8163) or for a positive change (i.e. to increase licking – odors 3 and 4 – unpaired t-test p = 0.8131). However, SERT-Cre mice showed slower changes in neural signals after reversal both in response to odors 1 and 2 (unpaired t-test p = 0.0030) and 3 and 4 (unpaired t-test p = 0.0023). Grey dots represent individual mice for odors 1 and 3, grey dots with darker edge represent individual mice for odors 2 and 4. Black dots represent mean ± s.e.m. in each condition. Right: Mean across mice of the difference between fluorescence and corresponding licking time constants showing that activity of serotonin neurons changes significantly slower than the behavior. * p < 0.05, ** p < 0.01, *** p < 0.001

Considering that DA and 5-HT may be acting in concert, the difference in the speed to which the two systems adapt to environmental change gave rise to a potentially important asymmetry in adaptation to positive and negative reversals. During a change from negative (or neutral) to positive outcomes (**Figure 4.17b**), because the buildup of 5-HT is much slower than that of DA, the difference signal is temporarily biased toward DA. Conversely, during a reversal from positive to negative outcome association (**Figure 4.17a**), because 5-HT neuronal signals evoked by positive CS's persist longer than those of DA, the difference is temporarily biased toward 5-HT. The implications of the difference in dynamics and resulting asymmetry are discussed below.

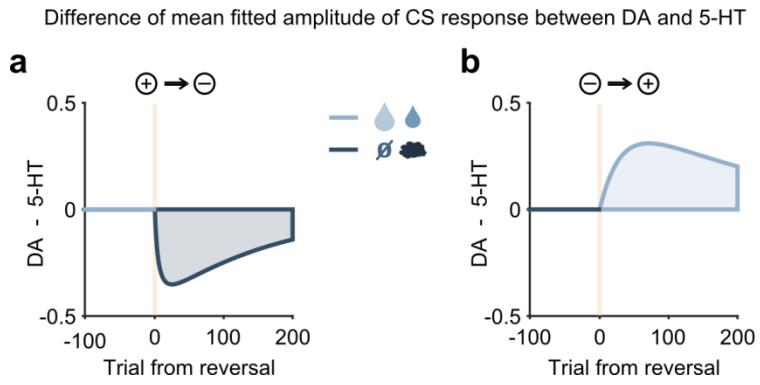

Figure 4.17. After reversal the difference signal is biased towards one neuromodulator or the other.

Difference of mean fitted amplitude of CS response change between DA and 5-HT during a negative change (a, need to stop licking, odors 1 and 2) and during a positive change (b, need to start licking, odors 3 and 4).

4.3 Discussion

Here, we studied in parallel activity-dependent fluorescence signals from populations of midbrain DA neurons and DRN 5-HT neurons during a reversal-learning paradigm. We found that midbrain DA neurons, as expected from previous theory and observations, showed transient responses consistent with a signed reward prediction error[140,143]. More unexpectedly, 5-HT neurons were also strongly sensitive to the unexpected outcomes that occur after sudden reversal of cue-reward associations. Importantly, 5-HT neurons responded to both positive and negative surprises with increases in activity; they also showed enhanced responses to rewards and even neutral events (tones) when they were delivered at unexpected times. These results suggest that 5-HT neurons report an unsigned prediction error, that is, a signal that conveys surprise rather than valence. Thus, 5-HT neurons appear to report a form of uncertainty, a function recognized to be critical for reinforcement learning and behavioral control[331,332], but previously assigned to norepinephrine and acetylcholine[332]. Also consistent with the concept of a value-neutral signal, 5-HT neurons respond positively to mildly aversive air puffs as well as rewards[93,130]. This is unlikely to reflect two distinct 5-HT populations since the same bi-valent response profiles exist in single neurons[93]. However, whereas anticipatory licking showed that mice learned cue-reward associations, there was no behavioral evidence that mice learned cue-air puff associations. This could explain why, compared to water-evoked responses, serotonin

air-puff responses were less sensitive to expectations. A related possibility is that the persistence of air puff responses relates not to inability of the mice to predict but to their inability to control the aversive stimulus through their behavioral response, as has been reported in eyelid conditioning studies using comparable trace periods[326,327]. Predictable but uncontrollable shocks robustly activate the immediate early gene c-*fos* in DRN 5-HT neurons[129] and this activation is lowered by controllability signals from the ventral medial prefrontal cortex[333,334]. Thus 5-HT transients may report "control errors" rather than prediction errors.

These observations provide insight into the functions of 5-HT in reversal learning and, by extension, adaptive behavior in general. Surprise signals that a learned association or internal model may be invalid. A first potential role for 5-HT in reversal learning is using this information to directly inhibit behaviors based on the erroneous model. The responses of 5-HT neurons to cues reported here were rapid enough to inhibit cue-evoked anticipatory licking after reversal. Invigorating DA cue responses and inhibiting 5-HT cue responses would tend to cancel one another. However, the difference in the time scale at which DA and 5-HT adapted over trials to changes in CS-reward associations implies an asymmetry in DA/5-HT balance depending on the directionality of environmental change. Because CS-evoked 5-HT responses adapt more slowly than do DA responses, withdrawal of rewards will favor 5-HT and behavioral inhibition, helping to avoid perseveration, whereas encountering new rewards will favor DA and behavioral invigoration. A second role for surprise signals is with respect to learning. Surprise signals, unlike signed prediction errors, cannot be used to drive a corrective learning process. But they do indicate increased uncertainty in an environment, a signal that in Bayesian accounts calls for enhanced learning[331]. Surprising events are known to accelerate the rate of learning[335] and our data suggest that 5-HT transients are well suited to contribute to this process. Thus, 5-HT may contribute to adaption to abrupt environmental changes not only by inhibiting inappropriate behaviors, but by boosting the rate at which the brain itself adapts. Direct activation of 5-HT neurons does not appear to cause appetitive or aversive learning[118,119,178,336,337], but serotonin enhances cortical plasticity[338,339] and neurogenesis[340]. 5-HT might also augment, depress or modulate the impact of other learning processes, such as those mediated by DA-dependent or Hebbian learning[341,342]. Taken together with previous data, our results suggest that a value-neutral surprise-related signal can best account for a range of data on the firing of 5-HT neurons. This in turns suggests that the contribution of 5-HT to affective control and mood disorders is the consequence of more primary functions in prediction, control and learning.

4.4 Methods

Animals

All procedures were reviewed and performed in accordance with the Instituto Gulbenkian de Ciência and the Champalimaud Centre for the Unknown Ethics Committee guidelines, and approved by the Portuguese Veterinary General Board (Direcção Geral de Veterinária, approval ID 018831). Twenty two C57BL/6 male mice between 2 and 9 months of age were used in this study. Mice resulted from the backcrossing of BAC transgenic mice into Black C57BL for at least six generations, which express the Cre recombinase under the control of specific promoters. Eighteen mice expressed Cre under the serotonin transporter gene (Tg(Slc6a4-cre)ET33Gsat/Mmucd) from GENSAT[220], and 4 mice under the tyrosine hydroxylase gene, 2 mice (Tg(Th-cre)FI12Gsat/Mmucd) from GENSAT[220], and 2 mice (B6.Cg-Tg(Th-Cre)1Tmd/J) from The Jackson Laboratory[343]. Animals (25 – 45 g) were group-housed prior to surgery and individually housed post-surgery and kept under a normal 12 hour light/dark cycle. All experiments were performed in the light phase. Mice had free access to food. After training initiation, mice used in behavioral experiments had water availability restricted to the behavioral sessions.

Stereotaxic viral injections and fiber implantation

Mice were deeply anaesthetized with isoflurane mixed with O_2 (4% for induction and 0.5–1% for maintenance) and placed in a stereotaxic apparatus (David Kopf Instruments). Butorphanol (0.4 mg/kg) was injected subcutaneously for analgesia and Lidocaine (2%) was injected subcutaneously before incising the scalp and exposing the skull. For SERT-Cre mice a craniotomy was drilled over lobule 4/5 of the cerebellum and a pipette filled with a viral solution was lowered to the DRN (bregma -4.55 anterioposterior (AP), -2.85 dorsoventral (DV)) with a 32° angle toward the back of the animal. For the 2 TH-Cre mice from The Jackson Laboratory the pipette was targeted to the VTA (bregma -3.3 AP, 0.35 mediolateral (ML), -4.2 DV) with a 10° lateral angle, and for the 2 TH-Cre mice from GENSAT we targeted the SNc (bregma -3.15 AP, 1.4 ML, -4.2 DV). Viral solution was injected using a Picospritzer II (Parker Hannifin) at a rate of approximately 38 nl per minute. The expression of all fluorophores was Cre-dependent and all viruses were obtained from University of Pennsylvania (with 10^{12} or 10^{13} GC/mL). For analysis of GCaMP6s specific expression in 5-HT neurons 4 SERT-Cre mice were transduced in the DRN with 1µl of viral stock solution of AAV2/1 - Syn.Flex.GCaMP6s.WPRE.SV40. For behavioral experiments in control mice (4 SERT-Cre mice) 1.5 µl of a mixture of equal volumes of AAV2/1.EF1a.DIO.eYFP.WPRE.hGH and of AAV2/1.CAG.FLEX.tdTomato.WPRE.bGH was used. The remaining mice were injected with a mixture of equal volumes of AAV2/1.Syn.Flex.GCaMP6s.WPRE.SV40 and of AAV2/1.CAG.FLEX.tdTomato.WPRE.bGH: 1.5 µl was injected in 10 SERT-Cre mice (distributed around 6 points around the target coordinates) and 0.75 µl was injected in 4 TH-Cre mice (distributed around 4 points around the target).

For behavioral experiments, optical fiber implantation was done after infection and a head plate for head fixation was placed above Bregma: the skull was cleaned and covered with a layer of

Super Bond C&B (Morita). An optical fiber (300 µm, 0.22 NA) housed inside a connectorized implant (M3, Doric Lenses) was inserted in the brain, with the fiber tip positioned at the target for SERT-Cre mice and 200 µm above the infection target for TH-Cre mice. The implants were secured with dental acrylic (Pi-Ku-Plast HP 36, Bredent).

Behavioral training and testing protocol

Mice were water deprived in their homecage on the day of surgery or up to 5 days before it. During water deprivation mice weight was maintained above 80% of their original values. Following infection and implantation surgery, mice were habituated to the head-fixed setup by receiving water every 4s (6 µl drops) for 3 days, after which training in the odor-guided task started. A mouse poke (007120.0002, Island Motion Corporation) was adapted and used as a lickometer; sounds signaling the beginning of the trial and the outcomes were amplified (PCA1, PYLE Audio Inc.) and presented through speakers (Neo3 PDRW W/BC, Bohlender-Graebener), water valves (LHDA1233115H, The Lee Company) were calibrated and a custom made olfactometer designed by Z.F.M. (Island Motion) was used for odor delivery. The behavioral control system (Bcontrol) was developed by Carlos Brody (Princeton University) in collaboration with Calin Culianu, Tony Zador (Cold Spring Harbor Laboratory) and Z.F.M. Odors were diluted in mineral oil (Sigma-Aldrich) at 1:10 and 25 µl of each diluted odor was placed inside a syringe filter (2.7 µm pore size, 6823-1327, GE Healthcare) to be used in two sessions (~100 trials for each odor). Odorized air was delivered at 1000 $ml.min^{-1}$. Odors used were carvone (R)-(-), 2-octanol (S)-(+) , amyl acetate and cuminaldehyde, which were associated with large reward (4 µl water drop), small reward (2 µl water drop), neutral (no outcome) and punishment (air puff to the eye) before reversal, and with punishment, neutral, small reward and big reward after reversal of the cue-outcome associations, respectively. In each trial, white noise was played to signal the beginning of the trial and to mask odor valve sounds. A randomly selected odor was presented during 1s. Following a 2s trace period the corresponding outcome was available. Mice did one session per day and started training by being presented only with the large and small reward trials, followed by the introduction of the neutral type of trial in the next session and finally the punishment trial in the following one. Punishment trials were presented gradually until all 4 types of trials had the same probability of occurrence and each session consisted of 140 - 346 trials (minimum to maximum, 223 ± 30 mean ± SD). Time to odor (foreperiod), trace period and ITI were also gradually increased during training until mice could do the task with their final values: foreperiod was 3 to 4 s, taken from a uniform distribution, trace was fixed at 2 s, ITI was 4 to 8 s taken from a uniform distribution. These intervals were chosen to allow us to easily distinguish changes in GCaMP6s fluorescence for different events in a trial.

We ensured that mice could correctly perform the task in at least 3 consecutive days before reversing the odor-outcome contingency. We called these 3 days before reversal the expert phase (n = 18 mice, total of 48 sessions). In the day of reversal, mice started the session as before and the contingencies were reversed between the 32th and the 100th trial of that session (70 ± 15, mean ± SD). Two mice were excluded from the data analysis: one SERT-Cre and one TH-Cre mouse for bad fiber placement assessed after histology analysis (more than 400 µm

away from the infection area). Additionally, another SERT-Cre mouse was discarded from the reversal data analysis because of experimental problems with the fiber during the reversal session. After reversal, mice performed at least 3 sessions with the new contingencies. In 4 SERT-Cre mice and in all TH-Cre mice, at 5 to 6 days after reversal, we introduced surprise trials during the task. These surprise trials represented approximatly 20% of the total number of trials in a session during which no odor cue was presented: the typical white noise of the foreperiod was immediately followed by one of the four possible outcomes, randomly selected (11 ± 4 surprise vs 44 ± 8 cued trials per session, mean ± SD).

Fiber photometry

The dual-color bulk fluorescence acquisition setup consists of a 3-stage tabletop black case containing optical components (filters, dichroic mirrors, collimator), two light sources for excitation and two photomultiplier tubes (PMTs) for acquisition of fluorescence of a green (GCaMP6s) and of a red (tdTomato) fluorophore.

We used a 473 nm (maximum power: 30mW) and a 561 nm (maximum power: 100mW) diode-pumped solid-state laser (both from Crystalaser) for excitation of GCaMP6s and of tdTomato, respectively. Beamsplitters (BS007, Thorlabs) and photodiodes (SM1PD1A, Thorlabs) were used to monitor the output of each laser. The laser beams were attenuated with absorptive neutral density filters (Thorlabs) and each was aligned to one of the two entrances of the 3-stage tabletop black case (Doric Lenses). At the corresponding entrances the excitation filters used were 473 nm (LD01-473/10-25 Semrock) and 561nm (LL02-561-25 Semrock). Inside the black case 3 interchangeable/stackable cubes (Doric Lenses) with dichroic mirrors were used: one to separate the 473nm excitation light from longer wavelengths (Chroma T495LP), one to collect the emission light of GCaMP6s (FF552-Di02-25x36 Semrock), and one to separate the 561nm excitation light from tdTomato's fluorescence (Di01-R561-25x36). A collimator (F = 12 mm NA = 0.50, Doric Lenses) focused the laser beams in a single multimode silica optical fiber with 300 µm core and 0.22 NA (MFP_300/330/900-0.22_2.5m-FC_CM3, Doric Lenses), which was used for transmission of all excitation and emission wavelengths. The 3-stage tabletop black case had two exits, one for each fluorophore emission, at which we placed the corresponding emission filters (Chroma ET525/50m for GCaMP6s and Semrock LP02-568RS-25 for tdTomato), and convergent lenses (F = 40 mm and F = 50 mm, Thorlabs) before the photodetectors (photomultiplier tube module H7422-02, Hamamatsu Photonics). The output signals of the PMTs were amplified by a preamplifier (C7319, Hamamatsu) and acquired in a Micro1401-3 unit at 5000 Hz and visualized in Spike2 software (Cambridge Electronic Design). Light power at the tip of the patchcord fiber was 200 µW for each wavelength (473nm and 561 nm) for all experiments (measured before each experiment with a powermeter PM130D, Thorlabs). This patchcord fiber was attached to the fiber cannula each animal had implanted (MFC_300/330-0.22_5mm_RM3_FLT Fiber Polymicro, polymide removed) through a titanium M3 thread receptacle.

Data Analysis

All data were analysed in MATLAB.

Fluorescence data were downsampled to 1 kHz and smoothed using convolution with a gaussian filter of 100 ms. For each trial, the relative change in fluorescence, $\Delta F/F_0 = (F-F_0)/F_0$, was calculated by considering F_0 the mean fluorescence during 1 s before the odor presentation for both the red and the green channels ($[\Delta F/F_0]_{GREEN}$ and $[\Delta F/F_0]_{RED}$). For each session of each mouse, the distribution of green to red values of $\Delta F/F_0$ was fitted by the sum of two Gaussians along the red channel and the crossing point between these 2 Gaussians was used as a boundary (excluding the first and last 1000 ms of each trial because of filtering artifacts). All values of $[\Delta F/F_0]_{RED}$ below this boundary were used, together with the corresponding $[\Delta F/F_0]_{GREEN}$, to fit a linear regression line. Then, for each trial we corrected the green $\Delta F/F_0$ values using the parameters (*a* - slope; *b* - offset) obtained with the regression model of that mouse in that session: $[\Delta F/F_0]_{GREEN\_corr} = [\Delta F/F_0]_{GREEN} - a*[\Delta F/F_0]_{RED} - b$.
Behavioral data was organized as a function of US type and divided in CS and US responses. $[\Delta F/F_0]_{GREEN\_corr}$ US responses were normalized by subtracting the mean $[\Delta F/F_0]_{GREEN\_corr}$ of the interval of 1 s before US onset. The CS or US response was considered the mean of the signal during 1.5 s after CS or US onset respectively. For each mouse, all CS and US responses were z-scored in the expert phase to compare the amplitudes of responses to the different events. Analysis of US response across time was done by z-scoring all US responses of each mouse across days for each US type. Statistical analysis was done by comparing each day with pre-reversal days -1 and -2. For each mouse, mean amplitude of response to each US on the reversal day was also compared to the day before reversal. For analysis of surprise trials, four days of each mouse were pooled together due to the small number of surprise trials of each US type in each session.
For analysis of CS response time course during reversal, each mean amplitude change across trials was fitted by an exponential with maximum time constant of 225 trials (minimum number of trials after reversal for any US type of any mouse). Fits were done only if responses on the last 100 trials were significantly different from those of the 100 trials before reversal (only 1 odor in 1 mouse did not pass this criterion). Odors were pooled together in pairs (odors 1 and 2, odors 3 and 4) which correspond to the need to stop licking or to start licking after reversal.

Immunohistochemistry and anatomical verification

Mice were deeply anesthetized with pentobarbital (Eutasil, CEVA Sante Animale), exsanguinated transcardially with cold saline and perfused with 4% paraformaldehyde (P6148, Sigma-Aldrich). Coronal sections (40 µm) were cut with a vibratome and used for immunohistochemistry. For SERT-Cre mice used in expression specificity analysis, anti-5-HT (36 h incubation with rabbit anti-5-HT antibody 1:2000, Immunostar, followed by 2h incubation with Alexa Fluor 594 goat anti-rabbit 1:1000, Life Technologies) and anti-GFP immunostainning (15 h incubation with mouse anti-GFP antibody 1:1000, Life Technologies, followed by 2h incubation with Alexa Fluor 488 goat anti-mouse 1:1000, Life Technologies) were performed sequentially. For SERT-Cre mice used in behavioral experiments, anti-GFP immunostainning was performed (15h incubation with rabbit polyclonal anti-GFP antibody 1:1000, Life

Technologies, followed by 2h incubation with Alexa Fluor 488 goat anti-rabbit 1:1000, Life Technologies).

For TH-Cre mice, anti-GFP (15h incubation with rabbit polyclonal anti-GFP antibody 1:1000, Life Technologies, followed by 2h incubation with Alexa Fluor 488 goat anti-rabbit 1:1000, Life Technologies) and anti-TH immunostainning (15h incubation with mouse monoclonal anti-TH antibody 1:5000, Immunostar, followed by 2h incubation with Alexa Fluor 647 goat anti-mouse, 1:1000, Life Technologies) were performed sequentially.

To quantify the specificity of GCaMP6s expression in 5-HT neurons of SERT-Cre mice we used a confocal microscope (Zeiss LSM 710, Zeiss) with a 20X objective (optical slice thickness of 1.8 µm) to acquire z-stacks of three slices around the center of infection. Images for DAPI, GFP and Alexa Fluor 592 were acquired and quantification of cells expressing GCaMP6s and of cells stained with 5-HT antibody were quantified in a 200 x 200 µm window in the center of the DRN. The same was done for quantification of specificity in DA neurons of TH-Cre mice, but acquising Alexa Fluor 647 instead of 592 and taking the 200 x 200 µm window on the infection side. To evaluate fiber location in relation to infection, images for DAPI, YFP or GFP and tdTomato were acquired with an upright fluorescence scanning microscope (Axio Imager M2, Zeiss) equipped with a digital CCD camera (AxioCam MRm, Zeiss) with a 10X objective. The location of the fiber tip was determined by the most anterior brain damage made by the optical fiber subtracted by its radius. The center of infection was estimated through visual inspection of slices as the location where there were most infected cells. The distance between the fiber tip location and center of infection was calculated as an anterior-posterior distance which was estimated by comparing each corresponding location in the mouse brain atlas[344]. To determine the overlap between cells expressing YFP or GCaMP6s and tdTomato in SERT-Cre mice, we used a confocal microscope (Zeiss LSM 710, Zeiss) with a 20X objective (optical slice thickness of 1.8 µm) to image three slices around the center of infection (slices -1, 0 and 1, relative to it). All cell counts were done using the Cell Counter plugin of Fiji.

5. General Discussion

In this chapter, first I briefly discuss the main advantage and disadvantage of our technical approach and summarize what the studies shown in Chapters 3 and 4 have common: the conclusion that what had been theorized to be strict opponency is actually a form of complementarity between two neural systems. Then I proceed to a more detailed discussion about our findings regarding the activity of serotonergic neurons during reversal learning and the interaction between this neuromodulator and dopamine.

5.1 The use of fiber photometry to record activity of genetically defined neural populations

Neural population activity represents important information for understanding the large-scale dynamics of the brain[345]. However, understanding how the activity of different neurons relates to that global activity also offers insights on neural processes involved in behavior[346].

Our fiber photometry setup was developed for recoding neural population signals from genetically defined cell types in behaving mice. As a limitation, it is not possible to get single cell activity from it, and thus we cannot know if the signals we record are generated by all neurons in a uniform way or if they result from an integration of heterogeneous responses across neurons. Similarly, we don't know if the signals we recorded are generated only by spiking activity or if sub-threshold activity also contributes for them.

Nevertheless, this technique is appropriate to test hypothesis about the general role of a genetically defined population of neurons, such as neurons that express certain types of receptors or that produce important neuromodulators.

We used fiber photometry the hypothesis of opponency between two systems in two different situations. Theories of opponent processes have populated neuroscience research to explain approach and avoidance, invigoration and inhibition, incentive and withdrawal, as well as cellular and molecular mechanisms.

Here we have shown that in the two situations we studied, striatopallidal versus striatonigral pathways, and DRN 5-HT neurons versus midbrain DA neurons, pairs of systems might in fact drive opponent processes. However, their opponency is not strict in the sense that when one is active the other is inhibited. It seems that their activity is more complementary than strictly opposite. This means that they are generally balanced and, in the case of the striatopallidal and striatonigral pathways an imbalance between the two might compromise motor control, while in the case of 5-HT and DA the imbalance might be needed to allow for proper behavioral adaptation.

Based on the population signals we recorded from DA neurons and their similarity to the ones observed in previous studies, we can conclude that our approach provides a good readout of the spiking activity of a population of neurons, even if calcium signals are an indirect measure of such activity. Therefore, it is an appropriate tool to compare different neural populations under the same behavioral conditions.

5.2 An integrated view for the phasic activity of 5-HT neurons

We used fiber photometry to record neural activity from populations of DRN 5-HT neurons while mice were engaged in a reversal learning task. We performed the exact same acquisition in VTA/SNc DA neurons and observed that, as expected from the reward prediction error theory of DA's phasic activity, these neurons were activated by learned reward predicting cues and unexpected rewards, while they were inhibited by unexpected reward omission or reward omission coupled with unexpected air puff.

We observed that the activity of 5-HT neurons had some points in common with DA neurons, but it had also important differences. These neurons were activated by learned reward predicting cues, predicted and unpredicted air puffs, and unexpected outcomes of any valance.

Diverse and heterogeneous activity of DRN neurons has been reported for several years. As mentioned in the introduction, Barry Jacobs' group has hypothesized that increased activity in cat DRN neurons would facilitate motor output[19], but the majority of other theories on 5-HT function involve it in behavioral motor inhibition[40,41,111,134,347], generally coupled with aversive processing.

Ranade and Mainen 2009[179] reported that DRN neurons in behaving rats responded to a variety of events, such as movements, stimulus identity, reward omission, response direction, and sound clicks. Kae Nakamura's group has mostly found reward related activity in recorded DRN neurons from non-human primates, both in terms of phasic and of tonic activity[43,131,176,177]. Other studies showed reward related activity too[180,215], but responses to punishments or aversive contexts have also been repeatedly reported[130,217,348,349].

All these studies showed how heterogeneous the responses of DRN neurons can be, and called for the need to perform cell type specific recordings.

This was carried out by Cohen *et al*., 2015[93], to find that DRN 5-HT neurons indeed showed transient responses to reward predicting cues and to air puffs, but also to unpredicted rewards, albeit with small amplitude. Interestingly, they found that single 5-HT neurons could respond to both reward predicting cues and to air puffs. Similarly, Hayashi *et al.*, 2015[131] found that single non-identified DRN neurons could respond to both rewarding and aversive events.

This suggests that the heterogeneity that had been attributed to DRN responses and that was often justified by the possibility of having different cell populations coding for different events might have to be reevaluated. Although it is likely that different cell groups of 5-HT neurons have specific specializations, it is also plausible to think that single 5-HT neurons show such (from our perspective) heterogeneous responses.

Our technical approach of using fiber photometry ran the risk of not showing any clear results if 5-HT neurons fired asynchronously and heterogeneously to events. However, we recorded patters of activity that were consistent across mice and event identities.

Our results and the aforementioned observations from other studies[93,131] suggest that the classification of 5-HT responses based on the valance of the events that triggered them might not be the most appropriate approach to understand 5-HT neurons' phasic activity.

Of course the use of rewarding and aversive events in animal studies is widespread and a critical aspect for the survival of animal species is to approach rewards, such as food, water or possible mating partners, and to avoid danger, such as predators or other life-risking situations. According to adaptive control theory animals learn actions to maximize rewards and minimize punishments[350]. To accomplish this, animals must not only perceive such events as good or bad, but they also need to learn to associate predictive cues (such as stimuli, contexts, etc) of such events with their expected value. Once these associations are established, animals can adopt adequate behaviors when presented with such cues, namely approach in the case of

predicted rewards, or avoidance in the case of predicted aversive events. We can parse these basic functions in 3 general stages: attribution of valance to unconditioned stimuli, learning about the cues that predict them by attributing motivational properties to these, and generating the appropriate behaviors to match the motivations and emotions elicited by them.
We think that there are two ways in which we can look at our results in the context of the remaining literature on 5-HT function. The phasic activity of 5-HT neurons that we observed can be integrated as reporting:

1) either an unsigned prediction error, also called surprise, or uncertainty signal;
2) or a "control error" signal, reporting the inadequacy of a response (or lack of it) to the motivational context in which it is generated.

Either of these options needs to be valid for either reward or aversive processing and the system does not have to be necessarily biased towards one or the other. The difference between these two proposed signals is subtle but potentially very relevant: while the first one is about triggering learning about new predictions and models of the world, the second one is about the link between an emotion or motivation (which can be triggered by conditioned or unconditioned stimuli) and the appropriate behavior. I will discuss this difference in more detail in the next section. Later, I will present some requirements that are common to these two signals and which DRN 5-HT neurons are in a privileged position to fulfill. These include access to information from limbic, motor and higher level centers, widespread efferent projections, the capacity to induce behavioral adaptation and neural plasticity (the direction of which might be determined in combination with other signals or neuromodulators that might have privileged information about the valance of the situation).

5.2.1 Unsigned prediction error or "control error" signal?

Surprise signals have long been studied in behavioral research and shown to play a pivotal role in enhancing the speed of learning[351]. Accelerated learning has been observed as a consequence of the delivery of surprising reinforcers[352,353], but also of surprising neutral stimuli[354–356]. Pearce and Hall[335] proposed a model in 1980 in which animals learn CS-US associations by updating the associative strength, or associability, of these two stimuli depending on the degree to which the CS already predicts the US. This means that associability between a CS and a US is modulated by how surprising the US is (in absolute value, *i.e.*, independent of valence). So the more surprising a stimulus is, the larger will be the learning rate, and as it becomes predictable, the learning rate will decrease. Courville *et al.*, 2006[331] proposed a Bayesian account of such surprise signals' capacity (whether reinforcers or neutral) to enhance learning: they contribute to increase uncertainty in a changing world which is done by decreasing the weight of old evidence over new one. Uncertainty is, in Bayesian inference, the equivalent to associability in Pearce and Hall's model, and surprising events signal change in the environment and thus increase uncertainty and speed up learning.
Our reversal task only depends on the unpredictable new association between CS's and US's and we didn't test if, after this reversal or after the introduction of surprising US's at the time of

CS, animals created a model about the speed of change in the environment. It is likely that they did, because the speed of adaptation to reversals decreases when animals have experienced such situations and, interestingly, the effect of 5-HT depletion in the OFC also decreases with the number of reversals[44]. For the future, it will be interesting to monitor 5-HT activity in multiple reversals and also in a reversal performed after having cued the animals that the environment constantly changes (with neutral stimuli for instance) to test if 5-HT activity is decreased in these situations. If 5-HT is signaling surprise and the animals learn a model of the world as a permanently changing environment, then its influence will probably lose effect over time, something that could also be tested with inhibition experiments.

Other brain areas and neuromodulators have been associated with surprise or uncertainty information in the brain. For instance, Yu and Dayan 2005 have proposed that acetylcholine and norepinephrine would code information about different types of uncertainty[357]. In fact, basal forebrain cholinergic neurons show responses to reinforcers (rewards and punishments) which are modulated by their level of expectation[358], something that is also observed in amygdala neurons[359]. Non-cholinergic basal forebrain neurons show responses to motivationally salient events independent of valance which are thought to be important for attentional processes[358,360]. These include both primary reinforcers and the cues that predict them, but the responses to primary reinforcers are modulated by the level of expectation[360].
Surprise signals have also been reported in the anterior cingulate cortex (ACC) of monkeys and interpreted as carrying a signal for the need of adjusting behavior adaptively, useful to report the associatiability of actions and their outcomes and needed to update the predictive model used for behavior[361]. Interestingly, the ACC is an area with extensive NE projections which play an important role in determining decisions and behavioral choices by controlling the weight given to prior knowledge in ACC activity[362].

To consider the 5-HT neural activity observed in our results as a surprise signal, *i.e.* as an unsigned prediction error signal, it is important to take into account that the animals did not learn the odor – air puff association. Indeed, the 5-HT responses to the air puff were never transferred to the CS that predicted it, even after extensive training. This transfer of activity would be predicted for any general form of associative learning, and thus also for the representation of a pure signal for surprise or for motivational salience dependent or independent of valance. Similarly, we never saw an anticipatory eyeblink conditioned response, but such lack of response has been documented in eyelid conditioning paradigms with trace periods comparable to the one we used[326,363].
This is a limitation of this paradigm and it is unclear if mice learn the association or not, but clearly they cannot execute a proper response to avoid it. This might suggest that the inability of generating an appropriate action should be signaled as a “control error”.

We might get some insight by taking into consideration that other studies report that the activity of DRN 5-HT neurons is modulated by the degree of controllability over events. Non-identified DRN neurons showed no habituation to sensory stimuli (audio clicks and light flashes) that were

neutral and that were not supposed to trigger any type of response in the experimental setting[179,213,364]. Additionally, in aversive processing it has been shown that predictable but inescapable shocks activate *c-fos* expression in DRN 5-HT neurons[129]. Several studies have shown that 5-HT activity during inescapable shock (IS) is more elevated than during escapable shock[365,366], a difference that is needed for later demonstration of learned helplessness phenotype[367] in rats exposed to IS. This increased response under situations of uncontrollability is modulated by habenula input[368] and is under the control of the mPFCv: when rats have been exposed to situations in which they had control over a stressor, the mPFCv exerts inhibitory control over DRN 5-HT neurons in order to prevent the sequelae triggered by uncontrollable stress[334,369]. Similarly, optogenetic activation of the mPFC projection to the DRN promoted more active swimming behavior in the forced swim test[370].

Although attempts have been made to model controllability using a Bayesian framework[175], there is no accepted definition for it. Our task is Pavlovian, so there is nothing the animals can do to really avoid the air puff. This means that if we consider that there is a system creating a model about associations of environmental events and another system creating a model about the right motor programs to match them, in the case of the air puff trials, this last model cannot be made. Because in air puff trials the mice always get an air puff there is no possible mapping between whatever action and a safety outcome. Therefore, while a prior about the best action to undertake is not available, the control error will always be signaled. This would result in an absence of CS response to the odor that predicts air puff (but not to the odors that predict rewards, because in those cases the animals have control over the right action to take: lick). Interestingly, Nakamura *et al*., 2008[176] reported no prediction error activity in DRN neurons when they reversed cues associated with small and large rewards[176], but they did see some modulation of activity to unpredicted outcomes in a more recent paper[131]. A reversal involving rewards of different sizes should not generate control errors as the behavior elicited by both is the same. However, it should generate a reward prediction error, which indeed was observed in DA neurons in their study[176]. In our task we did include small and large rewards, but unfortunately we did not do any reversal between stimuli that required the same motor program. Performing an experiment with all types of reversals (rewards to no rewards, different types of rewards, different types of punishments, different neutrals, and combinations of all these) would maybe allow us to disentangle these two proposed signals.

This idea about a role for 5-HT as a controllability signal is also interesting because it seems more related to other functions performed by 5-HT at physiological and homeostatic levels. It could be the result of the natural evolution of an old mechanism to act at a higher level function. In fact, 5-HT seems to be important for control and adaptation of autonomic functions such as respiration[12,13,371], temperature regulation[12,16], food intake[14] and plant roots' growth[372]. These are functions that lose their adaptive responses under decreased 5-HT signaling, consequently increasing the risk of autonomic dysregulation.

So we do not have a definitive answer for this integrated signal that 5-HT neurons might be reporting. However, whether it is a surprise signal or a "control error" signal it does have to fulfill

some requirements to integrate the information needed for computing such signal and for broadcasting it to a relevant set of target structures. In the next sections we will discuss some of these characteristics.

5.2.2 5-HT neurons receive inputs from both aversive and reward centers

In the introduction we have already mentioned that 5-HT neurons receive input projections from several brain areas involved in reward and/or aversive processing.
For instance, lateral habenula neurons are known to be excited by reward omissions and aversive stimuli, representing negative motivational value[329,373]. This activity generally inhibits VTA/SNc DA neurons[374] through GABAergic neurons in the rostromedial tegmental nucleus (RMTg)[164,375]. The LHb also influences the DRN: direct projections to 5-HT neurons are mostly glutamatergic[82,83] while indirect projections through the RMTg are GABAergic[376,377].
DRN 5-HT neurons also receive strong input projections from the lateral hypothalamus[81], both glutamatergic and GABAergic[378].
Both negative and positive value representations have been observed in the amygdala[379,380], an important center of the limbic system. The amygdala, especially its central nucleus, also sends projections to DRN 5-HT neurons[81,83].
Finally, even though the projections from DRN 5-HT neurons to DA neurons are much stronger than the opposite[81,137], both VTA and SNc neurons (dopaminergic or not) project to 5-HT cells in the DRN[83,381].

5.2.3 5-HT stimulation is not rewarding nor aversive

Investigations on whether 5-HT increase is rewarding or reinforcing have had contradictory results. Pharmacological or lesion manipulations of the serotonergic system have reported facilitation of conditioned or unconditioned responses to rewards both in situations of presumed decreased[133,168,382] and increased[383] 5-HT availability. The same is true for attenuated conditioned responses to rewards[170,384]. However, in these results it is hard to isolate reward-related behavior from general arousal and motor output.
As for aversive stimuli, it is more generally accepted that 5-HT neurons respond to them[129,130,366] and that this influences typical behavioral adaptations[40,41,123,134,347,385,386]. However, 5-HT does not seem to be aversive *per se*. In fact, over-expression of the serotonin transporter, which reduces brain 5-HT levels, results in reduced sensitivity to both positive and negative reinforcers[387] and 5-HT depletion disinhibits behavioral responding under high incentive motivation, even if this motivation is appetitive[388].
The best way to answer this question is to use optogenetic stimulation of 5-HT neurons in behavioral paradigms sensitive to rewards and punishments. Liu *et al*., 2014[178] reported that photostimulation of DRN Pet-1 neurons (5-HT specific) was highly rewarding since it shifted sucrose preference, created region-of-interest preference, drove self-stimulation and facilitated sensory discrimination learning. However, the major contributor for these rewarding effects was the release of glutamate by DRN neurons in the VTA and possibly other areas[178]. While one

study showed that most projections from the DRN to the VTA are glutamatergic (but not serotonergic) and their activation increases DA release in the NAc which is reinforcing[389], other studies have reported that photostimulation of DRN Pet-1[336] or Tph2[118,336] or SERT[119,336,337] expressing neurons had no such effects. Besides, the study that used a Pet-1 (and Tph2 and SERT) mouse line shows that the projections from the DRN to the VTA that reinforce behavior are non-serotonergic[336], suggesting that the effects observed by Liu *et al*., 2014[178] are caused either by non-specific expression of ChR2 in DRN neurons or the effects are driven by a specific and very small population of DRN 5-HT neurons that also release glutamate in the VTA[87,389,390].
In our laboratory several paradigms were tested and in no situation animals showed appetitive or aversive responses to photostimulation. These included place preference tests[119] and a probabilistic choice task in which mice had to choose between two ports with different reward probabilities to have access to water: animals' choices matched the reward probabilities and were not affected by paired photostimulation of DRN 5-HT neurons with reward delivery in one side or the other[119].

5.2.4 5-HT neurons receive inputs from the anterior cortex and the basal ganglia

The ventral medial prefrontal cortex (mPFCv) projection to the DRN has been known for many years. This glutamatergic projection targets monosynaptically both 5-HT and GABA neurons[83,381], but its general effect in 5-HT neurons seems to be inhibitory[391,392], both through activation of GABAergic interneurons[393,394] and through activation of 5-HT1A autoreceptors[395].
The main cortical sources of projections to DRN 5-HT neurons originate from layer 5 of the insular, motor, orbital, infralimbic, prelimbic, and cingulate areas[81,83,381], which in turn also receive input from 5-HT neurons[73]. These areas are all involved in decision-making, behavioral control and uncertainty. For instance, surprise signals, or unsigned prediction errors, have been reported in the dorsal anterior cingulate cortex in primates[361,396] and the orbitofrontal cortex is intimately associated with uncertainty[397], prediction and evaluation of future outcomes[398–401]. It has been shown to code both appetitive and aversive information and preference[402–404] and its function is needed for cognitive flexibility in rodents[405] and primates[406–408]. Besides, depletion of 5-HT in the OFC disrupts probabilistic discrimination learning[409] and reversal learning[44,45] (discussed below).
In contrast, projections from the basal ganglia nuclei to DRN 5-HT neurons have been considered fairly weak. However, recent studies reported that the output nuclei of the basal ganglia, SNr and GPe, project monosynaptically to DRN 5-HT neurons. There are also direct projections from striatal medium spiny neurons to 5-HT neurons, most of which express D1 receptors, although some D2 expressing neurons were also identified[83]. This suggests the existence of parallel circuits capable of modulating 5-HT neurons, as well as being modulated by them[410], and directly involves 5-HT, together with DA, in a network for integration and control of motor behaviors in response to motivational events. This also invites reconsideration of

models of the basal ganglia control that did not account for such direct influence of the striatum in 5-HT neurons[299].

The observed projections suggests that 5-HT can impact movement parameters and could potentially influence action selection and movement control, but its influence in movement is likely indirect and dependent on other variables such as general motivation (but maybe not valance-dependent).

5.2.5 5-HT contributes for behavioral flexibility

We used a reversal learning task to monitor the activity of 5-HT neurons. Such a task is useful to test the prediction error theory of DA and 5-HT but also to understand their involvement in cognitive and behavioral flexibility. Cognitive flexibility is a broad concept used to name the capacity for modifying behavior when environmental conditions change.

5-HT signaling has been considered particularly important in behavioral adaptation when environments are volatile, such as when well-learned CS-US associations are suddenly reversed. A consistent line of studies has shown that 5-HT2C receptor antagonists improve spatial reversal learning in rats[320,321] and that OFC 5-HT depletions make marmosets more prone to make perseverative errors after reversal[44]. These results are interpreted as resulting from increased difficulty in disengaging from the previously rewarded stimulus, rather than by increased active avoidance to the previously non-rewarded stimulus[45]. Similar behavior has also been observed in rats[411]. SERT knockout mice, which should have higher extracellular 5-HT levels, show better performance in reversal learning than littermate controls[323]. However, monkeys with either two copies of the short allele of the SERT gene-linked polymorphic region[412] or with the TGT haplotype of the 3' untranslated region of SERT[413], both of which are thought to allow higher extracellular 5-HT levels than their counterparts, show reduced and increased cognitive flexibility, respectively. As for humans, no effect of this polymorphism was found[414]. Nevertheless, the latter results are hard to interpret because these are congenital variations that might lead to a series of compensatory mechanisms and it is not clear yet how they affect the levels of 5-HT in the brain[412–415].

Although some studies have claimed that in probabilistic reversal tasks 5-HT signaling is important for negative feedback and this necessarily involves it in aversive processing[416,417], other studies suggest that this is not the case and that 5-HT could be needed only for the feedback signal itself and for behavioral inhibition but not for reporting aversive outcomes[418,419]. Indeed, pharmacological manipulations of the 5-HT system in rats engaged in a reversal learning task affected both punishment and reward sensitivity, *albeit* in a dose dependent manner[420].

The surprise or control error signal that we observed in our data seems to be the perfect match for the function that the reversal learning results mentioned above seem to attribute to 5-HT: a signal that both reports the need for behavioral adaptation and promotes behavioral inhibition.

5.2.6 5-HT in undirected neural plasticity

Given the characteristics of the 5-HT system reviewed above, 5-HT neurons seem to be well positioned to constantly monitor environmental and contextual cues, current motivations and goals, as well as ongoing or planned motor programs. Could 5-HT neurons be receiving this multitude of information and integrating it to signal a prediction error or a "control error" signal? Such a signal would be useful to adapt behavior, and based on our data and the data reviewed above, it seems to do so towards behavioral inhibition.

Would there be a difference between unsigned prediction error signal-driven plasticity and control error-driven plasticity? This is a difficult question to answer, because we don't know much about the plasticity mechanisms that happen during reversal learning.

However, there are many evidences that 5-HT increases plasticity in several brain areas, which is a sign that it could in principle modulate behavior during reversal learning once a signal for the need for adaptation is triggered.

As we have already mentioned briefly, enhanced 5-HT triggers cortical plasticity in the visual cortex of adult amplyopic mice[338] and promotes cross-modal reorganization of the cortex after injury[339,421]. It also modulates developmental plasticity[422], promotes axonal growth[423], as well as dendritic remodelling[424] and neurogenesis in the hippocampus[425,426], an effect that has been linked to the antidepressive effects of SSRIs[340].

In addition, context-dependent modulation of plasticity by 5-HT has been reported in the auditory cortex[427] and 5-HT can also modulate the impact of learning processes mediated by DA-dependent or Hebbian plasticity[341,342].

Such a behavioral adaptation signal would be in accordance with a recent model[428] for 5-HT function in undirected plasticity which suggests that this neuromodulator is involved in undirected susceptibility to change. This means that 5-HT would open the gate for adaptation, but if this change is for the benefit of the individual or not depends on the environmental conditions. The author of this proposal uses this model to explain the complicated effects of SSRIs in the treatment of depression, which seem to work fairly well when combined with psychotherapy, but which in general do not have the desirable efficacy.

So we know that there is a lot of variability in the results obtained in both humans and experimental animals with psychiatric or behavioral disorders under treatment of SSRIs[429], and we also known that other neuromodulators are dysregulated in such conditions[430–432]. This is a strong indicator that 5-HT cannot be influencing them by its own: it has to interact with other systems.

5.2.7 Interplay between 5-HT and DA

Until now we have been discussing the role of DRN 5-HT neurons as an unsigned prediction error or as a control error, both of which are concerned with the information about the need to promote learning and adaptation to alter behavior. But we do have another piece of evidence which is very interesting: the fact that after reversal, serotonin neurons take longer to adapt their CS responses to the new contingencies than DA neurons.

Although serotonin has been proposed as an opponent to DA for a long time, evidence for this opponency has never been observed at the neural activity level. Here we show that if 5-HT is involved in behavioral inhibition, as has been proposed for decades[111,433], especially in the context of aversive learning[40,41,123,134,347], it could also be doing so in the context of working to obtain rewards, *i.e.* inhibiting motor outputs that are not appropriate to obtain them and therefore should be inhibited. More specifically, in the context of our task the fact that 5-HT neurons' CS responses are intrinsically slower than those of DA's in a positive reversal (that is, cues that predicted no rewards start predicting rewards after reversal), creates an unbalanced state in which DA neurons are actively predicting reward and driving behavioral invigoration (and thus licking) before 5-HT neurons start inhibiting possible competing motor programs. On the contrary, during a negative reversal (cues that predicted rewards start predicting no rewards after reversal) the fact that the dynamics of 5-HT neurons is slower creates an imbalance favoring 5-HT. This 5-HT signal that is overrunning dopamine's after the cue presentation might be needed to inhibit inappropriate motor programs which now include licking. Indeed the rate of adaptation for 5-HT neural activity was slower than that of anticipatory licking.

This suggests that in steady state conditions, when the environment is stable, DA and 5-HT equilibrate each other and drive actions according to the learned model. However, an environmental change triggers the realization that the prior model used by the animal is no longer valid, requiring new learning. Additionally, this environmental change uncovers the competition between 5-HT and DA by temporarily creating an imbalance in their activity due to their distinct dynamics.

Natural behavior is biased towards approaching rewards and avoiding punishments and this might be the reason why it has been so difficult to conciliate the involvement of 5-HT with reward processing. However, if we consider that both DA and 5-HT drive behaviors towards obtaining rewards and we consider rewards anything better than the average value of an environment so as to include escapes from punishment, then we might get a more unifying view of the role of these two neuromodulators. DA drives behaviors towards rewards by invigorating actions that lead to better-than-expected outcomes, while 5-HT inhibits actions that might compromise that goal. However, the problem must not be this simple, because in our reversal task, if we believe that the licking responses that are no longer needed are being suppressed by 5-HT's action then in this case 5-HT is not working towards or against rewards, it is just contributing to save energy resources. A role for 5-HT in maintaining energy balance is yet another theory of 5-HT function[434] that seems to encompass several of its functions in the control of physiological processes.

Another interesting consequence that might arise from the different time courses between DA and 5-HT after reversal is that, in the case of positive reversal, the window of time in which 5-HT has not yet matched the activity of DA neurons could be a time window for exploration (to obtain rewards). This is something that we cannot test in the context of the reversal task presented here because the animals are head-fixed, but which would be interesting to explore in a different behavioral setting, one in which animals would be freely moving and need to explore

an arena to find water or food, for instance. The slower increase in responses of 5-HT neurons to the new reward predicting cues could reflect a slow decrease in exploratory behaviors and concurrent tuning of the behavior towards the action that leads to reward. Supporting this view some studies have shown that 5-HT induces exploitation rather than exploration in invertebrates[435] and decreases exploration and/or locomotor activity[436–438].

Serotonin clearly represents a complex neuromodulatory system, and we did not do loss of function or activational studies in the context of this task to see if we can use it to change the behavior of the mice during reversal. That is obviously something that should be done in the future. We should also try to understand how 5-HT and DA could be interplaying in target structures involved in reversal learning, such as the OFC or the dorsal striatum.

For instance, distinct dynamics during reversal learning have also been observed in neural recordings done in the caudate nucleus of the striatum and in the PFC of behaving monkeys[439], two areas that are highly interconnected. Interestingly, the former showed faster adaptation to the reversed contingencies than the latter. This relates to our results with DA and 5-HT because the caudate nucleus is a major target of DA projections which are needed for reversal learning[440], while the PFC is one of the main targets of 5-HT projections important for avoiding perseverative errors in reversal learning[45]. In fact, in a different study the interaction between these two variables (DA in caudate putamen and 5-HT in OFC) explains most of the variability in a measure of behavioral flexibility in monkeys performing a reversal learning task[441]. Given how little we know about synaptic and circuit adaptations during reversal learning, studying the interplay and balance game between these two neuromodulators in these areas might shed some light on the control of behavior and cognitive flexibility.

5.3 Conclusion

The work presented in this dissertation has evolved from the development of an experimental technique for monitoring genetically defined population signals to testing proposed opponent processes in the brain.

As any other technique in neuroscience, fiber photometry has both advantages and limitations, which have been discussed in Chapter 2.

Here we used it to test two different brain systems that have been proposed to work through opposition of its elements and we show that, in both cases, these elements do not work in strict opposition. Instead, the functions of these systems seem to be sustained by a finely tuned balance between their elements.

First we recorded activity from striatonigral and striatopallidal neurons in the dorsal striatum to show that both striatal pathways are activated during contraversive movements. Optogenetic experiments have shown that the activity of both pathways is needed for these contraversive movements and that the balanced activity between the two is critical for spontaneous behaviors, since unbalanced activity can cause opposite effects to those predicted by observation of the natural activity of the two pathways.

Then we used an improved version to the fiber photometry setup to show that the activity of DA and 5-HT neurons do not show strictly opposite patterns.
We show that, with our technique, we could observe several characteristics of DA activity that are in accordance with the reward prediction error coding theory. As for 5-HT we also observed reward prediction error activity. However, unlike DA neurons, 5-HT neurons responded to both better-than-expected and worse-than-expected outcomes and even to surprising neutral outcomes. Such a signal is well positioned to facilitate behavioral plasticity and learning.
Additionally, we observed that 5-HT and DA's responses to reward predicting CS's showed different dynamics of adaptation following reversal: this asymmetry provides insight into why 5-HT may be more important in transitions from a good environment to a poor one than vice-versa.
Our data suggests that DRN 5-HT's activity could be useful both to trigger new learning and adaptation and to inhibit behaviors that are not useful for obtaining rewards.
DRN 5-HT is uniquely positioned to exert a global influence that is orchestrated by a localized set of neurons. It is in a privileged position to integrate diverse inputs and to broadcast a neural signal, and thus the tendency to hypothesize an integrative and overarching function for it is natural. Of course the diversity of receptors for 5-HT and the diversity of neurons that contain them are also well positioned to guarantee specific local responses to 5-HT signaling.
But how do 5-HT neurons compute such prediction or control error activity?
Although we might have contributed for some understanding of the role of 5-HT in learning, adaptation and behavioral control as well as for the nature of its opponency/complementation to DA's role, many questions remain without answer. Our technique and our analysis are based on the assumption that an integrated population signal of DRN 5-HT neurons codes a relevant message. However, this is debatable and our technique does not allow us to solve this issue straightforwardly. The signals we recorded in midbrain DA neurons show several aspects of the reward prediction error formalization by temporal difference models[139,140,142–144], as expected from a fairly homogeneous population of neurons. However, even for VTA and SNc DA neurons continued research is showing activity characteristics that do not fit this model and which seem to depend on the inputs and projection targets of the neurons[159,161–166].
It is likely that the same will happen with 5-HT neurons. In this case, the use of dynamic tasks such as reversal tasks might give us important insights into the events that trigger 5-HT activity compared to tasks that do not require adaptive learning. Some questions that need to be explored would be the possible coding of different types of prediction or control errors by different 5-HT neurons. Some 5-HT neurons respond to both rewarding and aversive events[93], but others seem to respond only to one or the other. Using genetic tools and retrograde viruses we should be able to record activity from projection-specific 5-HT neurons and maybe understand how the patterns of activity we observed here are generated based on their input signals.
It will be important to understand if distinct 5-HT neurons contribute differently to certain types of prediction error activity (or to other types of activity) depending on their projection pattern and/or

on the other signaling molecules that might be coexpressed by these neurons (these two characteristics seem to have some correlation[87–89]).
Looking for a unifying view of a DRN 5-HT signal might be a simplistic attempt to understand this complex system, but it is a good exercise to try to understand the organizing or functional principles of 5-HT, to make hypothesis about its effects, and to plan experiments.
Previously unexpected complexities such as the co-release of glutamate and GABA from single midbrain neurons have been recently revealed[442] and remind us that there are always exciting new avenues of research to be explored. Investigating how different neurotransmitters and neuromodulators complement each other to drive learning and adaptation through their activity patterns and dynamics must be one of the most exciting topics in neuroscience research.

As any findings involving the 5-HT system, these too could influence the way we look at the role of this neuromodulator in psychiatric disorders. As we have mentioned before, the fact that we observed a surprise type of signal in 5-HT neurons suggests that it can "open a gate for plasticity" by modulating other neural systems in different directions, which probably depend on its interaction with other neurotransmitters. In the case of depressive patients under SSRIs' treatment, the quality of the environment that surrounds them is very likely to influence the direction of the adaptation that takes place[428]. Related to this is the fact that unexpected external events can trigger an imbalance in the generally tightly controlled equilibrium of 5-HT and DA activity. This causes an inbalance between invigoration and inhibition of actions that might be necessary for for behavioral adaptation but which has to be reestablished after re-stabilization of the environmental conditions.
The lack of capacity to properly adapt behavior when needed or of stabilizing it in steady state conditions is at the root of many neuropsychiatric disorders, such as OCD, depression, attention-deficit/hyperactivity disorder, impulsivity, Parkinson's, Tourette's syndrome, etc. Our understading of the complex dynamics between different neuromodulatory systems during learning and adaptation will be fundamental to better prevent and treat these disorders[443].

Bibliography

1. Vialli, M. & Erspamer, V. Ricerche sul secreto delle cellule enterocromaffini. *Zeitschrift Zellforsch. und Mikroskopische Anat.* **27,** 81–99 (1937).
2. Erspamer, V. & Asero, B. Identification of Enteramine, the Specific Hormone of the Enterochromaffin Cell System, as 5-Hydroxytryptamine. *Nature* **169,** 800–801 (1952).
3. Rapport, M. Serum vasoconstrictor (Serotonin): V. The presence of creatinine in the complex. A proposed structure of the vasoconstrictor principle. *J. Biol. Chem.* **180,** 961–969 (1949).
4. Page, I. H. The vascular action of natural serotonin, 5- and 7-hydroxytryptamin and tryptamine. *J. Pharmacol. Exp. Ther.* **105,** 58–73 (1952).
5. Page, I. H. The discovery of serotonin. *Perspecttives Biol. Med.* **20,** 1–8 (1976).
6. Brodie, B. B. B. & Shore, P. A. A concept for a role of serotonin and norepinephrine as chemical mediators in the brain. *Ann. New York Acad. Sci.* **66,** 631–642 (1957).
7. Dahlstrom, A. & Fuxe, K. Evidence for the existence of monoamine-containing neurons in the central nervous system. I: Demonstrations of monoamines in the cell bodies of brainstem neurons. *Acta Physiol Scand* **62,** 1–55 (1964).
8. Fuxe, K. Evidence for the existence of monoamine neurons in the central nervous system III. The monoamine nerve terminal. *Zeitschrift für Zellforsch. und Mikroskopische Anat.* **65,** 573–596 (1965).
9. Woolley, D. W. & Shaw, E. A biochemical and pharmacological suggestions about certain mental disorders. *Proc. Natl. Acad. Sci. U. S. A.* **40,** 228–231 (1954).
10. Woolley, D. W. *The biochemical basis of psychosis. The serotonin hypothesis about mental diseases*. (J. Wiley & Sons Inc., New York, 1962).
11. Lovick, T. A. The medullary raphe nuclei: a system for integration and gain control in autonomic and somatomotor responsiveness? *Exp. Physiol.* **82,** 31–41 (1997).
12. Ray, R. S. *et al.* Impaired Respiratory and Body Temperature Control Upon Acute Serotonergic Neuron Inhibition. *Science* **333,** 637–642 (2011).
13. Depuy, S. D., Kanbar, R., Coates, M. B., Stornetta, R. L. & Guyenet, P. G. Control of Breathing by Raphe Obscurus Serotonergic Neurons in Mice. *J. Neurosci.* **31,** 1981–1990 (2011).
14. Wu, Q., Clark, M. S. & Palmiter, R. D. Deciphering a neuronal circuit that mediates appetite. *Nature* **483,** 594–597 (2012).
15. Mecawi, A. S., Fonseca, F. V, Araujo, I. G. de & Reis, L. C. in *Neurobiology of Body Fluid Homeostasis: Transduction and Integration* (eds. Luca, L. A. De, Menani, J. V. & Johnson, A. K.) (Frontiers in Neuroscience). at <http://www.ncbi.nlm.nih.gov/books/NBK200957/>
16. Audero, E. *et al.* Sporadic autonomic dysregulation and death associated with excessive serotonin autoinhibition. *Science* **321,** 130–133 (2008).
17. Dugué, G. P. *et al.* Optogenetic recruitment of dorsal raphe serotonergic neurons acutely decreases mechanosensory responsivity in behaving mice. *PLoS One* **9,** e105941 (2014).
18. Cai, Y., Wang, W., Hou, Y. & Pan, Z. Z. Optogenetic activation of brainstem serotonergic neurons induces persistent pain sensitization. *Mol. Pain* **10,** 70–79 (2014).
19. Jacobs, B. L. & Fornal, C. A. 5-HT and motor control: a hypothesis. *Trends Neurosci.* **16,** 346–352 (1993).
20. Fornal, C. a, Metzler, C. W., Marrosu, F., Ribiero-do-Valle, L. E. & Jacobs, B. L. A subgroup of dorsal raphe serotonergic neurons in the cat is strongly activated during oral-buccal movements. *Brain Res.* **716,** 123–33 (1996).

21. Wei, K. *et al.* Serotonin Affects Movement Gain Control in the Spinal Cord. *J. Neurosci.* **34,** 12690–12700 (2014).

22. Portas, C. M., Bjorvatn, B. & Ursin, R. Serotonin and the sleep / wake cycle : special emphasis on microdialysis studies. *Prog. Neurobiol.* **60,** (2000).

23. Ursin, R. Serotonin and sleep. *Sleep Med. Rev.* **6,** 57–69 (2002).

24. Sakai, K. Sleep-waking discharge profiles of dorsal raphe nucleus neurons in mice. *Neuroscience* 1–25 (2011). doi:10.1016/j.neuroscience.2011.09.024

25. Monti, J. M. Serotonin control of sleep-wake behavior. *Sleep Med. Rev.* **15,** 269–281 (2011).

26. Lorrain, D. S., Riolo, J. V, Matuszewich, L. & Hull, E. M. Dopamine : Implications for Sexual Satiety. *J. Neurosci.* **19,** 7648–7652 (1999).

27. Pfaus, J. G. Pathways of Sexual Desire. *J. Sex. Med.* **6,** 1506–1533 (2009).

28. Liu, Y. *et al.* Molecular regulation of sexual preference revealed by genetic studies of 5-HT in the brains of male mice. *Nature* **472,** 95–99 (2011).

29. Zhang, S., Liu, Y. & Rao, Y. Serotonin signaling in the brain of adult female mice is required for sexual preference. *Proc. Natl. Acad. Sci. U. S. A.* **110,** 9968–9973 (2013).

30. Paul, E. D. *et al.* Repeated social defeat increases reactive emotional coping behavior and alters functional responses in serotonergic neurons in the rat dorsal raphe nucleus. *Physiol. Behav.* **104,** 272–282 (2011).

31. Dölen, G., Darvishzadeh, A., Huang, K. W. & Malenka, R. C. Social reward requires coordinated activity of nucleus accumbens oxytocin and serotonin. *Nature* **501,** 179–184 (2013).

32. Beis, D. *et al.* Brain serotonin deficiency leads to social communication deficits in mice. *Biol. Lett.* **11,** 7–11 (2015).

33. Graeff, F. G. On serotonin and experimental anxiety. *Psychopharmacology (Berl).* **163,** 467–476 (2002).

34. Richardson-jones, J. W. *et al.* Serotonin-1A Autoreceptors Are Necessary and Sufficient for the Normal Formation of Circuits Underlying Innate Anxiety. *J. Neurosci.* **31,** 6008–6018 (2011).

35. Ohmura, Y., Tanaka, K. F., Tsunematsu, T. & Yamanaka, A. Optogenetic activation of serotonergic neurons enhances anxiety-like behaviour in mice. *Int. J. Neuropsychopharmacol.* **17,** 1777–1783 (2014).

36. Wong, D. T., Perry, K. W. & Bymaster, F. P. THE DISCOVERY OF FLUOXETINE HYDROCHLORIDE □ PROZAC □. *Nat. Rev.* **4,** 764–774 (2005).

37. Fischer, A. G., Jocham, G. & Ullsperger, M. Dual serotonergic signals: a key to understanding paradoxical effects? *Trends Cogn. Sci.* **19,** 21–26 (2015).

38. Urban, D. J. *et al.* Elucidation of The Behavioral Program and Neuronal Network Encoded by Dorsal Raphe Serotonergic Neurons. *Neuropsychopharmacology* 1–12 (2015). doi:10.1038/npp.2015.293

39. Fava, M. & Kendler, K. S. Major Depressive Disorder Review. *Neuron* **28,** 335–341 (2000).

40. Daw, N. D., Kakade, S. & Dayan, P. Opponent interactions between serotonin and dopamine. *Neural Networks* **15,** 603–616 (2002).

41. Cools, R., Nakamura, K. & Daw, N. D. Serotonin and Dopamine : Unifying Affective , Activational , and Decision Functions. *Neuropsychopharmacology* **36,** 98–113 (2011).

42. Donaldson, Z. R., Nautiyal, K. M., Ahmari, S. E. & Hen, R. Genetic approaches for understanding the role of serotonin receptors in mood and behavior. *Curr. Opin. Neurobiol.* **23,** 399–406 (2014).

43. Nakamura, K. The role of the dorsal raphé nucleus in reward-seeking behavior. *Front. Integr. Neurosci.* **7,** 60 (2013).

44. Clarke, H. F. Cognitive Inflexibility After Prefrontal Serotonin Depletion. *Science (80-.).* **304,** 878–880 (2004).

45. Clarke, H. F., Walker, S. C., Dalley, J. W., Robbins, T. W. & Roberts, a. C. Cognitive inflexibility after prefrontal serotonin depletion is behaviorally and neurochemically specific. *Cereb. Cortex* **17,** 18–27 (2007).

46. Whitaker-Azmitia PM, P. S. *The neuropharmacology of serotonin*. (New York Academy of Sciences, 1990).

47. Lucki, I. The spectrum of behaviors influenced by serotonin. *Biol. Psychiatry* **44,** 151–162 (1998).

48. Müller, C. P. & Jacobs, B. L. *Handbook of the Behavioral Neurobiology of Serotonin*. (Elsevier, 2010).

49. Jabobs, B. L. & Fornal, C. A. in *Psychopharmacology: The Fourth Generation of Progress* (eds. Bloom, F. E. & Kupfer, D. J.) 461–470 (Raven Press, New York, 1995).

50. Aghajanian, G. K., Marek, G. J. & Ph, D. Serotonin and Hallucinogens. *Neuropsychopharmacology* **21,** (1999).

51. Halberstadt, A. L. Recent advances in the neuropsychopharmacology of serotonergic hallucinogens. *Behav. Brain Res.* **277,** 99–120 (2015).

52. Trulson, M. E. & Jacobs, B. L. Long-Term Attphetamine Treatment Decreases Brain Serotonin Metabolism : Implications for Theories of Schizophrenia Trypto-. *Science* **205,** 1295–1297 (1979).

53. Grossberg, S. The Imbalanced Brain : From Normal Behavior to Schizophrenia. *Biol. Psychiatry* **48,** 81–98 (2000).

54. Remington, G. Alterations of dopamine and serotonin transmission in schizophrenia. *Prog. Brain Res.* **172,** 117–140 (2008).

55. Goddard, A. W., Shekhar, A., Whiteman, A. F. & Mcdougle, C. J. Serotoninergic mechanisms in the treatment of obsessive – compulsive disorder. *Drug Discov. Today* **13,** 325–332 (2008).

56. Maia, T. V & Cano-colino, M. The Role of Serotonin in Orbitofrontal Function and Obsessive-Compulsive Disorder. *Clin. Psychol. Sci.* **3,** 460–482 (2015).

57. Walther, D. J. & Bader, M. A unique central tryptophan hydroxylase isoform. *Biochem. Pharmacol.* **66,** 1673–1680 (2003).

58. Zhang, X., Beaulieu, J., Sotnikova, T. D., Gainetdinov, R. R. & Caron, M. G. Tryptophan Hydroxylase-2 Controls Brain Serotonin Synthesis. *Science* **305,** 27710 (2004).

59. Azmitia, E. C. G. Serotonin. *eLS* (2001). doi:10.1038/npg.els.0000124

60. Maejima, T., Masseck, O. A., Mark, M. D. & Herlitze, S. Modulation of firing and synaptic transmission of serotonergic neurons by intrinsic G protein-coupled receptors and ion channels. *Front. Integr. Neurosci.* **7,** Article 40 (2013).

61. Dankoski, E. C., Wightman, R. M., Garris, P. A. & State, I. Monitoring serotonin signaling on a subsecond time scale. *Front. Integr. Neurosci.* **7,** Article 44 (2013).

62. Ishimura, K., Takeuchi, Y. & Fujiwara, K. Quantitative analysis of the distribution of serotonin-immunoreactive cell bodies in the mouse brain. *Neurosci. Lett.* **91,** 265–270 (1988).

63. Hornung, J. The human raphe nuclei and the serotonergic system. *J. Chem. Neuroanat.* **26,** 331–343 (2003).

64. Hoyer, D., Hannon, J. P. & Martin, G. R. Molecular , pharmacological and functional diversity of 5-HT receptors. *Pharmacol. Biochem. Behavio* **71,** 533–554 (2002).

65. Barnes, N. M. & Sharp, T. A review of central 5-HT receptors and their function. *Neuropharmacoloy* **38,** 1083–1152 (1999).

66. Roth, B. L., Lopez, E., Patel, S. & Kroeze, W. K. The Multiplicity of Serotonin Receptors: Uselessly Diverse Molecules or an Embarrassment of Riches? *Neuroscientist* **6,** 252–262 (2000).

67. Jacobs, B. L., Ph, D., Fornal, C. A. & Ph, D. Activity of Serotonergic Neurons in Behaving Animals. *Neurospychopharmacology* **21,** (1999).

68. Wylie, C. J. *et al.* Distinct Transcriptomes Define Rostral and Caudal Serotonin Neurons. *J. Neurosci.* **30,** 670–684 (2010).

69. Tork, I. Anatomy of the Serotonergic System. 9–35

70. Jensen, P. *et al.* Redefining the serotonergic system by genetic lineage. *Nat. Neurosci.* **11,** 417–419 (2008).

71. Azmitia, C. An Autoradiographic Analysis of the Differential Ascending Projections of the Dorsal and Median Raphe Nuclei in the Rat. *J. Comp. Neurol.* **179,** 641–668 (1978).

72. Vasudeva, R. K., Lin, R. C. S., Simpson, K. L. & Waterhouse, B. D. Functional organization of the dorsal raphe efferent system with special consideration of nitrergic cell groups. *J. Chem. Neuroanat.* **41,** 281–293 (2011).

73. Bang, S. J., Jensen, P., Dymecki, S. M. & Commons, K. G. Projections and interconnections of genetically defined serotonin neurons in mice. *Eur. J. Neurosci.* **35,** 85–96 (2012).

74. Muzerelle, A., Scotto-lomassese, S., Bernard, J. F., Soiza-Reilly, M. & Gaspar, P. Conditional anterograde tracing reveals distinct targeting of individual serotonin cell groups (B5 – B9) to the forebrain and brainstem. *Brain Struct. Funct.* (2014). doi:10.1007/s00429-014-0924-4

75. Villar, M. J., Vitale, M. L., Hokfelt, T. & Verhofstad, A. A. J. Dorsal Raphe Serotoninergic Branching Neurons Projecting Both to the Lateral Geniculate Body and Superior Colliculus : A Combined Retrograde Tracing- Immunohistochemical Study in the Rat. *J. Comp. Neurol.* **140,** 126–140 (1988).

76. Jacobs, B. L. & Azmitia, E. C. Structure and function of the brain serotonin system. *Physiol. Rev.* **72,** 165–229 (1992).

77. Wickersham, I. R. *et al.* Monosynaptic Restriction of Transsynaptic Tracing from Single , Genetically Targeted Neurons. *Neuron* **53,** 639–647 (2007).

78. Tronche, F., Casanova, E., Turiault, M., Sahly, I. & Kellendonk, C. When reverse genetics meets physiology : the use of site-specific recombinases in mice. *FEBS Lett.* **529,** 116–121 (2002).

79. Kuhlman, S. J. & Huang, Z. J. High-Resolution Labeling and Functional Manipulation of Specific Neuron Types in Mouse Brain by Cre- Activated Viral Gene Expression. *PLoS One* **3,** e2005 (2008).

80. Atasoy, D., Aponte, Y., Su, H. H. & Sternson, S. M. A FLEX Switch Targets Channelrhodopsin-2 to Multiple Cell Types for Imaging and Long-Range Circuit Mapping. *J. Neurosci.* **28,** 7025–7030 (2008).

81. Ogawa, S., Cohen, J., Hwang, D., Uchida, N. & Watabe-Uchida, M. Organization of Monosynaptic Inputs to the Serotonin and Dopamine Neuromodulatory Systems. *Cell Rep.* **8,** 1–14 (2014).

82. Weissbourd, B. *et al.* Presynaptic Partners of Dorsal Raphe Serotonergic and GABAergic Neurons. *Neuron* **83,** 645–662 (2014).

83. Pollak Dorocic, I. *et al.* A Whole-Brain Atlas of Inputs to Serotonergic Neurons of the Dorsal and Median Raphe Nuclei. *Neuron* **83,** 663–678 (2014).

84. Steinbusch, H. W. M., Kooy, D. VAN DER, Verhofstad, A. A. J. & Pellegrino, A. Serotonergic and non-serotonergic projections from the nucleus raphe dorsalis to the

caudate-putamen complex in the rat, studied by a combined immunofluorecence and fluorescent retrograde axonal labeling technique. *Neurosci. Lett.* **19,** 137–142 (1980).

85. Michelsen, K. A., Prickaerts, J. & Ã, H. W. M. S. in *Progress in Brain Research* (eds. Giovanni, G. Di, Matteo, V. D. & Esposito, E.) **172,** 233–264 (2008).

86. Commons, K. G. Locally collateralizing glutamate neurons in the dorsal raphe nucleus responsive to substance P contain vesicular glutamate transporter 3 (VGLUT3). *J. Chem. Neuroanat.* **38,** 273–281 (2009).

87. Hioki, H. *et al.* Vesicular glutamate transporter 3-expressing nonserotonergic projection neurons constitute a subregion in the rat midbrain raphe nuclei. *J. Comp. Neurol.* **518,** 668–686 (2010).

88. Fu, W. *et al.* Chemical Neuroanatomy of the Dorsal Raphe Nucleus and Adjacent Structures of the Mouse Brain. *J. Comp. Neurol.* **3494,** 3464–3494 (2010).

89. Lu, Y., Simpson, K. L. & Weaver, K. J. Coexpression of Serotonin and Nitric Oxide in the Raphe Complex : Cortical Versus Subcortical Circuit. *Anat. Rec.* **1965,** 1954–1965 (2010).

90. Jackson, J., Bland, B. H. & Antle, M. C. Nonserotonergic projection neurons in the midbrain raphe nuclei contain the vesicular glutamate transporter VGLUT3. *Synapse* **63,** 31–41 (2009).

91. Bang, S. J. & Commons, K. G. Forebrain GABAergic Projections From the Dorsal Raphe Nucleus Identified by Using GAD67 – GFP Knock-In Mice. *J. Comp. Neurol.* **4167,** 4157–4167 (2012).

92. Descarries, L., Watkins, K. C. & Garcia, S. The Serotonin Neurons in Nucleus Raphe Dorsalis of Adult Rat : A Light and Electron Microscope Radioautographic Study. *J. Comp. Neurol.* **207,** 239–254 (1982).

93. Cohen, J. Y., Amoroso, M. W. & Uchida, N. Serotonergic neurons signal reward and punishment on multiple timescales. *Elife* **4:e06346,** (2015).

94. Mcginty, D. J. & Harper, R. M. Dorsal raphe neurons : depression of firing during sleep in cats. *Brain Res.* **101,** 569–575 (1976).

95. Kirby, L. G., Pernar, L., Valentino, R. J. & Beck, S. G. Distinguishing characteristics of serotonin and non-serotonin-containing cells in the dorsal raphe nucleus: electrophysiological and immunohistochemical studies. *Neuroscience* **116,** 669–683 (2003).

96. Beck, S. G. *et al.* Median and Dorsal Raphe Neurons Are Not Electrophysiologically Identical. *J. Neurophysiol.* **91,** 994–1005 (2004).

97. Marinelli, S. *et al.* Serotonergic and Nonserotonergic Dorsal Raphe Neurons Are Pharmacologically and Electrophysiologically Heterogeneous. *J. Neurophysiol.* **92,** 3532–3537 (2004).

98. Allers, K. a. & Sharp, T. Neurochemical and anatomical identification of fast- and slow-firing neurones in the rat dorsal raphe nucleus using juxtacellular labelling methods in vivo. *Neuroscience* **122,** 193–204 (2003).

99. Kocsis, B., Varga, V., Dahan, L. & Sik, A. Serotonergic neuron diversity : Identification of raphe neurons with discharges time-locked to the hippocampal theta rhythm. (2005).

100. Urbain, N. *et al.* Electrophysiological diversity of the dorsal raphe cells across the sleep – wake cycle of the rat. *J. Physiol.* **573,** 679–695 (2006).

101. Hajós, H. *et al.* Neurochemical identification of stereotypic burst-firing neurons in the rat dorsal raphe nucleus using juxtacellular labelling methods. *Eur. J. Neurosci.* **25,** 119–126 (2007).

102. Schweimer, J. V, Mallet, N., Sharp, T. & Ungless, M. A. Spike-timing relationship of neurochemically-identified dorsal raphe neurons during costical slow oscillations. *Neuroscience* **196,** 115–123 (2011).

103. Mccormick, D. A. Neurotransmitter actions in the thalamus and cerebral cortex and their role in neuromodulation of thalamocortical activity. *Prog. Neurobiol.* **39,** 337–388 (1992).

104. Dugué, G. P. & Mainen, Z. F. How serotonin gates olfactory information flow. *Nat. Neurosci.* **12,** 673–675 (2009).

105. Steinfels, G. F., Heym, J., Strecker, R. E. & Jacobs, B. L. Raphe Unit Activity in Freely Moving Cats is Altered by Manipulations of Central but not Peripheral Motor Systems. *Brain Res.* **279,** 77–84 (1983).

106. Trulson, M. E. & Jacobs, B. L. Raphe unit activity in freely moving cats: correlation with level of behavioral arousal. *Brain Res.* **163,** 135–150 (1979).

107. Trulson, M. E., Jacobs, B. L. & Morrison, A. R. Raphe unit activity during REM sleep in normal cats in pontine lesioned cats displaying rem sleep without atonia. *Brain Res.* **226,** 75–91 (1981).

108. Veasey, S. C., Fornal, C. A., Metzler, C. W. & Jacobs, B. L. Single-unit responses of serotonergic dorsal raphe neurons to specific motor challenges in freely moving cats. *Neuroscience* **79,** 161–169 (1997).

109. Kravitz, E. Hormonal control of behavior: amines and the biasing of behavioral output in lobsters. *Science* **241,** 1775–1781 (1989).

110. Ma, P., Beltz, B. & Kravitz, E. Serotonin-containing neurons in lobsters: their role as gain-setters in postural control mechanisms. *J. Neurophysiol.* **68,** 36–54 (1992).

111. Soubrié, P. Reconciling the role of central serotonin neurons in human and animal behavior. *Behav. Brain Sci.* **9,** 319–346 (1986).

112. Wise, C. D., Berger, B. D. & Stein, L. Evidence of alpha-noradrenergic reward receptors and serotonergic punishment receptors in the rat brain. *Biol. Psychiatry* **6,** 3–21 (1973).

113. Miyazaki, K. W., Miyazaki, K. & Doya, K. Activation of the central serotonergic system in response to delayed but not omitted rewards. *Eur. J. Neurosci.* 1–8 (2010). doi:10.1111/j.1460-9568.2010.07480.x

114. Miyazaki, K., Miyazaki, K. W. & Doya, K. Activation of Dorsal Raphe Serotonin Neurons Underlies Waiting for Delayed Rewards. *J. Neurosci.* **31,** 469–479 (2011).

115. Miyazaki, K. W., Miyazaki, K. & Doya, K. Activation of the central serotonergic system in response to delayed but not omitted rewards. *Eur. J. Neurosci.* **33,** 153–160 (2011).

116. Miyazaki, K. W., Miyazaki, K. & Doya, K. Activation of Dorsal Raphe Serotonin Neurons Is Necessary for Waiting for Delayed Rewards. *J. Neurosci.* **32,** 10451–10457 (2012).

117. Miyazaki, K., Miyazaki, K. W. & Doya, K. The Role of Serotonin in the Regulation of Patience and Impulsivity. *Mol. Neurobiol.* (2012). doi:10.1007/s12035-012-8232-6

118. Miyazaki, K. W., Miyazaki, K., Tanaka, K. F., Yamanaka, A. & Takahashi, A. Optogenetic Activation of Dorsal Raphe Serotonin Neurons Enhances Patience for Future Rewards. *Curr. Biol.* **24,** 1–8 (2014).

119. Fonseca, M. S., Murakami, M. & Mainen, Z. F. Activation of Dorsal Raphe Serotonergic Neurons Promotes Waiting but Is Not Reinforcing. *Curr. Biol.* **25,** 1–10 (2015).

120. Doya, K. Metalearning and neuromodulation. *Neural Networks* **15,** 495–506 (2002).

121. Doya, K. Modulators of decision making. *Nat. Neurosci.* 410–416 (2008). doi:10.1038/nn2077

122. Wise, C. D., Berger, B. D. & Stein, L. Serotonin: a possible mediator of behavioral suppression induced by anxiety. *Dis. Nerv. Syst.* **31,** Suppl:34–37 (1970).

123. Deakin K.F.W. in *Theory of Phychopharmacology* (ed. Cooper S.J.) Vol. 2, 149–193 (Academic Press, New York, 1983).

124. Graeff, F. G. Tryptamine antagonists and punished behavior. *J. Pharmacol. Exp. Ther.* **180,** 344–350 (1974).

125. Deakin and Graeff - 5-HT and mechanisms of defence.pdf.

126. Faulkner, P. & Deakin, J. F. W. The role of serotonin in reward , punishment and behavioural inhibition in humans : Insights from studies with acute tryptophan depletion. *Neurosci. Biobehav. Rev.* **46,** 365–378 (2014).

127. Deakin, J. F. W. The origins of ‘ 5-HT and mechanisms of defence ’ by Deakin and Graeff : A personal perspective. *J. Psycho* **27,** 1084–1089 (2015).

128. Montagne-clavel, J., Oliveras, J. & Martin, G. Single unit recordings at dorsal raphe nucleus in the awake-anesthetized rat: spontaneous activity and responses to cutaneous innocuous and noxious stimulations. *Pain* **60,** 303–310 (1995).

129. Takase, L. F. *et al.* Inescapable shock activates serotonergic neurons in all raphe nuclei of rat. *Behav. Brain Res.* **153,** 233–239 (2004).

130. Schweimer, J. V. & Ungless, M. a. Phasic responses in dorsal raphe serotonin neurons to noxious stimuli. *Neuroscience* **171,** 1209–1215 (2010).

131. Hayashi, K., Nakao, K. & Nakamura, K. Appetitive and Aversive Information Coding in the Primate Dorsal Raphe Nucleus. *J. Neurosci.* **35,** 6195–6208 (2015).

132. Azmitia, E. C. in *Handbook of Psychopharmacology (Vol.9) Chemical pathways in the brain* (eds. Iversen, L. L., Iversen, S. D. & Snyder, S.) 233–314 (Plenum Press, 1978).

133. Fletcher, P. J. Dopamine receptor blockade in nucleus accumbens or caudate nucleus differentially affects feeding induced by 8-OH-DPAT injected into dorsal or median raphe. *Brain Res.* **552,** 181–189 (1991).

134. Boureau, Y. & Dayan, P. Opponency Revisited : Competition and Cooperation Between Dopamine and Serotonin. *Neuropsychopharmacology* **36,** 74–97 (2011).

135. Solomon, R. L. An opponent-process theory of motivation. I. Temporal dynamics of affect. *Psychol. Rev.* **81,** 119–145 (1974).

136. Grossberg. *Neural networks and natural intelligence*. (MIT Press, Cambridge, MA, 1988).

137. Watabe-uchida, M., Zhu, L., Ogawa, S. K., Vamanrao, A. & Uchida, N. Whole-Brain Mapping of Direct Inputs to Midbrain Dopamine Neurons. *Neuron* **74,** 858–873 (2012).

138. Wise, R. A. Dopamine, learning and motivation. *Nat. Rev. Neurosci.* **5,** (2004).

139. Montague, P. R., Dayan, P. & Sejnowski, T. J. A framework for mesencephalic dopamine systems based on predictive Hebbian learning. *J. Neurosci.* **16,** 1936–1947 (1996).

140. Schultz, W., Dayan, P. & Montague, P. R. A neural substrate of prediction and reward. *Science* **275,** 1593–1599 (1997).

141. Fiorillo, C. D., Tobler, P. N. & Schultz, W. Discrete coding of reward probability and uncertainty by dopamine neurons. *Science* **299,** 1898–1902 (2003).

142. Fiorillo, C. D., Newsome, W. T. & Schultz, W. The temporal precision of reward prediction in dopamine neurons. *Nat. Neurosci.* **11,** 966–973 (2008).

143. Cohen, J. Y., Haesler, S., Vong, L., Lowell, B. B. & Uchida, N. Neuron-type-specific signals for reward and punishment in the ventral tegmental area. *Nature* **482,** 85–88 (2012).

144. Eshel, N. *et al.* Arithmetic and local circuitry underlying dopamine prediction errors. *Nature* **525,** 243–246 (2015).

145. Sutton, R. S. Learning to Predict by the Methods of Temporal Differences. **3,** 9–44 (1988).

146. Sutton, R. S. & Barto, A. G. in *Learning and computational neuroscience* (eds. Gabriel, M. & Moore, J. W.) 497–537 (MIT Press, Cambridge, MA, 1990).

147. Sutton, R. S. & Barto, a G. Reinforcement learning: an introduction. *IEEE Trans. Neural Netw.* **9,** 1054 (1998).

148. Reynolds, J. N., Hyland, B. I. & Wickens, J. R. A cellular mechanism of reward-related learning. *Nature* **413,** 67–70 (2001).

149. Stuber, G. D. *et al.* Reward-predictive cues enhance excitatory synaptic strength onto midbrain dopamine neurons. *Science* **321,** 1690–1692 (2008).

150. Morris, G., Schmidt, R. & Bergman, H. Striatal action-learning based on dopamine concentration. *Exp. Brain Res.* **200,** 307–317 (2010).

151. Tsai, H. *et al.* Phasic Firing in Dopaminergic Neurons is Sufficient for Behavioral Conditioning. *Science* **324,** (2009).

152. Witten, I. B. *et al.* Recombinase-driver rat lines: Tools, techniques, and optogenetic application to dopamine-mediated reinforcement. *Neuron* **72,** 721–733 (2011).

153. Kim, K. M. *et al.* Optogenetic Mimicry of the Transient Activation of Dopamine Neurons by Natural Reward Is Sufficient for Operant Reinforcement. *PLoS One* **7,** 1–8 (2012).

154. Steinberg, E. E. *et al.* A causal link between prediction errors, dopamine neurons and learning. *Nat Neurosci* **16,** 966–973 (2013).

155. Niv, Y., Daw, N. D., Joel, D. & Dayan, P. Tonic dopamine: Opportunity costs and the control of response vigor. *Psychopharmacology (Berl).* **191,** 507–520 (2007).

156. Berridge, K. C. The debate over dopamine's role in reward: The case for incentive salience. *Psychopharmacology (Berl).* **191,** 391–431 (2007).

157. Berridge, K. C., Robinson, T. E. & Aldridge, J. W. Dissecting components of reward: 'liking','wanting', and learning. **9,** 65–73 (2009).

158. Flagel, S. B. *et al.* A selective role for dopamine in stimulus-reward learning. *Nature* **469,** 53–57 (2011).

159. Matsumoto, M. & Hikosaka, O. Two types of dopamine neuron distinctly convey positive and negative motivational signals. *Nature* **459,** 837–841 (2009).

160. Fiorillo, C. D., Song, M. R. & Yun, S. R. Multiphasic temporal dynamics in responses of midbrain dopamine neurons to appetitive and aversive stimuli. *J. Neurosci.* **33,** 4710–25 (2013).

161. Fiorillo, C. D. Two Dimensions of Value : Dopamine Neurons Represent Reward But Not Aversiveness. *Science (80-.).* **341,** 546–549 (2013).

162. Bromberg-martin, E. S., Matsumoto, M. & Hikosaka, O. Dopamine in Motivational Control: Rewarding, Aversive, and Alerting. *Neuron* **68,** 815–834 (2010).

163. Lammel, S., Ion, D. I., Roeper, J. & Malenka, R. C. Projection-Specific Modulation of Dopamine Neuron Synapses by Aversive and Rewarding Stimuli. *Neuron* **70,** 855–862 (2011).

164. Lammel, S. *et al.* Input-specific control of reward and aversion in the ventral tegmental area. *Nature* **491,** 212–217 (2012).

165. Menegas, W. *et al.* Dopamine neurons projecting to the posterior striatum form an anatomically distinct subclass. *Elife* 10.7554/eLife.10032 (2015).

166. Lerner, T. N. *et al.* Intact-Brain Analyses Reveal Distinct Information Carried by SNc Dopamine Subcircuits. *Cell* **162,** 635–647 (2015).

167. Daw, N. D. & Touretzky, D. S. Long-Term Reward Prediction in TD Models of the Dopamine System. *Neural Comput.* **2583,** 2567–2583 (2002).

168. Fletcher, P. J., Ming, Z. & Higgins, G. A. Conditioned place preference induced by microinjection of 8-OH-DPAT into the dorsal or median raphe nucleus. *Psychopharmacology (Berl).* **113,** 31–36 (1993).

169. Fletcher, P. J., Tampakerast, M. & Yeomanst, J. S. Median Raphe Injections of 8-OH-DPAT Lower Frequency Thresholds for Lateral Hypothalamic Self-Stimulation. *Pharmacol. Biochem. Behav.* **52,** 65–71 (1995).

170. Fletcher, P. J., Korth, K. M. & Chambers, J. W. Selective destruction of brain serotonin neurons by 5 , 7-dihydroxytryptamine increases responding for a conditioned reward. *Pharmacology* **147,** 291–299 (1999).

171. Fletcher, P. J. & Korth, K. M. Activation of 5-HT 1B receptors in the nucleus accumbens reduces amphetamine-induced enhancement of responding for conditioned reward. *Neuropsychopharmacology* **142,** 165–174 (1999).

172. Kapur, S. & Remington, G. Serotonin–dopamine interaction and its relevance to schizophrenia. *Am. J. Psychiatry* **153,** 466–476 (1996).

173. Jones, S. & Kauer, J. A. Amphetamine Depresses Excitatory Synaptic Transmission via Serotonin Receptors in the Ventral Tegmental Area. *J. Neurosci.* **19,** 9780–9787 (1999).

174. Mahadevan, S. Average Reward Reinforcement Learning : Foundations , Algorithms , and Empirical Results. *Mach. Learn.* **22,** 159–195 (1996).

175. Huys, Q. J. M. & Dayan, P. A Bayesian formulation of behavioral control. *Cognition* **113,** 314–328 (2009).

176. Nakamura, K., Matsumoto, M. & Hikosaka, O. Reward-dependent modulation of neuronal activity in the primate dorsal raphe nucleus. *J. Neurosci.* **28,** 5331–5343 (2008).

177. Bromberg-Martin, E. S., Hikosaka, O. & Nakamura, K. Coding of task reward value in the dorsal raphe nucleus. *J. Neurosci.* **30,** 6262–6272 (2010).

178. Liu, Z. *et al.* Dorsal Raphe Neurons Signal Reward through 5-HT and Glutamate. *Neuron* **81,** 1360–1374 (2014).

179. Ranade, S. P. & Mainen, Z. F. Transient firing of dorsal raphe neurons encodes diverse and specific sensory, motor, and reward events. *J. Neurophysiol.* **102,** 3026–37 (2009).

180. Inaba, K. *et al.* Neurons in Monkey Dorsal Raphe Nucleus Code Beginning and Progress of Step-by-Step Schedule , Reward Expectation , and Amount of Reward Outcome in the Reward Schedule Task. *J. Neurosci.* **33,** 3477–3491 (2013).

181. Lima, S. Q., Hromádka, T., Znamenskiy, P. & Zador, A. M. PINP : A New Method of Tagging Neuronal Populations for Identification during In Vivo Electrophysiological Recording. *PLoS One* **4,** e6099 (2009).

182. Mayevsky, A. & Chance, B. in *Advances in Experimental Medicine and Biology* 239–244 (1973).

183. Chance, B., Legallais, V., Sorge, J. & Graham, N. A Versatile Time-Sharing Multichannel Spectrophotometer, Reflectometer, and Fluorometer. *Anal. Biochem.* **66,** 498–514 (1975).

184. Gunaydin, L. a. *et al.* Natural neural projection dynamics underlying social behavior. *Cell* **157,** 1535–1551 (2014).

185. Mayevsky, A. & Chance, B. Oxidation-Reduction State Measured in situ by a Multichannel fiber-optic Fluorometer. *Science* **217,** 537–540 (1982).

186. Mayevsky, A. Brain NADH redox state monitored in vivo by fiber optic surface fluorometry. *Brain Res. Rev.* **7,** 49–68 (1984).

187. Mottin, S., Laporte, P., Jouvet, M. & Cespuglio, R. Determination of NADH in the rat brain during sleep-wake states with an optic fibre sensor and time-resolved fluorescence procedures. *Neuroscience* **79,** 683–693 (1997).

188. Stosiek, C., Garaschuk, O., Holthoff, K. & Konnerth, A. In vivo two-photon calcium imaging of neuronal networks. *Proc. Natl. Acad. Sci. U. S. A.* **100,** 7319–7324 (2003).

189. Paredes, R. M., Etzler, J. C., Watts, L. T., Zheng, W. & Lechleiter, J. D. Chemical calcium indicators. *Methods* **46,** 143–51 (2008).

190. Adelsberger, H., Garaschuk, O. & Konnerth, A. Cortical calcium waves in resting newborn mice. *Nat. Neurosci.* **8,** 988–990 (2005).

191. Grienberger, C. *et al.* Sound-evoked network calcium transients in mouse auditory cortex in vivo. *J. Physiol.* **590,** 899–918 (2012).

192. Stroh, A. *et al.* Making Waves: Initiation and Propagation of Corticothalamic Ca2+ Waves In Vivo. *Neuron* **77,** 1136–1150 (2013).

193. Berridge, M. J., Lipp, P. & Bootman, M. D. The versatility and universality of calcium signalling. *Nat. Rev. Mol. Cell Biol.* **1,** 11–21 (2000).

194. Helmchen, F. & Sakmann, B. Ca2 + Buffering and Action Potential-Evoked Ca2 + Signaling in Dendrites of Pyramidal Neurons. *Biophys. Journalournal* **70,** 1069–1081 (1996).

195. Kerr, J. N. D., Greenberg, D. & Helmchen, F. Imaging input and output of neocortical networks in vivo. **102,** 14063–14068 (2005).

196. Grienberger, C. & Konnerth, A. Imaging Calcium in Neurons. *Neuron* **73,** 862–885 (2012).

197. Deisseroth, K. Optogenetics: 10 years of microbial opsins in neuroscience. *Nat. Neurosci.* **18,** 1213–1225 (2015).

198. Adamantidis, A. *et al.* Optogenetics: 10 years after ChR2 in neurons - views from the community. *Nat. Neurosci.* **18,** 1213–1225 (2015).

199. Miyawaki, A. *et al.* Fluorescent indicators for Ca 2 + based on green fluorescent proteins and calmodulin. *Nature* **388,** 882–887 (1997).

200. Heim, N. *et al.* Improved calcium imaging in transgenic mice expressing a troponin C – based biosensor. *Nat. Methods* **4,** 2006–2008 (2007).

201. Wallace, D. J. *et al.* Single-spike detection in vitro and in vivo with a genetic Ca 2 + sensor. *Nat. Methods* **5,** 797–804 (2008).

202. Mank, M. & Griesbeck, O. Genetically Encoded Calcium Indicators. *Chem. Rev.* **108,** 1550–1564 (2008).

203. Hires, S. A., Tian, L. & Looger, L. L. Reporting neural activity with genetically encoded calcium indicators. *Brain Cell Biol.* **36,** 69–86 (2008).

204. Tian, L. *et al.* Imaging neural activity in worms , flies and mice with improved GCaMP calcium indicators. *Nat. Methods* **6,** 875–881 (2009).

205. Chen, T.-W. *et al.* Ultrasensitive fluorescent proteins for imaging neuronal activity. *Nature* **499,** 295–300 (2013).

206. Betley, J. N. & Sternson, S. M. Adeno-Associated Viral Vectors for Mapping , Monitoring , and Manipulating Neural Circuits. *Hum. Gene Ther.* **22,** 669–677 (2011).

207. Lütcke, H. Optical recording of neuronal activity with a genetically-encoded calcium indicator in anesthetized and freely moving mice. *Front. Neural Circuits* **4,** 1–12 (2010).

208. LeChasseur, Y. *et al.* A microprobe for parallel optical and electrical recordings from single neurons in vivo. *Nat. Methods* **8,** 319–325 (2011).

209. Cui, G. *et al.* Concurrent activation of striatal direct and indirect pathways during action initiation. *Nature* **494,** 238–242 (2014).

210. Cui, G. *et al.* Deep brain optical measurements of cell type–specific neural activity in behaving mice. *Nat. Protoc.* **9,** 1213–1228 (2014).

211. Chen, Y., Lin, Y.-C., Kuo, T.-W. & Knight, Z. A. Sensory Detection of Food Rapidly Modulates Arcuate Feeding Circuits. *Cell* **160,** 829–841 (2015).

212. Le Moal, M. & Olds, M. E. Unit responses to auditory input in the dorsal and median raphe nuclei of the rat. *Physiol. Behav.* **22,** 11–5 (1979).

213. Heym, J., Trulson, M. E. & Jacobs, B. L. Raphe unit activity in freely moving cats: effects of phasic auditory and visual stimuli. *Brain Res.* **232,** 29–39 (1982).

214. Veasy, S., Fornal, C. A., CW, M. & Jacobs, B. L. Single-unit responses of serotonergic dorsal raphe neurons to specific motor challenges in freely moving cats. *Neuroscience* **79,** 161–169 (1997).

215. Kulichenko, A. M. & Pavlenko, V. B. Self-Initiated Behavioral Act-Related Neuronal Activity in the Region of the. **36,** 50–57 (2004).

216. Waterhouse, B. D., Devilbiss, D., Seiple, S. & Markowitz, R. Sensorimotor-related discharge of simultaneously recorded, single neurons in the dorsal raphe nucleus of the awake, unrestrained rat. *Brain Res.* **1000,** 183–91 (2004).

217. Li, Y., Dalphin, N. & Hyland, B. I. Association with Reward Negatively Modulates Short Latency Phasic Conditioned Responses of Dorsal Raphe Nucleus Neurons in Freely Moving Rats. *J. Neurosci.* **33,** 5065–5078 (2013).

218. Dayan, P. & Huys, Q. Serotonin ' s many meanings. 3–5 (2015). doi:10.7554/eLife.06346

219. UPenn. University of Pennsylvania Vector Core. https://www.med.upenn.edu/gtp/vectorcore/

220. Gong, S. *et al.* Targeting Cre recombinase to specific neuron populations with bacterial artificial chromosome constructs. *J. Neurosci.* **27,** 9817–9823 (2007).

221. GENSAT. www.gensat.org

222. Fiji. http://fiji.sc/

223. Baubet, V. *et al.* Chimeric green fluorescent protein-aequorin as bioluminescent Ca2+ reporters at the single-cell level. *Proc. Natl. Acad. Sci. U. S. A.* **97,** 7260–7265 (2000).

224. Naumann, E. A., Kampff, A. R., Prober, D. A., Schier, A. F. & Engert, F. Monitoring neural activity with bioluminescence during natural behavior. *Nat. Neurosci.* **13,** 513–520 (2010).

225. Crystalaser. http://www.crystalaser.com/

226. Semrock. www.semrock.com

227. Chroma. www.chroma.com

228. Doric Lenses. http://doriclenses.com/

229. Thorlabs. http://www.thorlabs.com/

230. Hamamatsu. http://www.hamamatsu.com/

231. Shannon, N. J., Gunnet, J. W. & Moore, K. E. A Comparison of Biochemical Indices of 5-Hydroxytryptaminergic Neuronal Activity Following Electrical Stimulation of the Dorsal Raphe Nucleus. *J. Neurochem.* **47,** 958–965 (1986).

232. FHC. http://www.fh–co.com/

233. Scientifica. http://www.scientifica.uk.com/

234. AM Systems. https://www.a–msystems.com/

235. Cambridge Electronic Design. http://ced.co.uk/

236. Albin, R. L., Young, A. B. & Penney, J. B. The functional anatomy of basal ganglia disorders. *Trends Neurosci.* **12,** 366–375 (1989).

237. Jin, X. & Costa, R. M. Start / stop signals emerge in nigrostriatal circuits during sequence learning. *Nature* **466,** 457–462 (2010).

238. Gerfen, C. R. *et al.* D1 and D2 dopamine receptor-regulated gene expression of striatonigral and striatopallidal neurons. *Science* **250,** 1429–1432 (1990).

239. Bateup, H. S. *et al.* Distinct subclasses of medium spiny neurons differentially regulate striatal motor behaviors. *Proc. Natl. Acad. Sci. U. S. A.* **107,** 14845–14850 (2010).

240. Kravitz, A. V *et al.* Regulation of parkinsonian motor behaviours by optogenetic control of basal ganglia circuitry. *Nature* **466,** 622–6 (2010).

241. Playstation. www.playstation.com

242. Lopes, G., Bonacchi, N., Frazão, J. & Neto, J. Bonsai: An event-based framework for processing and controlling data streams. *Front. Neuroinform.* **9,** (2015).

243. Mathworks. http://www.mathworks.com/products/matlab/

244. National Instruments. www.ni.com

245. Tecuapetla, F., Matias, S., Dugue, G. P., Mainen, Z. F. & Costa, R. M. Balanced activity in basal ganglia projection pathways is critical for contraversive movements. *Nat. Commun.* **5,** 4315 (2014).

246. Shcherbo, D. *et al.* Far-red fluorescent tags for protein imaging in living tissues. **574,** 567–574 (2009).

247. Furler, S., Paterna, J., Weibel, M. & Bu, H. Recombinant AAV vectors containing the foot and mouth disease virus 2A sequence confer efficient bicistronic gene expression in cultured cells and rat substantia nigra neurons. *Gene Ther.* **8,** 864–873 (2001).

248. Trichas, G., Begbie, J. & Srinivas, S. Use of the viral 2A peptide for bicistronic expression in transgenic mice. *BMC Biol.* **4,** (2008).

249. Bullock, T. H. Signals and signs in the nervous system : The dynamic anatomy of electrical activity is probably information-rich. *Proc. Natl. Acad. Sci. U. S. A.* **94,** 14–19 (1997).

250. Engel, A. K., Fries, P. & Singer, W. Dynamic predictions: Oscillations and synchrony in top-down processing. *Nat. Rev. Neurosci.* **2,** 704–716 (2001).

251. Kenet, T., Arieli, A., Tsodyks, M. & Grinvald, A. in *23 Problems in Systems Neuroscience* (eds. van Hemmen, J. L. & Sejnowski, T. J.) (Oxford University Press, 2006).

252. Ghosh, K. K. *et al.* Miniaturized integration of a fluorescence microscope. *Nat. Methods* **8,** 872–878 (2011).

253. Inscopix. http://www.inscopix.com/

254. Vincent, P. *et al.* Live imaging of neural structure and function by fibred fluorescence microscopy. *EMBO Rep.* **7,** (2006).

255. Wilt, B. A. *et al.* Advances in Light Microscopy for Neuroscience. *Annu. Rev. Neurosci.* **32,** 435–506 (2009).

256. Mehta, A. D., Jung, J. C., Flusberg, B. A. & Schnitzer, M. J. Fiber optic in vivo imaging in the mammalian nervous system. *Curr. Opin. Neurobiol.* **14,** 1–12 (2004).

257. Jung, J. C. *et al.* In Vivo Mammalian Brain Imaging Using One- and Two-Photon Fluorescence Microendoscopy In Vivo Mammalian Brain Imaging Using One- and Two-Photon Fluorescence Microendoscopy. *J. Neurochem.* **92,** 3121–3133 (2004).

258. Wang, C. & Ji, N. Pupil-segmentation-based adaptive optical correction of a high-numerical-aperture gradient refractive index lens for two-photon fluorescence endoscopy. *Opt. Lett.* **37,** 2001–2003 (2012).

259. Wang, C. & Ji, N. Characterization and improvement of three- dimensional imaging performance of GRIN-lens- based two-photon fluorescence endomicroscopes with adaptive optics. *Opt. Express* **21,** 27142–27154 (2013).

260. Kajikawa, Y. & Schroeder, C. E. How local is the local field potential? *Neuron* **72,** 847–858 (2011).

261. Lindén, H. *et al.* Modeling the Spatial Reach of the LFP. *Neuron* **72,** 859–872 (2011).

262. Akerboom, J. *et al.* Genetically encoded calcium indicators for multi-color neural activity imaging and combination with optogenetics. *Front. Mol. Neurosci.* **6,** 1–29 (2013).

263. Heilman, K. M., Bowers, D., Coslett, H. B., Whelan, H. & Watson, R. T. Directional hypokinesia: prolonged reaction times for leftward movements in patients with right hemisphere lesions and neglect. *Neurology* **35,** 855–596 (1985).

264. Karnath, H. O., Himmelbach, M. & Rorden, C. The subcortical anatomy of human spatial neglect: putamen, caudate nucleus and pulvinar. *Brain* **125,** 350–360 (2002).

265. Schwarcz, R., Fuxe, K., Agnati, L. F., Hökfelt, T. & Coyle, J. T. Rotational behaviour in rats with unilateral striatal kainic acid lesions: a behavioural model for studies on intact dopamine receptors. *Brain Res.* **170,** 485–95 (1979).

266. Brasted, P. J., Humby, T., Dunnett, S. B. & Robbins, T. W. Unilateral lesions of the dorsal striatum in rats disrupt responding in egocentric space. *J Neurosci* **17,** 8919–8926 (1997).

267. Kuriyama, K. & Kurihara, E. Correlation between rotational behaviors and neurochemical changes associated with damage of rat striatum: Analysis using unilateral microinjection of kainic acid. *Neurochem. Int.* **4,** 551–5 (1982).

268. Kitama, T., Ohno, T., Tanaka, M., Tsubokawa, H. & Yoshida, K. Stimulation of the caudate nucleus induces contraversive saccadic eye movements as well as head turning in the cat. *Neurosci. Res.* **12,** 287–92 (1991).

269. Thanos, P. K., Jhamandas, K. & Beninger, R. J. N-methyl-D-aspartate unilaterally injected into the dorsal striatum of rats produces contralateral circling: antagonism by 2-amino-7-phosphonoheptanoic acid and cis-flupenthixol. *Brain Res.* **589,** 55–61 (1992).

270. DeLong, M. R. Primate models of movement disorders of basal ganglia origin. *Trends Neurosci.* **13,** 281–285 (1990).

271. Alexander, G. & Crutcher, M. Functional architecture of basal ganglia circuits: neural substrates of parallel processing. *Trends Neurosci.* **13,** 266–71 (1990).

272. Kravitz, A. V *et al.* Neuro Paper Prompt 2. *Nature* **466,** 622–6 (2010).

273. Tai, L.-H., Lee, a M., Benavidez, N., Bonci, A. & Wilbrecht, L. Transient stimulation of distinct subpopulations of striatal neurons mimics changes in action value. *Nat. Neurosci.* **15,** 1281–1289 (2012).

274. Durieux, P. F., Schiffmann, S. N. & de Kerchove d'Exaerde, A. Differential regulation of motor control and response to dopaminergic drugs by D1R and D2R neurons in distinct dorsal striatum subregions. *EMBO J.* **31,** 640–653 (2012).

275. Mink, J. W. the Basal Ganglia: Focused Selection and Inhibition of Competing Motor Programs. *Prog. Neurobiol.* **50,** 381–425 (1996).

276. Hikosaka, O., Takikawa, Y. & Kawagoe, R. Role of the basal ganglia in the control of purposive saccadic eye movements. *Physiol. Rev.* **80,** 953–978 (2000).

277. Hikida, T., Kimura, K., Wada, N., Funabiki, K. & Nakanishi, S. Distinct Roles of Synaptic Transmission in Direct and Indirect Striatal Pathways to Reward and Aversive Behavior. *Neuron* **66,** 896–907 (2010).

278. Sano, H., Chiken, S., Hikida, T., Kobayashi, K. & Nambu, a. Signals through the Striatopallidal Indirect Pathway Stop Movements by Phasic Excitation in the Substantia Nigra. *J. Neurosci.* **33,** 7583–7594 (2013).

279. Han, X. A high-light sensitivity optical neural silencer: development and application to optogenetic control of non-human primate cortex. *Front. Syst. Neurosci.* **5,** 18 (2011).

280. Dang, M. T. *et al.* Disrupted motor learning and long-term synaptic plasticity in mice lacking NMDAR1 in the striatum. *Proc. Natl. Acad. Sci. U. S. A.* **103,** 15254–15259 (2006).

281. Shuen, J. a., Chen, M., Gloss, B. & Calakos, N. Drd1a-tdTomato BAC Transgenic Mice for Simultaneous Visualization of Medium Spiny Neurons in the Direct and Indirect Pathways of the Basal Ganglia. *J. Neurosci.* **28,** 2681–2685 (2008).

282. McGeorge, a J. & Faull, R. L. The organization of the projection from the cerebral cortex to the striatum in the rat. *Neuroscience* **29,** 503–537 (1989).

283. Madisen, L. *et al.* A toolbox of Cre-dependent optogenetic transgenic mice for light-induced activation and silencing. *Nat. Neurosci.* **15,** 793–802 (2012).

284. Nambu, A. Seven problems on the basal ganglia. *Curr. Opin. Neurobiol.* **18,** 595–604 (2008).

285. Cazorla, M. *et al.* Dopamine D2 Receptors Regulate the Anatomical and Functional Balance of Basal Ganglia Circuitry. *Neuron* **81,** 153–164 (2014).

286. Mallet, N. *et al.* Dichotomous Organization of the External Globus Pallidus. *Neuron* **74,** 1075–1086 (2012).

287. Jin, X., Tecuapetla, F. & Costa, R. M. Basal ganglia subcircuits distinctively encode the parsing and concatenation of action sequences. *Nat. Neurosci.* **17,** 423–430 (2014).

288. Mink, J. W. The basal ganglia and involuntary movements: impaired inhibition of competing motor patterns. *Arch. Neurol.* **60,** 1365–1368 (2003).

289. Wichmann, T. & Delong, M. R. Functional and pathophysiological models of the basal ganglia. *Curr. Opin. Neurobiol.* **6,** 751–758 (1996).

290. Tecuapetla, F., Koo, T., Tepper, J. M., Kabbani, N. & Yeckel, M. F. Differential Dopaminergic Modulation of Neostriatal Synaptic Connections of Striatopallidal Axon Collaterals. *J. Neurosci.* **29,** 8977–8990 (2009).

291. Taverna, S. *et al.* Recurrent Collateral Connections of Striatal Medium Spiny Neurons Are Disrupted in Models of Parkinson ' s Disease. *J. Neurosci.* **28,** 5504–5512 (2008).

292. Deurwaerdère, P. De, Bonhomme, N., Lucas, G., Moal, M. Le & Spampinato, U. Serotonin Enhances Striatal Dopamine Outflow In Vivo Through Dopamine Uptake Sites. *J. Neurochem.* **66,** 210–215 (1996).

293. Navailles, S. & Deurwaerdère, P. De. Presynaptic control of serotonin on striatal dopamine function. *Psychopharmacology (Berl).* **213,** 213–242 (2011).

294. Mathur, B. N. & Lovinger, D. M. Parkinsonism and Related Disorders Serotonergic action on dorsal striatal function. *Park. Relat. Disord.* **18,** S129–S131 (2012).

295. Dray, a, Davies, J., Oakley, N. R., Tongroach, P. & Vellucci, S. The dorsal and medial raphe projections to the substantia nigra in the rat: electrophysiological, biochemical and behavioural observations. *Brain Res.* **151,** 431–442 (1978).

296. Guiard, B. P., Mansari, M. El, Merali, Z. & Blier, P. Functional interactions between dopamine , serotonin and norepinephrine neurons : an in-vivo electrophysiological study in rats with monoaminergic lesions. *Int. J. Neuropsychopharmacol.* **11,** 625–639 (2008).

297. Carta, M., Carlsson, T., Kirik, D. & Björklund, A. Dopamine released from 5-HT terminals is the cause of L-DOPA-induced dyskinesia in parkinsonian rats. *Brain* **130,** 1819–1833 (2007).

298. Muñoz, A. *et al.* Serotonin neuron-dependent and -independent reduction of dyskinesia by 5-HT 1A and 5-HT 1B receptor agonists in the rat Parkinson model. *Exp. Neurol.* **219,** 298–307 (2009).

299. Reed, M. C., Nijhout, H. F. & Best, J. Computational studies of the role of serotonin in the basal ganglia. *Front. Integr. Neurosci.* **7,** 1–8 (2013).

300. The Jackson Laboratory. https://www.jax.org/

301. Parker Hannifin. http://www.parker.com/

302. Drummond Scientific. www.drummondsci.com/

303. UNC Vector Core. http://www.med.unc.edu/genetherapy/vectorcore

304. Laserglow Technologies. www.laserglow.com

305. CNI Lasers. www.cnilaser.com

306. AA Opto Electronic. http://www.aaoptoelectronic.com/

307. Innovative-Neurophysiology. http://www.inphysiology.com

308. Blackrock Microsystems. www.blackrockmicro.com

309. Plexon Inc. www.plexon.com

310. A.M.P.I. http://www.ampi.co.il/

311. Aravanis, A. M. *et al.* An optical neural interface: in vivo control of rodent motor cortex with integrated fiberoptic and optogenetic technology. *J. Neural Eng.* **4,** S143–S156 (2007).

312. Zeiss. www.zeiss.com

313. MBF Bioscience. http://www.mbfbioscience.com/

314. The Imaging Source. http://www.theimagingsource.com/

315. Tracker, S. M. Simple Mouse Tracker. https://github.com/joseaccruz/SimpleMouseTracker

316. Systat. www.systat.com

317. Boulougouris, V., Castañé, A. & Robbins, T. W. Dopamine D2 / D3 receptor agonist quinpirole impairs spatial reversal learning in rats : investigation of D3 receptor involvement in persistent behavior. *Psychopharmacology (Berl).* **202,** 611–620 (2009).

318. Clatworthy, P. L. *et al.* Dopamine Release in Dissociable Striatal Subregions Predicts the Different Effects of Oral Methylphenidate on Reversal Learning and Spatial Working Memory. *J. Neurosci.* **29,** 4690–4696 (2009).

319. Rutledge, R. B. *et al.* Dopaminergic Drugs Modulate Learning Rates and Perseveration in Parkinson ' s Patients in a Dynamic Foraging Task. *J. Neurosci.* **29,** 15104–15114 (2009).

320. Boulougouris, V., Glennon, J. C. & Robbins, T. W. Dissociable effects of selective 5-HT2A and 5-HT2C receptor antagonists on serial spatial reversal learning in rats.pdf. *Neuropsychopharmacology* **33,** 2007–2019 (2008).

321. Boulougouris, V. & Robbins, T. W. Enhancement of spatial reversal learning by 5-HT2C receptor antagonism is neuroanatomically specific. *J. Neurosci.* **30,** 930–938 (2010).

322. Nonkes, L. J. P. & Homberg, J. R. Perseverative instrumental and Pavlovian responding to conditioned stimuli in serotonin transporter knockout rats. *Neurobiol. Learn. Mem.* **100,** 48–55 (2013).

323. Brigman, J. L. *et al.* Pharmacological or genetic inactivation of the serotonin transporter improves reversal learning in mice. *Cereb. Cortex* **20,** 1955–1963 (2010).

324. Berg, B. A., Schoenbaum, G. & Mcdannald, M. A. The dorsal raphe nucleus is integral to negative prediction errors in Pavlovian fear. *Eur. J. Neurosci.* **40,** 3096–3101 (2014).

325. Takahashi, Y. K. *et al.* Expectancy-related changes in firing of dopamine neurons depend on orbitofrontal cortex. *Nat. Neurosci.* **14,** 1590–1597 (2011).

326. Reynolds, B. The acquisition of a trace conditioned response as a function of the magnitude of the stimulus trace. *J. Exp. Psychol.* **35,** 15–30 (1945).

327. Boneau, C. A. The interstimulus interval and the latency of the conditioned eyelid response. *J. Exp. Psychol.* **56,** 464–471 (1958).

328. Pan, W., Brown, J. & Dudman, J. T. Neural signals of extinction in the inhibitory microcircuit of the ventral midbrain. *Nat. Neurosci.* **16,** 71–78 (2013).

329. Matsumoto, M. & Hikosaka, O. Lateral habenula as a source of negative reward signals in dopamine neurons. *Nature* **447,** (2007).

330. Tian, J. & Uchida, N. Habenula Lesions Reveal that Multiple Mechanisms Underlie Dopamine Prediction Errors. *Neuron* **87,** 1–13 (2015).

331. Courville, A. C., Daw, N. D. & Touretzky, D. S. Bayesian theories of conditioning in a changing world. *Trends Cogn. Sci.* **10,** 294–300 (2006).

332. Dayan, P. & Yu, A. J. Phasic norepinephrine: a neural interrupt signal for unexpected events. *Netw. Comput. Neural Syst.* **17,** (2006).

333. Bland, S. T. *et al.* Stressor Controllability Modulates Stress-Induced Dopamine and Serotonin Efflux and Morphine-Induced Serotonin Efflux in the Medial Prefrontal Cortex. *Neuropsychopharmacology* **28,** 1589–1596 (2003).

334. Amat, J. *et al.* Medial prefrontal cortex determines how stressor controllability affects behavior and dorsal raphe nucleus. **8,** 365–371 (2005).

335. Pearce, J. M. & Hall, G. A model for Pavlovian learning: variations in the effectiveness of conditioned but not of unconditioned stimuli. *Psychol. Rev.* **87,** 532–552 (1980).

336. Mcdevitt, R. A. *et al.* Serotonergic versus Nonserotonergic Dorsal Raphe Projection Neurons : Differential Participation in Reward. *Cell Rep.* **8,** 1857–1869 (2014).

337. Correia, P. A. *et al.* Optogenetic activation of dorsal raphe serotonergic neurons reduces movement, without affecting motor coordination or inducing reinforcing responses in behaving mice. *Prep.* (2015).

338. Maya Vetencourt, J. F. *et al.* The antidepressant fluoxetine restores plasticity in the adult visual cortex. *Science (80-.).* **320,** 385–388 (2008).

339. Jitsuki, S. *et al.* Article Serotonin Mediates Cross-Modal Reorganization of Cortical Circuits. *Neuron* **69,** 780–792 (2011).

340. Santarelli, L. *et al.* Requirement of Hippocampal Neurogenesis for the Behavioral Effects of Antidepressants. *Science (80-.).* **301,** 805–809 (2003).

341. Kojic, L., Gu, Q., Douglas, R. M. & Cynader, M. S. Serotonin facilitates synaptic plasticity in kitten visual cortex: an in vitro study. *Dev. Brain Res.* **101,** 299–304 (1997).

342. He, K. *et al.* Distinct Eligibility Traces for LTP and LTD in Cortical Synapses. *Neuron* **88,** 1–11 (2015).

343. Savitt, J. M., Jang, S. S., Mu, W., Dawson, V. L. & Dawson, T. M. Bcl-x is required for proper development of the mouse substantia nigra. *J. Neurosci.* **25,** 6721–6728 (2005).

344. Paxinos, G and Franklin, K. B. J. *Mouse Brain in Stereotaxic Coordinates*. (2001).

345. Harris, K. D. *et al.* How do neurons work together ? Lessons from auditory cortex. *Hear. Res.* **271,** 37–53 (2011).

346. Moore, T., Hofer, S. B., Mrsic-flogel, T. D., Carandini, M. & Harris, K. D. Diverse coupling of neurons to populations in sensory cortex ´. *Nature* **521,** 511–515 (2015).

347. Deakin, J. F. W. & Graeff, F. G. 5-HT and mechanisms of defence. *J. Psychopharmacol.* **5,** 305–315 (1991).

348. Khanbabian, M. V, Kirakosyan, M. P. & Sargsyan, R. S. Electrophysiological and Pharmacological Analysis of Neuronal Activity in the Midbrain Medial Raphe Nucleus after Acute Immobilization Stress. *Neurophysiology* **34,** 147–149 (2002).

349. Walletschek, H. & Raab, a. Spontaneous activity of dorsal raphe neurons during defensive and offensive encounters in the tree-shrew. *Physiol. Behav.* **28,** 697–705 (1982).

350. Dickinson, A. & Balleine, B. in *Stevens' Handbook of Experimental Psychology* (ed. Gallistel, C.) Vol. 3: 497–533 (Wiley: New York, N.Y., 2002).

351. Mackintosh, N. J. A theory of attention: Variations in the associability of stimuli with reinforcement. *Psychol. Rev.* **82,** 276–298 (1975).

352. Hall, G. & Pearce, J. M. Latent inhibition of a CS during CS-US pairings. *J. Exp. Psychol. Anim. Behav. Process.* **5,** 31–42 (1979).

353. Blaisdell, A. P., Denniston, J. C. & Miller, R. R. Unblocking with Qualitative Change of Unconditioned Stimulus. *Learn. Motiv.* **279,** 268–279 (1997).

354. Wilson, P. N. *et al.* Restoration of the orienting response to a light by a change in its predictive accuracy in its Predictive Accuracy. *Q. J. Exp. Psychol. Sect. B* **44B,** 17–36 (1992).

355. Holland, P. C. Brain mechanisms for changes in processing of conditioned stimuli in Pavlovian conditioning : Implications for behavior theory. *Anim. Learn. Behav.* **25,** 373–399 (1997).

356. Blaisdell, A., Bristol, A., Gunther, L. & Miller, R. Overshadowing and latent inhibition counteract each other: support for the comparator hypothesis. *J. Exp. Psychol. Anim. Behav. Process* **24,** 335–351 (1998).

357. Yu, A. J. & Dayan, P. Uncertainty , Neuromodulation , and Attention. *Neuron* **46,** 681–692 (2005).

358. Hangya, B., Ranade, S. P., Lorenc, M. & Kepecs, A. Central Cholinergic Neurons Are Rapidly Recruited by Reinforcement Feedback Article Central Cholinergic Neurons Are Rapidly Recruited by Reinforcement Feedback. *Cell* **162,** 1155–1168 (2015).

359. Belova, M. A., Paton, J. J., Morrison, S. E. & Salzman, C. D. Expectation Modulates Neural Responses to Pleasant and Aversive Stimuli in Primate Amygdala. *Neuron* **55,** 970–984 (2007).

360. Lin, S. & Nicolelis, M. A. L. Neuronal Ensemble Bursting in the Basal Forebrain Encodes Salience Irrespective of Valence. *Neuron* **59,** 138–149 (2008).

361. O'Reilly, J. X., Schüffelgen, U., Cuell, S. F., Behrens, T. E. J. & Mars, R. B. Dissociable effects of surprise and model update in parietal and anterior cingulate cortex. *Proc. Natl. Acad. Sci. U. S. A.* **110,** E3660–E3669 (2013).

362. Tervo, D. G. R. *et al.* Behavioral Variability through Stochastic Choice and Its Gating by Anterior Cingulate Cortex. *Cell* **159,** 21–32 (2014).

363. Boneau, C. A. THE INTERSTIMULUS INTERVAL AND THE LATENCY OF THE CONDITIONED EYELID RESPONSE 1 The effect upon eyelid conditioning of the time interval between the CS and the UCS has been studied in detail , with a rather precise specifica- tion of the shape of the func. *J. Exp. Psychol.* **56,** 464–471 (1958).

364. Rasmussen, K., Strecker, R. E. & Jacobs, B. L. Single unit response of noradrenergic , serotonergic and dopaminergic neurons in freely moving cats to simple sensory stimuli. *Brain Res.* **369,** 336–340 (1986).

365. Maswood, S., Barter, J. E., Watkins, L. R. & Maier, S. F. Exposure to inescapable but not escapable shock increases extracellular levels of 5-HT in the dorsal raphe nucleus of the rat. *Brain Res.* **783,** 115–120 (1998).

366. Grahn, R. E. *et al.* Activation of serotonin-immunoreactive cells in the dorsal raphe nucleus in rats exposed to an uncontrollable stressor. *Brain Res.* **826,** 35–43 (1999).

367. Maier, S., Grahn, R. & Watkins, L. 8-OH-DPAT microinjected in the region of the dorsal raphe nucleus blocks and reverses the enhancement of fear conditioning and interference with escape produced by exposure to inescapable shock. *Behav. Neurosci.* **109,** 404–412 (1995).

368. Amat, J. *et al.* The role of the habenular complex in the elevation of dorsal raphe nucleus serotonin and the changes in the behavioral responses produced by uncontrollable stress. *Brain Res.* **917,** 118–126 (2001).

369. Amat, J., Paul, E., Zarza, C., Watkins, L. R. & Maier, S. F. Previous Experience with Behavioral Control over Stress Blocks the Behavioral and Dorsal Raphe Nucleus Activating Effects of Later Uncontrollable Stress : Role of the Ventral Medial Prefrontal Cortex. *J. Neurosci.* **26,** 13264–13272 (2006).

370. Warden, M. R. *et al.* A prefrontal cortex–brainstem neuronal projection that controls response to behavioural challenge. *Nature* **492,** 428–432 (2012).

371. Brust, R. D. *et al.* Functional and Developmental Identification of a Molecular Subtype of Brain Serotonergic Neuron Specialized to Regulate Breathing Dynamics Article Functional and Developmental Identification of a Molecular Subtype of Brain Serotonergic Neuron Specialized. *Cell Rep.* **9,** 2152–2165 (2014).

372. Pelagio-Flores, R., Ortíz-Castro, R., Méndez-Bravo, A., Macías-Rodríguez, L. & López-Bucio, J. Serotonin, a Tryptophan-Derived Signal Conserved in Plants and Animals ,

Regulates Root System Architecture Probably Acting as a Natural Auxin Inhibitor in Arabidopsis thaliana. *Plant Cell Physiol.* **52,** 490–508 (2011).

373. Matsumoto, M. & Hikosaka, O. Representation of negative motivational value in the primate lateral habenula. *Nat. Neurosci.* **12,** 77–84 (2009).

374. Christoph, G. R., Leonzio, R. J. & Wilcox, K. S. Stimulation of the Lateral Habenula Inhibits Dopamine-Containing Neurons in the Substantia Ventral Tegmental Area of the Rat. *J. Neurosci.* **6,** 613–619 (1986).

375. Jhou, T. C., Fields, H. L., Baxter, M. G., Saper, C. B. & Holland, P. C. The Rostromedial Tegmental Nucleus (RMTg), a GABAergic Afferent to Midbrain Dopamine Neurons , Encodes Aversive Stimuli and Inhibits Motor Responses. *Neuron* **61,** 786–800 (2009).

376. Varga, V., Kocsis, B. & Sharp, T. Electrophysiological evidence for convergence of inputs from the medial prefrontal cortex and lateral habenula on single neurons in the dorsal raphe nucleus. *Eur. J. Neurosci.* **17,** 280–286 (2003).

377. Sego, C. *et al.* Lateral habenula and the rostromedial tegmental nucleus innervate neurochemically distinct subdivisions of the dorsal raphe nucleus in the rat. *J. Comp. Neurol.* **522,** 1454–1484 (2014).

378. Celada, P., Casanovas, J. M., Paez, X. & Artigas, F. Control of serotonergic neurons in the dorsal raphe nucleus by the lateral hypothalamus. *Brain Res.* **932,** 79–90 (2002).

379. Paton, J. J., Belova, M. A., Morrison, S. E. & Salzman, C. D. The primate amygdala represents the positive and negative value of visual stimuli during learning. *Nature* **439,** (2006).

380. Belova, M. a, Paton, J. J. & Salzman, C. D. Moment-to-moment tracking of state value in the amygdala. *J. Neurosci.* **28,** 10023–10030 (2008).

381. Weissbourd, B. *et al.* Presynaptic Partners of Dorsal Raphe Serotonergic and GABAergic Neurons. *Neuron* **83,** 645–662 (2014).

382. Liu, Z. & Ikemoto, S. The midbrain raphe nuclei mediate primary reinforcement via GABA A receptors. *Eur. J. Neurosci.* **25,** 735–743 (2007).

383. Sasaki-Adams, D. M. & Kelley, A. E. Serotonin-Dopamine Interactions in the Control of Conditioned Reinforcement and Motor Behavior. *Neuropsychopharmacology* **25,** 410–452 (2001).

384. Bellew, L. T. L. T. J. G., Grote, K. A. & Neisewander, J. L. Serotonin depletion attenuates cocaine seeking but enhances sucrose seeking and the effects of cocaine priming on reinstatement of cocaine seeking in rats. *Psychopharmacology (Berl).* **157,** 340–348 (2001).

385. Cools, R., Roberts, A. C. & Robbins, T. W. Serotoninergic regulation of emotional and behavioural control processes. *Trends Cogn. Sci.* **12,** 31–40 (2007).

386. Dayan, P. & Huys, Q. J. M. Serotonin in Affective Control. *Annu. Rev. Neurosci.* **32,** 95–126 (2009).

387. Line, S. J. *et al.* Reduced sensitivity to both positive and negative reinforcement in mice over-expressing the 5-hydroxytryptamine transporter. *Eur. J. Neurosci.* **40,** 3735–3745 (2014).

388. Den Ouden, H. E. M. & Swart, J. C. Acute serotonin depletion releases motivated inhibition of response vigour. *Psychopharmacology (Berl).* **232,** 1303–1312 (2015).

389. Qi, J. *et al.* A glutamatergic reward input from the dorsal raphe to ventral tegmental area dopamine neurons. *Nat. Commun.* **5,** 1–13 (2014).

390. Shutoh, F., Ina, A., Yoshida, S., Konno, J. & Hisano, S. Two distinct subtypes of serotonergic fibers classified by co-expression with vesicular glutamate transporter 3 in rat forebrain. *Neurosci. Lett.* **432,** 132–136 (2008).

391. Hajo, M., Richards, C. D. & Sze, A. D. An electrophysiological and neuroanatomical study of the medial prefrontal cortex projection to the midbrain raphe nuclei in the rat. *Neuroscience* **87,** 95–108 (1998).

392. Jankowski, M. P. & Sesack, S. R. Prefrontal Cortical Projections to the Rat Dorsal Raphe Nucleus : Ultrastructural Features and Associations with Serotonin and gamma - Aminobutyric Acid Neurons. *J. Comp. Neurol.* **529,** 518–529 (2004).

393. Peyron, C., Petit, J. M., Rampon, C., Jouvet, M. & Luppi, P. H. Forebrain afferents to the rat dorsal raphe nucleus demonstrated by retrograde and anterograde tracing methods. *Neuroscience* **82,** 443–468 (1997).

394. Csillag, A., Sharp, T., Hajo, M., Varga, V. & Sze, A. D. Evidence for a role of GABA interneurons in the cortical modulation of midbrain 5-hydroxytryptamine neurons. *Neuroscience* **106,** 783–792 (2001).

395. Celada, P., Puig, M. V., Casanovas, J. M., Guillazo, G. & Artigas, F. Control of Dorsal Raphe Serotonergic Neurons by the Medial Prefrontal Cortex : Involvement of Serotonin-1A , GABA A , and Glutamate Receptors. *J. Neurosci.* **21,** 9917–9929 (2001).

396. Hayden, B. Y., Heilbronner, S. R., Pearson, J. M. & Platt, M. L. Surprise Signals in Anterior Cingulate Cortex : Neuronal Encoding of Unsigned Reward Prediction Errors Driving Adjustment in Behavior. *J. Neurosci.* **31,** 4178–4187 (2011).

397. Kepecs, A., Uchida, N., Zariwala, H. A. & Mainen, Z. F. Neural correlates, computation and behavioural impact of decision confidence. *Nature* **455,** (2008).

398. Gottfried, J. a, O'Doherty, J. & Dolan, R. J. Encoding predictive reward value in human amygdala and orbitofrontal cortex. *Science* **301,** 1104–1107 (2003).

399. Schoenbaum, G., Saddoris, M. P. & Stalnaker, T. A. Reconciling the Roles of Orbitofrontal Cortex in Reversal Learning and the Encoding of Outcome Expectancies. *Ann. New York Acad. Sci.* **1121,** 320–335 (2007).

400. Schoenbaum, G., Roesch, M. R. & Stalnaker, T. A. A new perspective on the role of the orbitofrontal cortex in adaptive behaviour. *Nat. Rev. Neurosci.* **10,** 885–892 (2009).

401. Rudebeck, P. H. & Murray, E. A. The Orbitofrontal Oracle : Cortical Mechanisms for the Prediction and Evaluation of Specific Behavioral Outcomes. *Neuron* **84,** 1143–1156 (2014).

402. Tremblay, L. & Schultz, W. Relative reward preference in primate orbitofrontal cortex. *Nature* **398,** 704–708 (1999).

403. Morrison, S. E. & Salzman, C. D. Representations of appetitive and aversive information in the primate orbitofrontal cortex. *Ann. New York Acad. Sci.* **1239,** 59–70 (2011).

404. Hosokawa, T., Kato, K., Inoue, M. & Mikami, A. Neurons in the macaque orbitofrontal cortex code relative preference of both rewarding and aversive outcomes. *Neurosci. Res.* **57,** 434–445 (2007).

405. McAlonan, K. & Brown, V. J. Orbital prefrontal cortex mediates reversal learning and not attentional set shifting in the rat. *Behav. Brain Res.* **146,** 97–103 (2003).

406. Rogers, R. D., Andrews, T. C., Grasby, P. M., Brooks, D. J. & Robbins, T. W. Contrasting Cortical and Subcortical Activations Produced by Attentional-Set Shifting and Reversal Learning in Humans. *J. Cogn. Neurosci.* **12,** 142–162 (2000).

407. Fellows, L. K. & Farah, M. J. Ventromedial frontal cortex mediates affective shifting in humans : evidence from a reversal learning paradigm. *Brain* **126,** 1830–1837 (2003).

408. Dias, R., Robbins, T. W. & Roberts, a C. Dissociation in prefrontal cortex of affective and attentional shifts. *Nature* **380,** 69–72 (1996).

409. Rygula, R. *et al.* Role of Central Serotonin in Anticipation of Rewarding and Punishing Outcomes: Effects of Selective Amygdala or Orbitofrontal 5-HT Depletion. *Cereb. Cortex* bhu102 (2014). doi:10.1093/cercor/bhu102

410. Mathur, B. N., Capik, N. A., Alvarez, V. A. & Lovinger, D. M. Serotonin Induces Long-Term Depression at Corticostriatal Synapses. *J. Neurosci.* **31,** 7402–7411 (2011).

411. Masaki, D., Yokoyama, C. & Kinoshita, S. Relationship between limbic and cortical 5-HT neurotransmission and acquisition and reversal learning in a go / no-go task in rats. *Psychopharmacology (Berl).* **189,** 249–258 (2006).

412. Izquierdo, A., Newman, T. K., Higley, J. D. & Murray, E. A. Genetic modulation of cognitive flexibility and socioemotional behavior in rhesus monkeys. *Proc. Natl. Acad. Sci. U. S. A.* **104,** 14128–14133 (2007).

413. Vallender, E. J., Lynch, L., Novak, M. A. & Miller, G. M. Polymorphisms in the 3'UTR of the Serotonin Transporter are Associated With Cognitive Flexibility in Rhesus Macaques. *Am. J. Med. Genet. Part B* **150B,** 467–475 (2008).

414. Den Ouden, H. E. M. *et al.* Dissociable effects of dopamine and serotonin on reversal learning. *Neuron* **80,** 1090–100 (2013).

415. Hariri, A. R. & Holmes, A. Genetics of emotional regulation : the role of the serotonin transporter in neural function. *Trends Cogn. Sci.* **10,** 182–191 (2006).

416. Cools, R., Robinson, O. J. & Sahakian, B. Acute Tryptophan Depletion in Healthy Volunteers Enhances Punishment Prediction but Does not Affect Reward Prediction. *Neuropsychopharmacology* **33,** 2291–2299 (2008).

417. Robinson, O. J., Cools, R. & Sahakian, B. J. Tryptophan depletion disinhibits punishment but not reward prediction : implications for resilience. *Psychopharmacology (Berl).* **219,** 599–605 (2012).

418. Evers, E. a T. *et al.* Serotonergic modulation of prefrontal cortex during negative feedback in probabilistic reversal learning. *Neuropsychopharmacology* **30,** 1138–1147 (2005).

419. Crockett, M. J., Clark, L. & Robbins, T. W. Reconciling the Role of Serotonin in Behavioral Inhibition and Aversion : Acute Tryptophan Depletion Abolishes Punishment-Induced Inhibition in Humans. *J. Neurosci.* **29,** 11993–11999 (2009).

420. Bari, A. *et al.* Serotonin modulates sensitivity to reward and negative feedback in a probabilistic reversal learning task in rats. *Neuropsychopharmacology* **35,** 1290–1301 (2010).

421. Mcallister, B. B., Spanswick, S. C., Patel, P. P., Barneto, A. A. & Dyck, R. H. The effects of chronic fluoxetine treatment following injury of medial frontal cortex in mice. *Behav. Brain Res.* **290,** 102–116 (2015).

422. Kirkwood, A. Serotonergic control of developmental plasticity. *Proc. Natl. Acad. Sci. U. S. A.* **97,** 1951–1952 (2000).

423. Tong, C. K. *et al.* Axonal Control of the Adult Neural Stem Cell Niche. *Cell Stem Cell* **14,** 500–511 (2014).

424. Mcavoy, K., Russo, C., Kim, S., Rankin, G. & Sahay, A. Fluoxetine Induces Input-Specific Hippocampal Dendritic Spine Remodeling Along the Septotemporal Axis in Adulthood and Middle Age. *Hippocampus* **1446,** 1429–1446 (2015).

425. Malberg, J. E., Eisch, a J., Nestler, E. J. & Duman, R. S. Chronic antidepressant treatment increases neurogenesis in adult rat hippocampus. *J. Neurosci.* **20,** 9104–9110 (2000).

426. Pechnick, R. N. *et al.* Antidepressants Stimulate Hippocampal Neurogenesis by Inhibiting p21 Expression in the Subgranular Zone of the Hipppocampus. *PLoS One* **6,** e27290 (2011).

427. Hurley, L. M. & Hall, I. C. Context-dependent modulation of auditory processing by serotonin. *Hear. Res.* **279,** 74–84 (2011).

428. Branchi, I. & Elena, V. R. The double edged sword of neural plasticity : Increasing serotonin levels leads to both greater vulnerability to depression and improved capacity to recover. *Psychoneuroendocrinology* **36,** 339–351 (2011).

429. Healy, D. Serotonin and depression. *BMJ* **350,** 41771 (2015).

430. Tye, K. M. *et al.* Dopamine neurons modulate neural encoding and expression of depression-related behaviour. *Nature* **493,** 537–541 (2013).

431. Chaudhury, D. *et al.* Rapid regulation of depression-related behaviours by control of midbrain dopamine neurons. *Nature* **493,** 532–536 (2013).

432. Russo, S. J. & Nestler, E. J. The brain reward circuitry in mood disorders. *Nat. Rev. Neurosci.* **14,** 609–625 (2013).

433. Deakin, J. F. W., File, S. E., Hyde, J. R. G. & Macleod, N. K. Ascending 5-HT Pathways and Behavioral Habituation. *Pharmacol. Biochem. Behavio* **10,** 687–694 (1979).

434. Tecott, L. H. Review Serotonin and the Orchestration of Energy Balance. *Cell Metab.* **6,** 352–361 (2007).

435. Flavell, S. W. *et al.* Serotonin and the Neuropeptide PDF Initiate and Extend Opposing Behavioral States in C . elegans. *Cell* **154,** 1023–1035 (2013).

436. Gately, P. F., Poon, S. L., Segal, D. S. & Geyer, M. A. Psycho pharmacology Depletion of brain serotonin by 5 , 7-dihydroxytryptamine alters the response to amphetamine and the habituation of locomotor activity in rats. *Psychopharmacology (Berl).* **87,** 400–405 (1985).

437. Lipska, B. K., Jaskiw, G. E., Arya, A. & Weinberger, D. R. Serotonin Depletion Causes Long-Term Reduction of Exploration in the Rat. *Pharmacol. Biochem. Behav.* **43,** 1247–1252 (1992).

438. Mogensen, J., Wörtwein, G., Plenge, P. & Mellerup, E. T. Serotonin, locomotion, exploration, and place recall in the rat. *Pharmacol. Biochem. Behav.* **75,** 381–395 (2003).

439. Pasupathy, A. & Miller, E. K. Different time courses of learning-related activity in the prefrontal cortex and striatum. *Nature* **433,** 873–876 (2005).

440. Clarke, H. F., Hill, G. J., Robbins, T. W. & Roberts, A. C. Dopamine, but not serotonin, regulates reversal learning in the marmoset caudate nucleus. *J. Neurosci.* **31,** 4290–4297 (2011).

441. Groman, S. M. *et al.* Monoamine levels within the orbitofrontal cortex and putamen interact to predict reversal learning performance. *Biol. Psychiatry* **73,** 756–762 (2013).

442. Root, D. H. *et al.* Single rodent mesohabenular axons release glutamate and GABA. *Nat. Neurosci.* **17,** 1543–1551 (2014).

443. Maia, T. V & Frank, M. J. From reinforcement learning models to psychiatric and neurological disorders. *Nat. Neurosci.* **14,** 154–162 (2011).